The Tropical Tropopause Layer – Detailed Thermal Structure, Decadal Variability and Recent Trends

A Dissertation

Submitted in Partial Fulfilment of the Requirements
for the Degree of
Doctor of Natural Sciences
(Dr. rer. nat)
to the department of **Fachbereich Geowissenschaften**
of the **Freie Universität Berlin**

by **Wuke Wang**

Berlin, 2015

Supervisor: Prof. Dr. Katja Matthes
Second examiner: Prof. Dr. Ulrike Langematz

Date of the Defense: 12th October 2015

Abstract

The tropical tropopause layer (TTL) is a key region for troposphere-stratosphere exchange and acts as a "gate" for trace gases entering the stratosphere. In particular, tropical tropopause temperatures (TPTs) control the content of stratospheric water vapour, which influences stratospheric chemistry, radiation and circulation and is also an important driver of surface climate. Decadal variability or even long-term trends in TPTs and stratospheric water vapour are of great interest but are still not well understood.

A comprehensive analysis of the TTL, including its detailed thermal structure, recent variability and dominant processes spanning time scales of years to decades, is conducted in this thesis using the recently available decade of high accuracy and high vertical resolution Global Positioning System Radio Occultation (GPS-RO) data, the Modern Era Retrospective-Analysis for Research and Applications (MERRA) reanalysis data, and a series of model simulations with NCAR's fully-coupled CESM model, which employs the chemistry climate model WACCM as its atmospheric component.

The GPS-RO data measures a significant warming of TPTs and a weakening of the strength of the tropopause inversion layer (TIL) since 2001. Based on a series of model simulations, which switch on/off the corresponding factors, this recent warming in the TTL is mainly due to internal variability, i.e. a decrease in sea surface temperatures (SSTs) and a strengthening in Quasi-Biennial Oscillation (QBO) associated westerlies. A version of WACCM with higher vertical resolution (~300 m) reproduces this recent temperature variability better than with the standard vertical resolution (~1 km).

This thesis provides the first evidence for a connection between TPTs and the Pacific Decadal Oscillation (PDO), from both observations and model simulations. The phase of the PDO, and in particular the change from positive to negative phases around the year 2000, can very well explain the recently observed TPT (multi-) decadal variability. This connection between SSTs and TPTs has consequences for stratospheric water vapour and may provide an important feedback on the Earth's global surface temperatures.

Additionally, the hotly debated (multi-) decadal variability in lower stratospheric (LS) water vapour between 1979 and 2014, can be well understood with the 11-year solar cycle, the decadal El-Niño Southern Oscillation (ENSO) and the PDO. LS water vapour lags the solar cycle by 2-3 years and can be explained using a link between the solar cycle, decadal ENSO variations and tropopause temperature variability.

This thesis highlights the importance of a fine vertical resolution for climate models and improves the understanding of the TTL temperature and LS water vapour variability over the recent decades. In particular it opens up a debate of the connection between stratospheric decadal to multidecadal variability and modes of SST variability, such as the PDO.

Zusammenfassung

Die Schicht um die tropische Tropopause (tropical tropopause layer - TTL) ist eine Schlüsselregion für den Austausch zwischen Tropo- und Stratosphäre und Haupteintragsregion von Spurengasen in die Stratosphäre. Tropische Tropopausentemperaturen bestimmen die Menge des stratosphärischen Wasserdampfes, der sowohl die stratosphärische Chemie, als auch die Strahlung und Zirkulation beeinflusst und ein wichtiger Treiber des Klimas an der Erdoberfläche ist. Dekadische Variabilität oder sogar langfristige Trends in den Tropopausentemperaturen und im stratosphärischen Wasserdampf sind daher von großem Interesse, jedoch bisher nicht gut verstanden.

In dieser Arbeit wird eine umfassende Analyse der TTL, einschließlich ihrer detaillierten thermischen Struktur und ihrer aktuellen Variabilität auf Zeitskalen von Jahren bis Jahrzehnten durchgeführt. Dazu werden die nun für eine Dekade verfügbaren, sehr genauen und vertikal hoch aufgelösten Global Positioning System Radio Occultation (GPS-RO) Daten, die MERRA (Modern Era Retrospective-analysis for Research and Applications) Reanalysedaten, sowie eine Reihe von Modellsimulationen mit einem voll gekoppelten Klima-Chemiemodell vom NCAR (CESM-WACCM), welches bis in die Thermosphäre reicht, verwendet.

Die GPS-RO Daten zeigen eine signifikante Erwärmung der Tropopausentemperaturen und eine Abschwächung der Stärke der Inversionsschicht oberhalb der Tropopause (Tropopause Inversion Layer – TIL) seit 2001. Basierend auf einer Reihe von Modellsimulationen, in welchen die entsprechenden natürlichen und anthropogenen Faktoren ein- bzw. ausgeschaltet werden, kann diese Erwärmung in der TTL vor allem auf interne Variabilität zurückgeführt werden. Dafür verantwortlich sind insbesondere eine Abnahme der Meeresoberflächentemperaturen und eine Verstärkung der Westphase der stratosphärischen Quasi-Biennial Oscillation (QBO). Eine vertikal höher aufgelöste Modellversion (~300 m in der TTL) reproduziert diese Temperaturvariabilität besser als die Standardauflösung (~1 km).

Im Rahmen dieser Arbeit wird erstmalig ein Zusammenhang zwischen den Tropopausentemperaturen und der PDO (Pacific Decadal Oscillation) sowohl in Beobachtungs- als auch Modelldaten hergestellt und ein Mechanismus vorgeschlagen. Die Phase der PDO, und insbesondere die Änderungen von einer positiven zu einer negativen Phase um das Jahr 2000, können die beobachtete (multi-)dekadische Variabilität der Tropopausentemperaturen gut erklären. Die Verbindung zwischen Meeresoberflächen- und Tropopausentemperaturen beeinflusst wiederum den stratosphärischen Wasserdampf und könnte eine wichtige Wechselwirkung zur globalen Erdbodentemperatur darstellen.

Die momentan stark diskutierte (multi-)dekadische Variabilität im Wasserdampf der unteren Stratosphäre zwischen 1979 und 2014 kann mit dem 11-jährigen Sonnenfleckenzyklus, der dekadischen El-Niño Southern Oscillation (ENSO) und der PDO Variabilität erklärt

werden. Das Wasserdampfsignal ist zwei bis drei Jahre nach einem Sonnenfleckenmaximum am stärksten und kann mit der Verbindung zwischen dekadischer ENSO Variabilität und Tropopausentemperaturen verstanden werden.

Diese Arbeit unterstreicht die Bedeutung einer feinen vertikalen Auflösung für Klimamodelle im Bereich der TTL und verbessert das Verständnis der Temperatur- und Wasserdampfvariabilität in der unteren Stratosphäre in den letzten Jahrzehnten. Insbesondere eröffnet sie eine Diskussion über den Zusammenhang zwischen dekadischer bis multidekadischer stratosphärischer Variabilität und Variabilitätsmoden im Ozean wie zum Beispiel der PDO.

Table of contents

Chapter 1

Introduction

1.1 The Tropical Tropopause Layer

In the tropics, the temperature decreases with height from the surface up to the tropopause region (~17 km), and then increases at higher altitudes through the stratosphere. The relative minimum temperature between the troposphere and the stratosphere is termed the cold point tropopause (CPT, the solid line in Fig. 1.1). The tropopause is a transition zone between the well-mixed, convectively active troposphere and the stably stratified and quieter stratosphere, rather than a line that isolates the troposphere from the stratosphere (*Fueglistaler et al.*, 2009; *Gettelman and Birner*, 2007; *Highwood and Hoskins*, 1998; *Plumb*, 2007; *Sherwood and Dessler*, 2001). This transition zone is now generally called the tropical tropopause layer (TTL, blue shaded area in Fig. 1.1a), within which the air has distinct properties of both the troposphere and the stratosphere. The vertical range of the TTL depends on its definition, i.e., it can be a shallower layer between 14-18.5 km (*Fueglistaler et al.*, 2009) or a deeper layer of about 12-19 km (*Gettelman and Forster*, 2002; *SPARC-CCMVal*, 2010, chapter 7). These definitions all capture the same key feature of transition from convectively to radiatively dominated regimes (Fig. 1.2).

The TTL acts like a "gate" for air entering into the stratosphere from the tropical troposphere, and thereby determines the amounts of atmospheric tracers entering the stratosphere, such as very short lived substances and water vapour, which both play an important role for stratospheric radiation and chemistry. The transition of atmospheric tracers between the troposphere and stratosphere is largely determined by the composition of the air near the tropical tropopause (*Hegglin et al.*, 2014; *Randel and Jensen*, 2013). The tracer concentration exhibits particularly strong vertical gradients through the TTL region, e.g., ozone begins to depart from its tropospheric background value at the level of minimum stability and increases strongly to high values, and water vapour reaches its stratospheric background value near

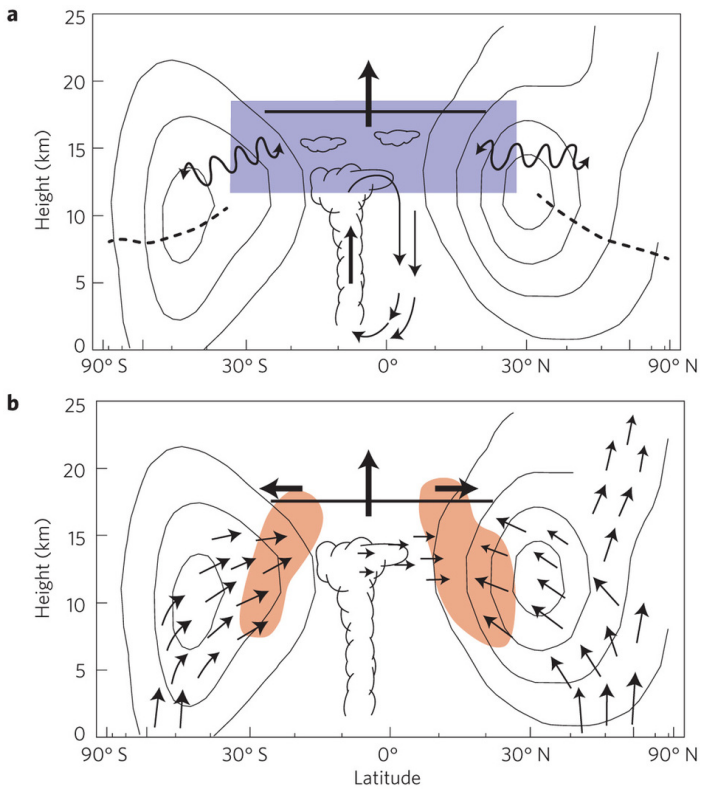

Fig. 1.1 Schematic of the large-scale structure and circulation of the TTL in the latitude-height plane. The influence of tropical deep convection and interactions with other regions of the atmosphere are highlighted. The solid line in the tropics near 17 km indicates the CPT, and the dotted lines denote the extratropical tropopause. Contours represent the zonal mean winds, and the wriggled lines highlight two-way transport between the TTL (blue region) and the extratropics. The upward arrow across the tropical tropopause indicates the large-scale upwelling associated with the Brewer-Dobson circulation. The latitude scale is proportional to area (weighted by cos (latitude)). **b**, Large-scale dynamical structure of the zonal mean atmosphere, highlighting the propagation of tropical and extratropical waves (denoted by arrows) that dissipate in the subtropics (red regions), inducing polewards motion in the subtropical lower stratosphere and time mean upwelling within the TTL. From *Randel and Jensen* (2013, their Figure 1).

the CPT (Fig. 1.2). The stratospheric constituents are therefore particularly sensitive to the mixing processes in the TTL. The TTL affects both the surface and stratospheric climate, because of the strong chemical effects of these tracers as well as the powerful radiative effects of water vapour (*Dessler et al.*, 2013; *Solomon et al.*, 2010). The TTL in turn is influenced by a variety of physical, dynamical and chemical processes (Fig. 1.1), and is highly sensitive to climate change, and hence is a potential indicator of climate change (*Santer et al.*, 2003; *Shepherd*, 2002).

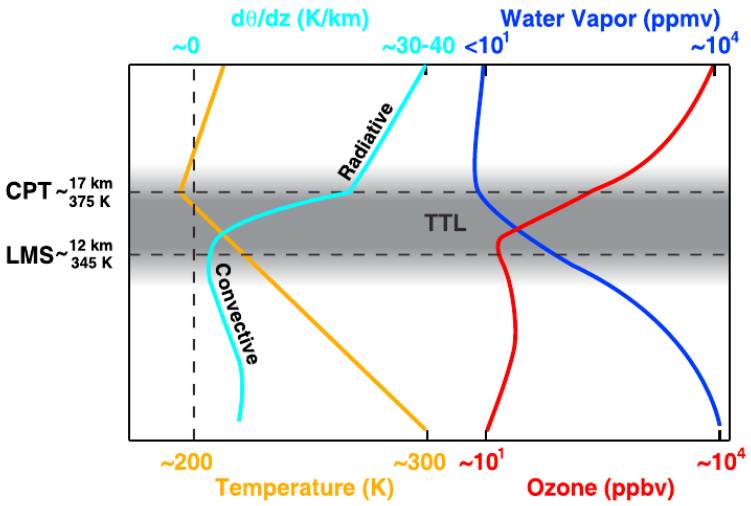

Fig. 1.2 Schematic of TTL based on the thermal structure and chemical tracer relationships. The schematic highlights the change of O_3 and H_2O at the two critical levels in the thermodynamic structure–O_3 begins to depart from its tropospheric background value at the level of minimum stability, and H_2O reaches its stratospheric background value near the CPT. The transitional air masses, as identified by the tracer-relationship, are well correlated with the level of minimum stability and the CPT. From *Pan et al.* (2014, their Figure 12).

1.2 Detailed structure of the TTL – Tropopause Inversion Layer (TIL)

1.2.1 The discovery of the TIL

Temperature is a fundamental state variable of the atmosphere, linking atmospheric motion, clouds, radiation, (moist) convection, and chemical reactions. Temperature observations with high vertical resolution from radiosondes have been available since the 1950s, albeit with relatively few stations, many of which do not have openly-accessible data. Since the 1970s, satellite measurements have provided layer average temperatures with global coverage, but poor vertical resolution. Since 2001, the Global Positioning System Radio Occultation (GPS-RO) data have provided data that are well-suited for studying the TTL, i.e. data with global coverage, weather independent, self-calibrating measurements, and very high vertical resolution of about 100 m (see details about the GPS-RO data in *Wickert et al.* (2001, 2009) and Chapter 2).

With this highly accurate and highly vertically resolved temperature data, the detailed vertical thermal structure of the TTL, the height of the tropopause, and the tropopause temperature, can now be precisely detected for every profile. However, because the tropopause

height and temperature vary with time and location, the main features of the TTL's vertical structure are blurred by a conventional sea-level based average, where the vertical coordinate is fixed in time and horizontal space. *Birner* (2006) instead computed the average with respect to the local, time-dependent altitude of the tropopause (i.e., a tropopause-based average), in order to preserve characteristic features that are coupled to the tropopause. This resulted in the discovery of the so-called Tropopause Inversion Layer (TIL), a narrow (1-2 km) band of temperature inversion above the tropopause associated with a region of enhanced static stability (Fig. 1.3), in radiosonde data (*Birner*, 2006; *Birner et al.*, 2002), which was later confirmed as a global feature with GPS-RO data (*Grise et al.*, 2010).

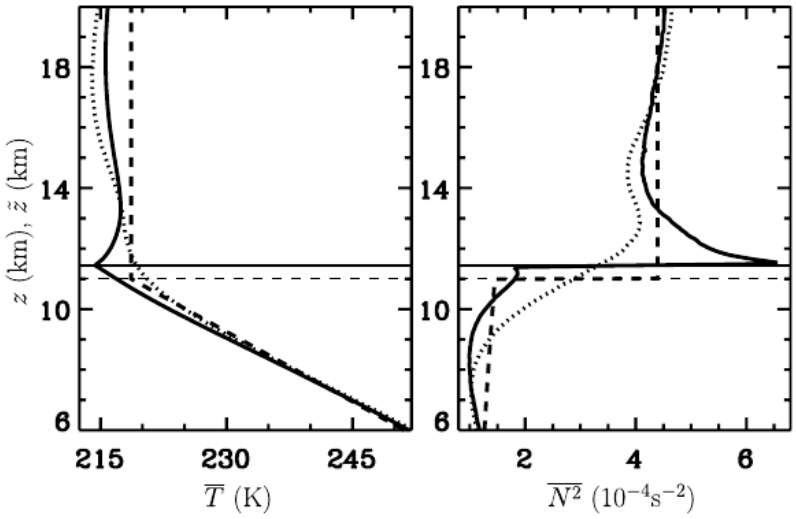

Fig. 1.3 Averaged profiles representative of about 45°N of (left) temperature and (right) buoyancy frequency squared from radiosonde data. Dotted lines indicate sea-level based average, solid lines indicate tropopause-based average, and dashed lines indicate profiles of the U.S. standard atmosphere at 45°N. Horizontal lines denote the height of the tropopause. From *Birner et al.* (2006, their Figure 8).

The thermal structure of the TIL sharply contrasts conventional, textbook climatologies of atmospheric temperature (~1 km vertical resolution), which typically show roughly constant temperature profiles in the mid-latitude lower stratosphere (dashed lines in Fig. 1.3), according to the U.S. standard atmosphere (USSA) (*Force*, 1976). The TIL, which is a particular aspect of the tropopause over the globe, is distinct with the conventional TTL, which constitutes the broader transition region from the troposphere to the stratosphere in the tropics.

1.2.2 Mechanisms for TIL formation

Wirth (2004) and *Wirth and Szabo* (2007), using an idealized model and dynamical framework, found that the sharp peak in squared buoyancy frequency (N^2) just above the tropopause occurrs primarily in anticyclonic flow. By taking into account the enhancement of gravity wave activity associated with the cyclone and jet stream during the development and mature stages of a cyclone, *Otsuka et al.* (2014) suggested that the vertical convergence from gravity waves associated with synoptic weather systems is a key process in the formation of the negative correlation between the strength of the TIL and the local relative vorticity at the tropopause. *Birner et al.* (2006) suggested that the existence of the TIL might result from large-scale eddy heat fluxes. These dynamical mechanisms were disputed by *Randel et al.* (2007), who showed that the TIL exists during any dynamic circulation regimes, and should have other causes, such as radiative processes resulting from the strong gradients of water vapour and ozone across the tropopause. This radiative mechanism was supported by the studies of *Hegglin et al.* (2009); *Kunz et al.* (2009); *Randel and Wu* (2010) and *Schmidt et al.* (2010). Furthermore, *Birner* (2010) showed this question to be more complex by pointing out that the residual circulation mainly caused the TIL in the winter midlatitudes, whereas radiation seems to dominate the formation of the polar summer TIL. The relative contribution of both, dynamical and radiative processes, was studied in a high-resolution model (*Miyazaki et al.*, 2010a,b), and supports the idea that radiative effects are important only in polar summer while dynamics dominate otherwise. The formation and maintenance of the TIL are not yet fully understood and are may be a combination of effects by both radiation and different scale dynamical processes.

1.2.3 The strength of the TIL and its potential impacts on climate

Randel et al. (2007) define the strength of the TIL (STIL) as the temperature difference between the temperature at 2 km above the tropopause and the tropopause temperature (TPT) in the extratropics. In this thesis we use a similar definition of the STIL, but with the temperature at 1 km instead of 2 km above the tropopause, since the maximum of N^2 occurs no more than 1 km above the tropopause (Fig. 1.3b, also *Grise et al.* (2010)) in the tropics. The maximum of N^2 is used as another indicator of STIL. There are at least three potential impacts of the TIL on stratospheric climate. First, as described above, the CPT dominates the water vapour amount entering the stratosphere from the troposphere (*Hegglin et al.*, 2014; *Randel and Jensen*, 2013). Whether such a temperature inversion just above the CPT also influences the water vapour dehydration while crossing the tropopause and entering into the lower stratosphere needs further study. Second, the buoyancy frequency N^2, which indicates

the stability of the atmosphere, determines the sensitivity of the temperature tendency to the vertical motion due to the thermodynamic balance (see section 1.3.1 below and also *Randel and Wu* (2015)). Finally, N^2 is an essential factor in controlling equatorial waves (*Alexander et al.*, 2010; *Fritts and Alexander*, 2003). A thin layer with dramatically increased N^2 potentially affects wave propagation, reflection and dissipation, and therefore influences momentum and energy transport (*Alexander et al.*, 2010; *Flannaghan and Fueglistaler*, 2013; *Fritts and Alexander*, 2003). The response of the STIL to climate change on decadal or longer time scales is still unclear. This thesis gives the first investigation of the long-term variability in the STIL, to improve the understanding of both TIL formation and maintenance mechanisms, and discuss potential impacts of the TIL on stratospheric climate (Chapter 2).

1.3 Seasonal-to-decadal variability of the TTL

As mentioned above and shown in Figs. 1.1 and 1.2, the temperature in the TTL is determined by combined influences of latent heat release by convection, dynamically driven vertical motion, and radiative cooling (*Fueglistaler et al.*, 2009; *Grise and Thompson*, 2012, 2013; *Kim and Alexander*, 2015; *Randel and Jensen*, 2013; *Randel and Wu*, 2015). These complex processes from both the troposphere and the stratosphere make analyzing the TTL temperature and its variability a complex task.

1.3.1 Thermodynamic balance

The zonal mean temperature can be analyzed and understood in a relatively simple theoretical framework. The zonal mean thermodynamic equation (in transformed Eulerian mean (TEM) coordinates (*Andrews et al.*, 1987)) is:

$$\overline{T}_t = -\overline{v}^*\overline{T}_y - \overline{w}^* S + \overline{Q} - e^{z/H}[e^{-z/H}(\overline{v'T'}\frac{\overline{T}_y}{S} + \overline{w'T'})]. \tag{1.1}$$

Here $\overline{T}$ is zonally averaged temperature, ($\overline{v}^*$, $\overline{w}^*$) are meridional and vertical components of the residual meridional circulation, $S = HN^2R$ is a stability parameter with the scale height of $H = 7km$, gas constant $R = 287m^2S^{-2}K^{-1}$, buoyancy frequency N^2, and Q is the zonal mean diabatic heating. The eddy terms in (1.1) are generally small (although not negligible near the tropical tropopause (*Abalos et al.*, 2013; *Randel and Wu*, 2015)), and the $\overline{v}^*$ term is also small in the deep tropics, so that the approximate thermodynamic balance is:

$$\overline{T}_t = -\overline{w}^* S + \overline{Q}. \tag{1.2}$$

In the troposphere, $\overline{Q}$ is mainly linked to large-scale convective heating and radiative cooling, while radiation dominates in the stratosphere (and $\overline{Q}$ is often approximated by a relaxation of the form $\overline{Q} = -\alpha(\overline{T} - \overline{T}_{eq})$, with $\overline{T}_{eq}$ a background equilibrium temperature and α an inverse radiative damping time scale (e.g., *Andrews et al.*, 1987)). Hence, zonal mean temperatures in the tropical tropopause region and above can be primarily understood in terms of (dynamically forced) upwelling $\overline{w}^*$ and the response to radiative effects. Any processes influencing the tropical upwelling, such as convection, tropospheric and stratospheric circulations and wave-mean flow interactions, or the radiative heating rate, e.g., solar irradiance, stratospheric water vapour, ozone and aerosols, should be considered.

1.3.2 Processes influencing its variability

The TTL temperature has seasonal to decadal variations, depending on altitude, depending on which processes dominate on a given time scale.

Fig. 1.4 (top panel) shows that the temperature in the TTL, especially around the tropopause, has a clear annual cycle. In the lower levels of the TTL (upper troposphere), the temperature shows weak seasonal variations and is broadly associated with the distribution of convection, e.g. the Intertropical Convergence Zone (ITCZ) (*Fueglistaler et al.*, 2009). Around the tropopause, the temperature shows a prominent annual cycle, which is mainly determined by the upward motion forced by equatorial and extratropical waves (*Abalos et al.*, 2014; *Randel and Wu*, 2015; *Taguchi*, 2009; *Yulaeva et al.*, 1994) and also influenced by the annual variations of lower stratospheric ozone (*Fueglistaler et al.*, 2011). The upward motion is the vertical component of the Brewer-Dobson circulation (BDC) in the tropics, which then moves poleward and descends at middle and high latitudes (see a recent review by *Butchart*, 2014). As addressed above in section 1.3.1, vertical motion is one key factor in dominating the thermodynamic balance.

Beside the annual cycle, the TTL temperatures also show interannual variations as shown in Fig. 1.4 (bottom panel). Above the tropopause in the tropical lower stratosphere, the temperature is dominated by the Quasi-Biennial Oscillation (QBO) (*Randel and Wu*, 2015). The QBO appears as easterly and westerly wind regimes that propagate down to the lowermost stratosphere, alternating with a variable period of about 28 months. It is the dominant mode of variability throughout the equatorial stratosphere, and has important impacts on the temperature structure as well as the distribution of chemical constituents

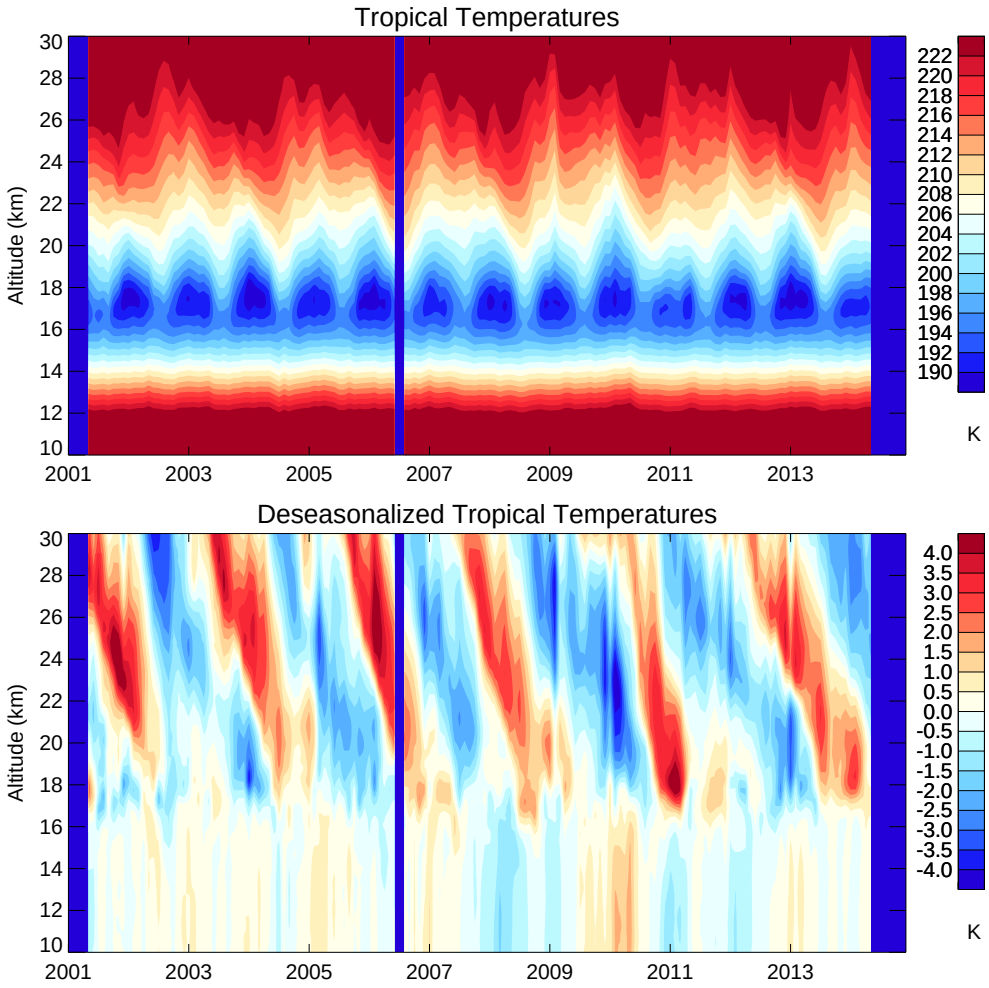

Fig. 1.4 Time-altitude cross section of temperatures in the tropics (10°S-10°N) from the GPS-RO data over the period 2001-2014. (**top**) Monthly time series and (**bottom**) deseasonalized monthly anomalies (defined as the departure of temperatures for a particular month from the long-term monthly mean). The dark blue columns in the early 2001, late 2014 and 2006 are due to the missing data.

like water vapour, methane and ozone (*Baldwin et al.*, 2001). It is mainly driven by upward propagating tropical atmospheric waves like gravity, inertia-gravity, Kelvin and Rossby-gravity waves. The QBO influences the tropical temperature above the tropopause mainly due to the thermal wind balance, which is a balance between temperature and the vertical shear of the zonal winds (*Andrews et al.*, 1987; *Baldwin et al.*, 2001), and also influences the temperature by modulating the upward motion of the BDC (*Flury et al.*, 2013), and the upward propagation of equatorial and extratropical waves (*Simpson et al.*, 2009).

Another interannual feature of the TTL temperature variability, which can be seen from the time series of the temperature anomalies in Fig. 1.5, is the El Niño–Southern Oscillation (ENSO) (*Yulaeva and Wallace*, 1994). ENSO is the leading mode of an empirical orthogonal function (EOF) analysis of global detrended monthly SST anomalies (details of method in *Deser et al.*, 2010). It is a seesaw between warm and cold SST anomalies in the equatorial Pacific with consequences for the regional and global weather and climate. SSTs are anomalously warm in the tropical Pacific ocean during a warm ENSO phase (El Niño), while cold anomalies can be found during a cold ENSO phase (La Niña). ENSO influences the tropical weather and also the extratropics via tropospheric teleconnections, e.g. the atmospheric bridge (*Alexander*, 2013). There seems to be also a stratospheric pathway of ENSO influencing the troposphere as recently summarized from reanalysis data by *Butler et al.* (2014). During ENSO warm phases, the Aleutian low is deepened, and the planetary wave number 1 interferes positively with the climatological wave structure (*Ineson and Scaife*, 2009). The resulting stronger wave forcing in turn leads to a weaker stratospheric polar vortex (*Ayarzagüena et al.*, 2013; *Manzini et al.*, 2006) and more Sudden Stratospheric Warming (SSW) events, which significantly influence the surface weather during winter in the Northern Hemisphere. Beside the tropospheric effects, ENSO also influences the TTL region because it modulates deep convection and extratropical wave propagation (*Calvo et al.*, 2010; *Garfinkel et al.*, 2013a,b; *Randel and Wu*, 2015; *Randel et al.*, 2009; *Scherllin-Pirscher et al.*, 2012; *Simpson et al.*, 2011) and also the upward motion of the BDC (*Oberländer et al.*, 2013) in the tropics.

The TTL temperature also exhibits clear decadal variability (Fig. 1.5). On this time scale, one important influence on the TTL temperature comes from the 11-year solar cycle (e.g. *Gray et al.*, 2010; *SPARC-CCMVal*, 2010). The 11-year solar cycle is the most pronounced variability in observed solar irradiance. Solar variability influences the temperature through direct radiative effects and also indirect effects. Indirect effects include by a "top-down" mechanism through radiative effects on stratospheric ozone and subsequent indirect dynamical effects, or a "bottom-up" mechanism through the long memory of SST response to the solar forcing and the corresponding feedbacks to the atmospheric circulations (e.g., *Meehl et al.*, 2009; *van Loon and Meehl*, 2014). The maximum temperature response occurs in the equatorial upper stratosphere during solar maximum conditions, and a distinct secondary temperature maximum can be found in the equatorial lower stratosphere around 100 hPa (*Gray et al.*, 2010; *SPARC-CCMVal*, 2010).

Another potential driver of decadal to multidecadal TTL variability is the Pacific Decadal Oscillation (PDO). The PDO is the leading EOF of monthly SST anomalies over the North Pacific (*Alexander*, 2013; *Deser et al.*, 2010; *Kamae et al.*, 2015). The PDO SST pattern is

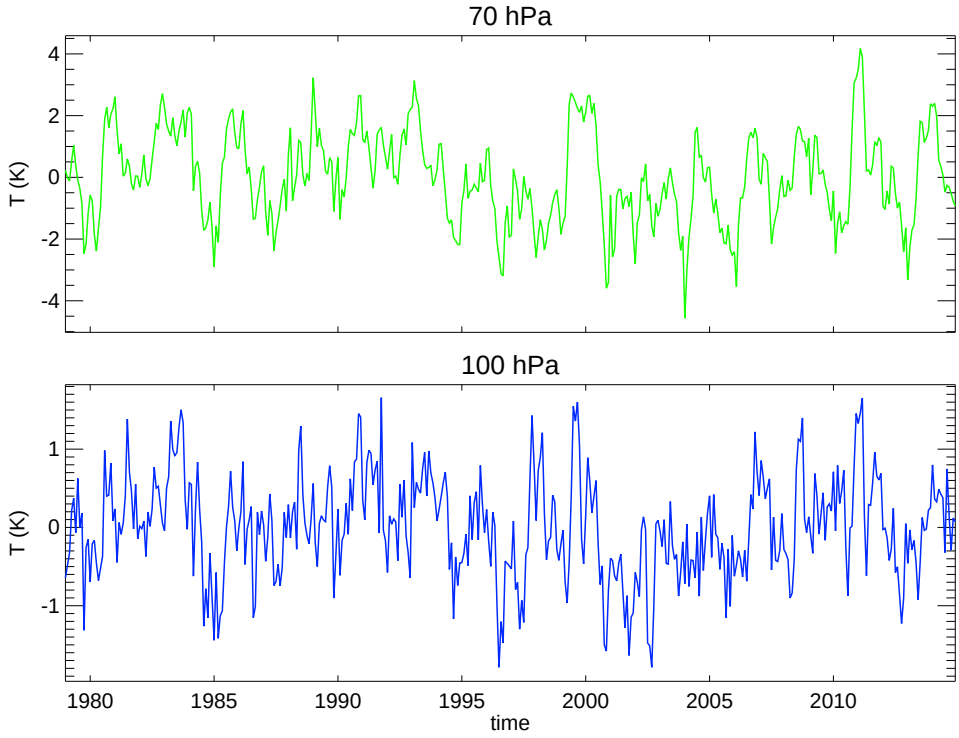

Fig. 1.5 Deseasonalized tropical (10°S-10°N) temperature anomalies at 100 (**bottom**) and 70 (**top**) hPa during 1979-2014, from the Modern Era Retrospective-Analysis for Research and Applications (MERRA) reanalysis data.

similar to that of ENSO, except for the relative weighting between the north and tropical Pacific: for the PDO, SST anomalies in the equatorial eastern Pacific are comparable to those in the North Pacific, whereas they are considerably larger for ENSO (*Deser et al.*, 2010, and references therein). The PDO may influence the TTL temperature similarly to ENSO, but on different time scales. The relative importance of the PDO for decadal to multidecadal TTL variability as well as the possible mechanism are still largely unknown. This is another focus of this thesis.

In addition to the single-factor effects, the processes described above may also be coupled. For example, the 11-year solar cycle can produce ENSO-like SST anomalies in the Pacific

(e.g., *Meehl et al.*, 2009; *van Loon and Meehl*, 2014), and though the mechanism is not clear, a lagged response in SSTs to the solar cycle has been seen in both the North Atlantic (*Gray et al.*, 2013; *Scaife et al.*, 2013; *Thieblemont et al.*, 2015) and the North Pacific (*Hood et al.*, 2013; *Meehl and Arblaster*, 2009; *Roy and Haigh*, 2012) regions. This indicates a potentially delayed solar signal in lower stratospheric water vapour (*Schieferdecker et al.*, 2015).

Another key issue regarding the tropopause temperature is its long-term trends. The National Centers for Environmental Prediction/National Center for Atmospheric Research (NCEP/NCAR) reanalysis data show a significant cooling in tropopause temperatures over the past decades (1981-2010), while the European Center for Medium rage Weather Forecasting (ECMWF) reanalysis data show an opposite signal (*Fueglistaler et al.*, 2013; *SPARC-CCMVal*, 2010; *Xie et al.*, 2014). Tropical tropopause temperature trends from radiosondes are highly uncertain because the radiosonde datasets do not have global coverage and are constructed by different approaches (*Wang et al.*, 2012), though the uncertainties and discrepancies may also be due to the decadal to multidecadal variability described above. For example, the TTL temperature in the MERRA reanalysis decreased during 1979-2000, but increased after 2001 (Fig. 1.5). Thus decadal to multidecadal variability increases uncertainty and reduces the statistical significance of potential long-term trends.

This thesis revisits processes described above influencing TTL temperatures, using both observations and a unique set of model simulations, which includes both an interactive ocean and an interactive chemistry module and reaches up to the thermosphere. In particular, decadal to multidecadal variability of the TTL temperature, as well as its connection to SSTs, will be investigated with the goal of improving our understanding of the recent TTL temperature variability.

1.3.3 Lower stratospheric water vapour

Stratospheric water vapour influences chemistry, radiation and circulation in the stratosphere, and is also an important driver of surface climate. Water vapour is the source of ozone-destroying HOx species, and therefore influences ozone depletion and associated chemical and dynamical processes in the stratosphere (*Randel and Jensen*, 2013; *Tian et al.*, 2009). As a powerful greenhouse gas, enhanced stratospheric water vapour content will cool the upper stratosphere through thermal emission of infrared (IR) wavelengths, while warming the troposphere through absorption of IR radiation from the troposphere. It cools the surface by reducing shortwave radiation arrived to the surface slightly, but strongly warms the surface by absorbing the upward and emitting the downward longwave radiation at the same time, and contributes to a net warming at the surface (Fig. 1.6). As also illustrated in Fig. 1.6, water vapour exhibits its maximal variations at the lower stratosphere. By these mechanisms, trends

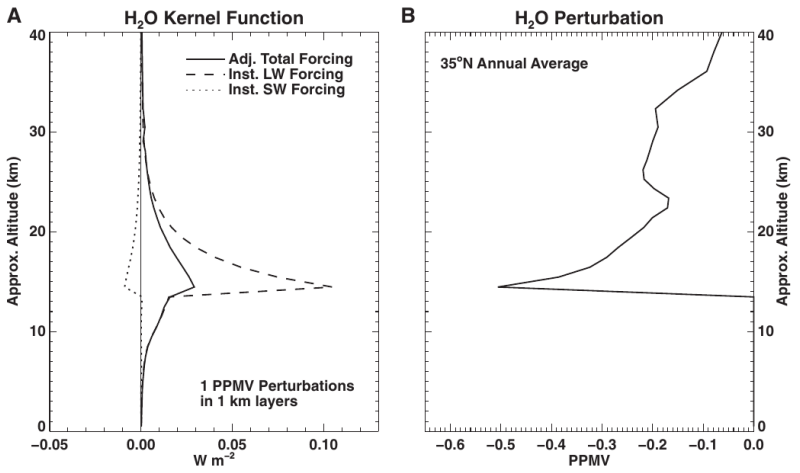

Fig. 1.6 Effect of stratospheric water vapour changes on radiative forcing of surface climate based on detailed line-by-line calculations. (A) Instantaneous longwave (LW) and instantaneous shortwave (SW) radiative forcing, along with the adjusted net total forcing (based on fixed-dynamical heating) versus altitude at 35°N obtained for a uniform change of 1 ppmv in 1-km layers using a line-by-line radiative transfer model; the largest sensitivity occurs close to the tropopause. **(B)**, The observed post-2000 water vapour decrease at 35°N, showing that the largest changes occurred in the most sensitive region. From *Solomon et al.* (2010, their Figure 2).

in lower stratospheric water vapour content significantly impact global surface temperatures (*Dessler et al.*, 2013; *Solomon et al.*, 2010).

Lower stratospheric water vapour is mainly controlled by the CPT, since it freeze-dries while crossing the tropopause (*Fueglistaler et al.*, 2009; *Randel and Jensen*, 2013). Like long-term trends in the tropical tropopause temperature, long-term trends in lower stratosphere water vapour are also not well quantified. Balloon measurements over Boulder, Colorado (USA) show an average increase of water vapour in the lower stratosphere from 1980 to 2010 (*Hurst et al.*, 2011), though other analyses have not found evidence for a long-term trend (*Hegglin et al.*, 2014). Further, clear decadal variability in stratospheric water vapour has been seen in both models and observations (*Dessler et al.*, 2014; *Fueglistaler et al.*, 2013; *Hurst et al.*, 2011). This decadal variability in lower stratospheric water vapour has been linked (with a 2-year lag) to the 11-year solar cycle (*Schieferdecker et al.*, 2015), though the mechanism is still unclear. While a possible lagged response in SSTs to the solar cycle has been discussed previously (*Gray et al.*, 2013; *Hood et al.*, 2013; *Meehl and Arblaster*, 2009; *Roy and Haigh*, 2012; *Scaife et al.*, 2013; *Thieblemont et al.*, 2015), this discovery reopened the debate of "top-down" versus "bottom-up" mechanism discussed in section 1.3.2.

The spatial distribution of lower stratospheric water vapour is also important, since it is strongly controlled by the spatial structure of tropopause temperature, and therefore a useful indicator of the lower stratospheric response to the surface (*Fu*, 2013; *Garfinkel et al.*, 2013a). As described above, both the tropopause temperature and lower stratospheric water vapour trends have significant zonal asymmetries (*Fu*, 2013; *Garfinkel et al.*, 2013a), which implies that the zonal mean may not be the best indicator of trends, especially when quantifying the relative contribution due to different processes, e.g. patterns in SST variations.

With respect to both the zonal mean and the spatial pattern, this thesis explains recent interannual to decadal variability of lower stratospheric water vapour. Special attention is paid to its connection to the 11-year solar cycle and SSTs.

1.4 TTL representation in climate models

Climate models are the primary tools available for investigating the response of the climate system to various forcings, for making climate predictions on seasonal to decadal time scales and for making projections of future climate over the coming century and beyond (*Flato et al.*, 2014). An advantage of models over observations is that we can run a number of realizations, and therefore increase the amount of data available for statistical analysis. Coupled Chemistry Climate Models (CCMs), including a fully resolved stratosphere with interactive radiative, chemical and dynamical processes, are state-of-the-art models for investigating the variability and physical characteristics of both the stratosphere and the TTL (*Eyring et al.*, 2006; *Morgenstern et al.*, 2010; *SPARC-CCMVal*, 2010). Many studies have used CCMs to study the processes in the stratosphere and the TTL, especially the responses and feedbacks to climate change (*Butchart et al.*, 2010; *Eyring et al.*, 2006, 2007; *Gettelman et al.*, 2009, 2010; *Li et al.*, 2008; *SPARC-CCMVal*, 2010). CCMs are able to reproduce the climatology, indicating both the annual cycle and interannual anomalies, of tropopause temperature, pressure, water vapour and ozone. Some common deficiencies, e.g., a large (10 K) spread in annual mean tropical CPTs and the annual cycle of water vapour in the lower stratosphere is shifted early, exist in many models (*Gettelman et al.*, 2009; *SPARC-CCMVal*, 2010). These deficiencies are partly due to the coarse vertical resolution of CCMs, which is specially investigated in this thesis. As an important driver, SSTs were prescribed in most of CCM simulations in Stratospheric Processes and their Role in Climate (SPARC) Chemistry-Climate Model Validation Activity (CCMVal-2) (*SPARC-CCMVal*, 2010), since the interactive chemistry is computationally expensive. However, without an interactive ocean, the internal damping of anomalies due to surface heat fluxes is enhanced and therefore reduces the variance in the atmosphere (e.g. *Barsugli and Battisti*, 1998; *Hansen et al.*,

2014). In this thesis, a set of model simulations with both fully-coupled ocean and interactive chemistry are performed to see the possible improvements for representing of the TTL.

1.4.1 TIL structure in Chemistry Climate Models (CCMs)

As mentioned above, the TTL region is affected by complex physical processes, including convection, cloud and trace gases related radiation, and large- and small-scale circulations (*Fueglistaler et al.*, 2009; *Randel and Jensen*, 2013). This makes comprehensive modeling of this region a daunting challenge (*Randel and Jensen*, 2013). It has been found, for example, that SPARC CCMVal-2 (*SPARC-CCMVal*, 2010) CCMs may not be able to quantitatively reproduce the structure of the observed TIL, due to their generally relatively coarse vertical resolution, which is about 1 km in the Upper Troposphere and Lower Stratosphere (UTLS). Such coarse vertical resolutions makes it difficult to adequately describe small-scale waves, such as Kelvin and gravity waves, which contribute to the detailed thermal structure in the TTL. In addition, the fast transition processes between the stratosphere and troposphere can not be well captured, which means that the subsequent radiative effects by the ozone and water vapour anomalies are also not fully represented.

1.4.2 TTL interannual variability and long-term trends in CCMs

Though only a few climate models are currently able to internally generate a QBO (because of the coarse vertical resolution of most models and poor resolution of small-scale waves), climate models may still capture QBO-influenced variations by simulating a so-called nudged QBO (*Baldwin et al.*, 2001; *Hansen et al.*, 2013; *Matthes et al.*, 2010; *Tian et al.*, 2006). Climate models, with a fully-coupled ocean or prescribed SSTs have also been used to estimate ENSO effects on both the TTL and the whole stratosphere (*Ayarzagüena et al.*, 2013; *Cagnazzo et al.*, 2009; *Calvo et al.*, 2010; *SPARC-CCMVal*, 2010). ENSO influences interannual variations of the lower stratospheric temperature (*Randel and Wu*, 2015; *Scherllin-Pirscher et al.*, 2012), water vapour (*Garfinkel et al.*, 2013b; *Xie et al.*, 2012) as well as dynamical circulations (*Calvo et al.*, 2010; *Manzini et al.*, 2006; *Simpson et al.*, 2011). Decadal variability in TTL temperatures related to 11-year solar cycle has also been investigated (*Austin et al.*, 2008; *Matthes et al.*, 2010; *SPARC-CCMVal*, 2010). The direct solar signal in the tropical upper stratosphere is acceptably represented in CCMs. However, larger differences in the vertical structure of the solar signal among the different CCMs as well as among different observational data sets occur below 10 hPa (*Gray et al.*, 2010; *Matthes et al.*, 2013; *SPARC-CCMVal*, 2010). Historical trends in tropopause pressure from reanalysis products can be generally simulated by CCMs. However, the long-term TTL

temperature trends from models have been found to be inconsistent with either observations or between different CCMs (*Gettelman et al.*, 2009; *Kim et al.*, 2013). This discrepancy is seen in lower stratospheric water vapour as well.

1.4.3 Importance of vertical resolution in climate models

High horizontal resolution is an important factor in the performance of climate models and has been investigated by many studies (e.g., *Jung et al.*, 2012; *Roeckner et al.*, 2006; *Staniforth and Thuburn*, 2012; *Zhou et al.*, 2001). Vertical resolution is also important and influences both the tropospheric and stratospheric temperature and dynamics (e.g. *Rind et al.*, 2007; *Roeckner et al.*, 2006). While the horizontal resolution of climate models has significantly increased during the last decade, similar changes were not accompanied in vertical resolution (*Richter et al.*, 2014a). Recently, as more attention has been given to the upper atmosphere, the interest in the role of vertical resolution in climate models has grown (e.g. *Bunzel and Schmidt*, 2013; *Richter et al.*, 2014a,b). The vertical resolution is important for a climate model to well simulate the interactions between the troposphere and the upper atmosphere; for example, it influences how a model simulates wave propagation from the troposphere to upper atmosphere and therefore is essential for a model to generate a realistic QBO (*Baldwin et al.*, 2001; *Bunzel and Schmidt*, 2013; *Giorgetta et al.*, 2002; *Richter et al.*, 2014b; *Xue et al.*, 2012). Well-reproduced wave activities and a realistic QBO in turn improve the simulation of temperature and mixing processes in the TTL (*Richter et al.*, 2014a).

1.4.4 The CESM-WACCM model with high vertical resolution

NCAR's Community Earth System Model (CESM) model (version 1.0 in this study), which is a fully coupled model system, including interactive ocean (POP2), land (CLM4), sea ice (CICE) and atmosphere (CAM/WACCM) model components, is used in this study. The Whole Atmosphere Community Climate Model (WACCM) is employed as atmospheric component. WACCM (version 4) is a CCM with detailed middle atmospheric chemistry and dynamics, extending from the surface to about 140 km (*Garcia et al.*, 2007; *Marsh et al.*, 2013). All simulations use a horizontal resolution of $1.9° \times 2.5°$(latitude $\times$ longitude) for the atmosphere and approximately 1 degree for the ocean. The standard version (W_L66) has 66 vertical levels, which means about 1 km vertical resolution in the TTL and in the lower stratosphere.

To better capture the fine-scale thermal structure of the atmosphere (i.e. the TIL) and to accurately describe the associated physical processes, several previous studies have used a

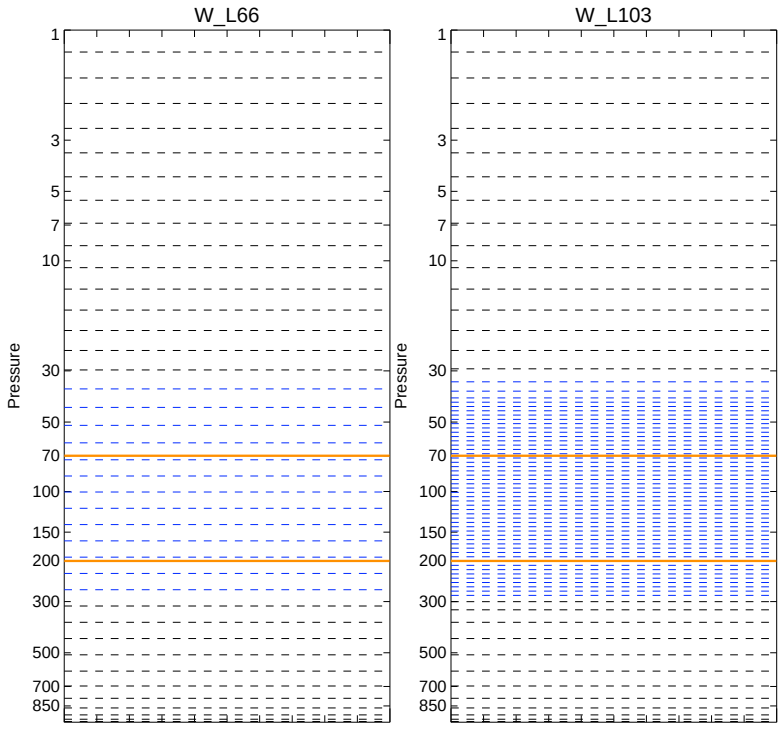

Fig. 1.7 Vertical levels in the standard WACCM model (W_L66, left) and WACCM with finer vertical resolutions (W_L103, right). The WACCM model top is at 10^{-6} *hPa*, only differences (blue area) until 1 *hPa* are shown to highlight the TTL (marked by red thick lines).

special high vertical resolution version (W_L103) of NCAR's WACCM model (*Gettelman and Birner*, 2007; *Gettelman et al.*, 2009). W_L103 has 103 vertical levels, with increased vertical resolution (about 300 m) in the UTLS (300-30 hPa), but the same vertical resolution as the W_L66 (Fig. 1.7). Evident improvements in the high vertical resolution version of WACCM include a better TIL structure (e.g., *Gettelman and Birner*, 2007; *Gettelman et al.*, 2009), though more detailed investigations of, for example, the detailed structure of the TIL and different scales of variability, have not yet been done. This thesis use this high vertical resolution WACCM model to further investigate the TTL characteristics as well as its interannual to decadal variability.

1.5 Scientific questions in this thesis

This thesis focuses on the detailed thermal structure of the TTL, its recent variability, and its influencing processes in different time-scale, such as the QBO, ENSO, the 11-year solar cycle, and the PDO. The following questions will be addressed in the coming chapters.

- **What is the recent TTL temperature variability measured by the GPS-RO data? How well can the WACCM model capture this variability?** (Chapter 2)
- **How do different natural and anthropogenic factors contribute to the recent TTL temperature variability? How important is the vertical resolution of a climate model for reproducing the TTL variability?** (Chapter 3)
- **How important is decadal to multidecadal variability in estimating the long-term trend of the tropical tropopause temperature, and which processes control it?** (Chapter 4)
- **Can we explain the recent variability in lower stratospheric water vapour? Which processes determine its decadal to multidecadal variability?** (Chapter 5)

This thesis will answer these questions using both observational data and a series of climate simulations with NCAR's CESM model, employing the WACCM as atmospheric component. The simulations are unique, since they include both an interactive ocean and an interactive chemistry module, reach up to the thermosphere and have relative long-term integration of about 150 years. Specified effects of main climate drivers, i.e., solar variability, SSTs, QBO and greenhouse gases, are separately simulated by switching on/off the corresponding factor in model configurations. We also perform simulations with a finer vertical resolution, with 103 vertical levels and about 300 m vertical resolution in the TTL and lower stratosphere (*Gettelman and Birner*, 2007). Details of the model and the setup of the simulations can be found in the respective chapters of this thesis.

The recent TTL temperature variability is investigated in Chapter 2, and Chapter 3 attributes this TTL variability to both natural and anthropogenic factors. A link between decadal to multidecadal variability of the tropical tropopause temperature and sea surface temperatures is addressed in Chapter 4. Chapter 5 explains the recent variability in lower stratospheric water vapour. Conclusions and discussions are given in Chapter 6.

Chapter 2

Recent variability of the Tropical Tropopause Inversion Layer

This chapter provides the first investigation of the long-term variability of tropical TIL over a decade, with GPS-RO data and WACCM model simulations. Over the past decade (2001-2011) the data show an increase of 0.8 K in tropical tropopause temperatures and a decrease of 0.4 K in the strength of the tropical TIL. The vertical temperature gradient has therefore declined, and static stability above the tropopause has weakened. WACCM simulations with finer vertical resolution improve the TIL structure and variability as compared with the standard WACCM runs. Model simulations show that the increased tropopause temperatures and the weaker tropopause inversion layer are related to weakened upwelling, i.e. weakened BDC in the tropics.

This chapter is a reprint of:

Wang, W., Matthes, K., Schmidt, T., and Neef, L.: Recent variability of the tropical tropopause inversion layer, Geophys. Res. Lett., 40, 6308–6313, doi:10.1002/2013GL058350, ulr:http://dx.doi.org/10.1002/2013GL058350, 2013.

Author contributions:

- W. Wang performed all the simulations, did all the analyses, produced all figures and wrote the manuscript.
- K. Matthes initiated the model experiments, contributed to ideas and discussions on the analysis and paper writing. T. Schmidt provided the GPS-RO data, contributed with discussions and comments on the manuscript. L. Neef contributed to discussions and comments on the manuscript.

Chapter 3

Quantifying contributions to the recent temperature variability in the tropical tropopause layer

This chapter attributes the recent TTL variability, as shown in Chapter 2, to natural and anthropogenic factors, such as solar variability, SSTs, the QBO, stratospheric aerosols, GHGs, as well as the dependence on the vertical resolution in the model.

A number of sensitivity simulations with NCAR's CESM-WACCM model were performed and analyzed to specifically quantify the factor contributions by switching on/off the corresponding factors. The results indicate that the recent TTL warming is mainly due to internal variability, i.e. the QBO and tropical SSTs, and partly caused by stratospheric aerosols. The vertical resolution can also strongly influence the TTL temperature response in addition to variability in the QBO and SSTs.

This chapter is a reprint of:

Wang, W., Matthes, K., and Schmidt, T.: Quantifying contributions to the recent temperature variability in the tropical tropopause layer, Atmos. Chem. Phys., 15, 5815-5826, doi:10.5194/acp-15-5815-2015, 2015.

Author contributions:

- W. Wang performed several simulations, did all the analyses, produced all figures and wrote the manuscript.
- K. Matthes initiated the model experiments, contributed to ideas and discussions on the analysis and paper writing. T. Schmidt provided the GPS-RO data, contributed with discussions and comments on the manuscript.

Atmos. Chem. Phys., 15, 5815–5826, 2015
www.atmos-chem-phys.net/15/5815/2015/
doi:10.5194/acp-15-5815-2015

Atmospheric Chemistry and Physics Open Access

Quantifying contributions to the recent temperature variability in the tropical tropopause layer

W. Wang[1,2], **K. Matthes**[2,3], **and T. Schmidt**[4]

[1]Freie Universität Berlin, Institut für Meteorologie, Berlin, Germany
[2]GEOMAR Helmholtz-Zentrum für Ozeanforschung Kiel, Kiel, Germany
[3]Christian-Albrechts Universität zu Kiel, Kiel, Germany
[4]Helmholtz Zentrum Potsdam, Deutsches GeoForschungsZentrum (GFZ), Potsdam, Germany

Correspondence to: W. Wang (wuke.wang@fu-berlin.de)

Received: 1 August 2014 – Published in Atmos. Chem. Phys. Discuss.: 28 August 2014
Revised: 22 April 2015 – Accepted: 8 May 2015 – Published: 26 May 2015

Abstract. The recently observed variability in the tropical tropopause layer (TTL), which features a warming of 0.9 K over the past decade (2001–2011), is investigated with a number of sensitivity experiments from simulations with NCAR's CESM-WACCM chemistry–climate model. The experiments have been designed to specifically quantify the contributions from natural as well as anthropogenic factors, such as solar variability (Solar), sea surface temperatures (SSTs), the quasi-biennial oscillation (QBO), stratospheric aerosols (Aerosol), greenhouse gases (GHGs) and the dependence on the vertical resolution in the model. The results show that, in the TTL from 2001 through 2011, a cooling in tropical SSTs leads to a weakening of tropical upwelling around the tropical tropopause and hence relative downwelling and adiabatic warming of 0.3 K decade^{-1}; stronger QBO westerlies result in a 0.2 K decade^{-1} warming; increasing aerosols in the lower stratosphere lead to a 0.2 K decade^{-1} warming; a prolonged solar minimum contributes about 0.2 K decade^{-1} to a cooling; and increased GHGs have no significant influence. Considering all the factors mentioned above, we compute a net 0.5 K decade^{-1} warming, which is less than the observed 0.9 K decade^{-1} warming over the past decade in the TTL. Two simulations with different vertical resolution show that, with higher vertical resolution, an extra 0.8 K decade^{-1} warming can be simulated through the last decade compared with results from the "standard" low vertical resolution simulation. Model results indicate that the recent warming in the TTL is partly caused by stratospheric aerosols and mainly due to internal variability, i.e. the QBO and tropical SSTs. The vertical resolution can also strongly influence the TTL temperature response in addition to variability in the QBO and SSTs.

1 Introduction

The tropical tropopause layer (TTL) is the transition layer from the upper troposphere to the lower stratosphere in the tropics, within which the air has distinct properties of both the troposphere and the stratosphere. The vertical range of the TTL depends on how it is defined, i.e. it can be a shallower layer between 14 and 18.5 km (Fueglistaler et al., 2009) or a deeper layer of about 12–19 km (Gettelman and Forster, 2002; SPARC-CCMVal, 2010, chapter 7). As a key region for the stratosphere–troposphere coupling, the TTL acts like a "gate" for air entering into the stratosphere from the tropical troposphere. The temperature in the TTL is determined by the combined influences of latent heat release, thermally as well as dynamically driven vertical motion and radiative cooling (Gettelman and Forster, 2002; Fueglistaler et al., 2009; Grise and Thompson, 2013). The thermal structure, static stability and zonal winds in the TTL affect the two-way interaction between the troposphere and the stratosphere (Flury et al., 2013; Simpson et al., 2009) as well as the surface climate, since the relative minimum temperature (usually known as the cold point tropopause) subsequently influences the radiation and water vapour budget (Andrews, 2010). The TTL reacts particularly sensitively to anthropogenically induced radiative, chemical and dynamical forc-

ings of the climate system and hence is a useful indicator for climate change (Fueglistaler et al., 2009).

Over the past decade, a remarkable warming has been captured by Global Positioning System Radio Occultation (GPS-RO) data in the TTL region (Schmidt et al., 2010; Wang et al., 2013). This might indicate a climate change signal, with possible important impacts on stratospheric climate: e.g. tropical tropopause temperatures dominate the amount of water vapour entering the stratosphere (Dessler et al., 2013, 2014; Solomon et al., 2010; Gettelman et al., 2009; Randel and Jensen, 2013). So far a long-term cooling in the lower stratosphere has been reported from the 1970s to 2000, although there are large differences between different data sets (Randel et al., 2009; Wang et al., 2012; Fueglistaler et al., 2013). The exact reason for the recent warming is therefore of great interest. An interesting issue is also whether this warming will continue or change in sign in the future and how well climate models can reproduce such a strong warming over 1 decade or longer time periods.

Based on model simulations, Wang et al. (2013) suggested that the warming around the tropical tropopause could be a result of a weaker tropical upwelling, which implies a weakening of the Brewer–Dobson circulation (BDC). However, the strengthening or weakening of the BDC is still under debate (Butchart, 2014, and references therein). Results from observations indicate that the BDC may have slightly decelerated (Engel et al., 2009; Stiller et al., 2012), while estimates from a number of chemistry–climate models (CCMs) show in contrast a strengthening of the BDC (Butchart et al., 2010; Li et al., 2008; Butchart, 2014). The reason for the discrepancy between observed and modelled BDC changes, as well as the mechanisms of the BDC response to climate change, is still under discussion (Oberländer et al., 2013; Shepherd and McLandress, 2011). The trends in the BDC may be different in different branches of the BDC (Lin and Fu, 2013; Oberländer et al., 2013). Bunzel and Schmidt (2013) show that the model configuration, i.e. the vertical resolution and the vertical extent of the model, can also impact trends in the BDC.

There are a number of other natural and anthropogenic factors besides the BDC which influence radiative, chemical and dynamical processes in the TTL. One prominent candidate for natural variability is the sun, which provides the energy source of the climate system. The 11-year solar cycle is the most prominent natural variation on the decadal timescale (Gray et al., 2010). Solar variability influences the temperature directly through radiative effects and indirectly through radiative effects on ozone and dynamical effects. The maximum response in temperature occurs in the equatorial upper stratosphere during solar maximum conditions, and a distinct secondary temperature maximum can be found in the equatorial lower stratosphere around 100 hPa (SPARC-CCMVal, 2010; Gray et al., 2010).

Sea surface temperatures (SSTs) also influence the TTL by affecting the dynamical conditions and subsequently the propagation of atmospheric waves and hence the circulation. Increasing tropical SSTs can enhance the BDC, which in turn cools the tropical lower stratosphere through enhanced upwelling (Grise and Thompson, 2012, 2013; Oberländer et al., 2013). The quasi-biennial oscillation (QBO) is the dominant mode of variability throughout the equatorial stratosphere and has important impacts on the temperature structure as well as the distribution of chemical constituents like water vapour, methane and ozone (Baldwin et al., 2001). Beside the switch between easterlies and westerlies with a period of about 28 months, the QBO undergoes some cycle-to-cycle variability, e.g. variations in period and amplitude and shifts to westerlies or easterlies, which may influence the long-term variability in the TTL (Kawatani and Hamilton, 2013). Stratospheric aerosols absorb outgoing long-wave radiation and lead to additional heating in the lower stratosphere, which maximizes around 20 km (Solomon et al., 2011; SPARC-CCMVal, 2010, chapter 8).

While greenhouse gases (GHGs) warm the troposphere, they cool the stratosphere at the same time by releasing more radiation into space. Warming of the troposphere and cooling of the stratosphere affect the temperature in the TTL directly, as well as indirectly, by changing chemical trace gas distributions and wave activities (SPARC-CCMVal, 2010).

In climate models, a sufficient high vertical resolution is important in order for models to correctly represent dynamical processes, such as wave propagation into the stratosphere and wave–mean flow interactions. High vertical resolution is also important to generate a self-consistent QBO (Richter et al., 2014). Meanwhile, vertical resolution is essential for a proper representation of the thermal structure in the model: e.g. models with coarse vertical resolution can not simulate the tropopause inversion layer (a narrow band of temperature inversion above the tropopause associated with a region of enhanced static stability) well (Wang et al., 2013; SPARC-CCMVal, 2010, chapter 7). Coarse vertical resolution is also still a problem for analysing the effects of El-Niño Southern Oscillation (ENSO) and the QBO onto the tropical tropopause (Zhou et al., 2001; SPARC-CCMVal, 2010, chapter 7).

In this study we use a series of simulations with NCAR's Community Earth System Model (CESM) model (Marsh et al., 2013) to quantify the contributions of the above discussed factors – Solar, SSTs, QBO, Aerosol and GHGs – to the recently observed variability in the TTL.

The details of the observational data, the model and numerical experiments, as well as a description of our methods, are given in Sect. 2. The observed temperature variability in the TTL and the contributions of various factors to the recent TTL variability are addressed in Sect. 3. Section 4 focuses on the importance of the vertical resolution in one climate model. The summary and discussion are presented in Sect. 5.

Table 1. Overview of fully coupled CESM-WACCM simulations (1955–2099).

Simulations	Natural forcings	GHGs
Natural	All natural forcings, including transit solar variability, fully coupled ocean, prescribed volcanic aerosols and nudged QBO	Fixed GHGs to 1960s state
SolarMean	Like the Natural run but with fixed solar radiation	Fixed
FixedSST	Like the Natural run but with fixed SSTs	Fixed
NOQBO	Like the Natural run but without QBO nudging	Fixed
RCP85	Like the Natural run	RCP8.5 scenario

2 Model simulations and method description

2.1 Fully coupled CESM-WACCM simulations

The model used here is NCAR's CESM version 1.0. CESM is a fully coupled model system, including an interactive ocean (POP2), land (CLM4), sea ice (CICE) and atmosphere (CAM/WACCM) component (Marsh et al., 2013). As the atmospheric component we use the Whole Atmosphere Community Climate Model (WACCM), version 4. WACCM4 is a CCM with detailed middle atmospheric chemistry and a finite volume dynamical core, extending from the surface to about 140 km (Marsh et al., 2013). The standard version has 66 (W_L66) vertical levels, which means about 1 km vertical resolution in the TTL and in the lower stratosphere. All simulations use a horizontal resolution of $1.9^\circ \times 2.5^\circ$ (latitude $\times$ longitude) for the atmosphere and approximately 1° for the ocean.

Table 1 gives an overview of all coupled CESM simulations. A control run was performed from 1955 to 2099 (Natural run hereafter) with all natural forcing including spectrally resolved solar variability (Lean et al., 2005), a fully coupled ocean, volcanic aerosols following the SPARC (Stratospheric Processes and their Role in Climate) CCMVal (Chemistry–Climate Model Validation) REF-B2 scenario recommendations (see details in SPARC-CCMVal, 2010) and a nudged QBO. The QBO is nudged by relaxing the modelled tropical zonal winds to observations between 22° S and N, using a Gaussian weighting function with a half width of 10° decaying latitudinally from the equator. Full vertical relaxation extends from 86 to 4 hPa, which is half the strength of the level below and above this range and 0 for all other levels (see details in Matthes et al., 2010; Hansen et al., 2013). The QBO forcing time series in CESM is determined from the observed climatology of 1953–2004 via filtered spectral decomposition of that climatology. This gives a set of Fourier coefficients that can be expanded for any day and year in the past and the future. Anthropogenic forcings like GHGs and ozone-depleting substances (ODSs) are set to constant 1960s conditions. Using the Natural run as a reference, a series of four sensitivity experiments were performed by systematically switching on or off several factors. The SolarMean run uses constant solar cycle values averaged over the past four observed solar cycles. The FixedSST run uses monthly varying climatological SSTs calculated from the Natural run and therefore neglects variability from varying SSTs such as ENSO. In the NOQBO run the QBO nudging has been switched off which means weak zonal mean easterly winds develop in the tropical stratosphere. An additional simulation, RCP85, uses the same forcings as the Natural run but in addition includes increases in anthropogenic GHGs and ODSs forcings. These forcings are based on observations from 1955 to 2005, after which they follow the representative concentration pathways (RCPs) RCP8.5 scenario (Meinshausen et al., 2011).

2.2 WACCM atmospheric stand-alone simulations

Instead of using the fully coupled CESM-WACCM version, WACCM can be integrated in an atmospheric stand-alone configuration with prescribed SSTs and sea ice. Beside the standard version with 66 vertical levels (W_L66), we have also performed simulations with a finer vertical resolution, with 103 vertical levels and about 300 m vertical resolution in the TTL and lower stratosphere (W_L103) (Gettelman and Birner, 2007; Wang et al., 2013).

With the atmospheric stand-alone version, an ensemble of three experiments was performed over the recent decade 2001–2010 with both WACCM versions (W_L66, W_L103) (see Table 2). Observed SSTs and spectrally resolved solar fluxes were used to produce the most realistic simulations of atmospheric variability over the past decade (2001–2010). The QBO is nudged using the same method as in the fully coupled runs discussed above. GHGs and ODSs are based on observations for the first 5 years (2001–2005) and then follow the IPCC RCP4.5 scenario for the next 5 years (2005–2010), since no observational data were available when the simulations were started. Atmospheric aerosols were relatively constant between 2001 and 2010 since no strong volcanic eruptions occurred and are the same as in the CESM-WACCM runs described above. All the forcings considered in this study are available from the CESM model input data repository (https://svn-ccsm-inputdata.cgd.ucar.edu/trunk/inputdata/). An additional run (W_Aerosol) was performed using the W_L103 version with more realistic observed stratospheric aerosol forcing from the Chemistry-Climate Model Initiative (CCMI, http://www.met.reading.ac.uk/ccmi/).

Table 2. Overview of WACCM atmospheric stand-alone simulations (2001–2010).

Simulations	Number of simulations	Vertical levels	Forcings	Stratospheric aerosols
W_L103	3	103	Observed solar variability and SSTs, nudged QBO, GHGs in RCP4.5 scenario	Volcanic aerosols from CCMVal-2
W_L66	3	66	As W_L103	As W_L103
W_Aerosol	1	103	As W_L103	Stratospheric aerosols from CCMI

2.3 Estimation of factor contributions

For a pair of reference and single-factor runs (e.g. Natural and SolarMean), all configuration and drivers are the same except for the long-term variability of the respective factor (e.g. Solar). Temperature differences $T_{\text{diff}}(x,t)$ between the reference and single-factor runs (e.g. Natural – SolarMean) can be estimated by a linear regression:

$$T_{\text{est}}(x,t) = c(x)X(t), \tag{1}$$

where $T_{\text{est}}(x,t)$ is an estimate of $T_{\text{diff}}(x,t)$ at each grid point (x) and each simulation time (t). $X(t)$ is the time series of the respective factor (e.g. Solar) and $c(x)$ are the coefficients of that factor at each grid point.

Then the contributions of that factor to the recent warming in the TTL can be estimated as

$$T_{\text{fac}}(x) = c(x)b_{\text{fac}}, \tag{2}$$

where $T_{\text{fac}}(x)$ represents the factor contribution to the recent temperature trend, $c(x)$ are the coefficients and b_{fac} is the observed linear trend of that factor during 2001–2011 (Fig. 1).

The standard error (SE) can be used to estimate the uncertainty of the regressed coefficients $c(x)$, which is defined by

$$(\text{SE})^2 = \frac{\sum_{t=1}^{n} e_t^2}{(n_{\text{eff}}-2)\sum_{t=1}^{n}(X_t-\overline{X})^2}, \tag{3}$$

where n is the sample size, $e = T_{\text{diff}} - T_{\text{est}}$ are the residuals and $\overline{X}$ is the mean value. n_{eff} is the effective number of degrees of freedom, with consideration of the effect of autocorrelation, which is determined by

$$n_{\text{eff}} = n\frac{1-r_{\text{a}}}{1+r_{\text{a}}}, \tag{4}$$

where r_{a} is the lag-1 autocorrelation coefficient (Wigley, 2006).

For the estimated coefficients c, the test statistics

$$t\_\text{test} = \frac{c}{\text{SE}} \tag{5}$$

has the Student's t distribution with $n_{\text{eff}} - 2$ degrees of freedom.

Beside the regressions described above, the Pearson's correlations (r) between temperature differences (T_{diff}) and the respective factor (X) were also estimated. The test statistics

$$t\_\text{test} = r\sqrt{\frac{n_{\text{eff}}-2}{1-r^2}} \tag{6}$$

has the Student's t distribution with $n_{\text{eff}} - 2$ degrees of freedom, and the effective number of degrees of freedom can be estimated by

$$\frac{1}{n_{\text{eff}}} = \frac{1}{n} + \frac{2}{n}r_{\text{a1}}r_{\text{a2}}, \tag{7}$$

where r_{a1}, r_{a2} are the lag-1 autocorrelation coefficients of the two time series in calculating the Pearson's correlation respectively.

Such regressions, correlations and 11-year trend estimations were applied to all factors, i.e. Solar, SSTs, QBO, GHGs and stratospheric aerosols.

Special attention is given to the region 20° S–20° N latitude and 16–21 km height, which is mainly the observed warming area in the TTL (see below). Hereafter, we use the average trend over this area to discuss the exact contribution of every factor to the temperature trend in the TTL.

2.4 Forcings in observations and model simulations

Figure 1 shows the time series of both natural and anthropogenic forcings over past and future decades in observations (black) and model experiments (blue). Observed linear trends during 2001–2011 are highlighted with straight lines.

Observations of the solar variability show that the total solar irradiance (TSI) exhibits a clear 11-year solar cycle variation of about 1 W m^{-2} between sunspot minimum (S_{min}) and sunspot maximum (S_{max}) in the past (Gray et al., 2010). The future projection in the Natural run is a repetition of the last four observed solar cycles (Fig. 1a, blue line). With a delayed and smaller amplitude return to maximum conditions, the observed TSI significantly (over 95 %) decreased during 2001–2011 (Fig. 1a, straight black line).

Figure 1b shows the variability of tropical (20° S–20° N) SSTs for the last 5 decades from observations (Hadley Center Updates and supplementary information available from http://www.metoffice.gov.uk/hadobs/hadisst, black lines) and up to 2099 from the Natural coupled CESM-WACCM model ex-

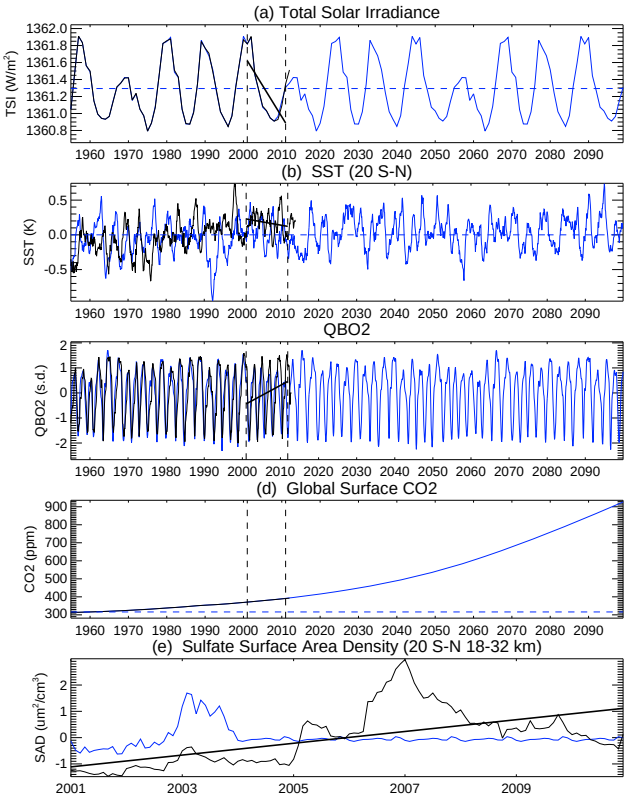

Figure 1. Time series of forcing data sets used for the simulations from 1955 through 2099. **(a)** TSI from observations (black), Natural (solid blue) and SolarMean (dashed blue) runs. **(b)** SST anomalies from HadISSTs (black), Natural (solid blue) and FixedSST (dashed blue) runs. **(c)** QBO2 (see text for details) from observations (black) and Natural (solid blue) run. **(d)** Global surface CO_2 concentration from observations (black, overlapped with the blue line), RCP85 (solid blue) and Natural (dashed blue) runs. **(e)** AOD (532 nm, 18–32 km) from the CCMI (black) and the CCMVal2 (blue) projects for the time 2001–2010. The black solid straight lines in each subfigure are the linear fits of the respective forcing during 2001–2011.

periment (blue line). Both the observed and simulated tropical SSTs show a statistically significant (over 95 %) decrease from 2001 to 2011. Note that there is a strong drop in SSTs around 1992 in the model, which does not occur in observations. This might be caused by an overestimated response to the Pinatubo eruption in the CESM-WACCM model (Marsh et al., 2013; Meehl et al., 2012).

The QBO variations are represented by a pair of orthogonal time series QBO1 and QBO2, which are constructed from the equatorial zonal winds over 70–10 hPa (Randel et al., 2009). The observed QBO2 (data from the FU Berlin: http://www.geo.fu-berlin.de/en/met/ag/strat/produkte/qbo/index.html), which is the dominate mode of QBO in the tropical lower stratosphere, shows an increase (a shift towards westerlies or stronger westerlies) during 2001–2011 (Fig. 1c, straight black line). Note that this short-term linear trend of the QBO2 is sensitive to the start and ending years. However, a further analysis for 2001–2012 ending with a relative minimum of QBO2 confirms this significant increase of QBO2 (not shown).

As shown in Fig. 1d, GHGs show a steady increase after 2001. The increasing rate of global CO_2 release from 2001 to 2011 is close to the RCP8.5 scenario.

Similar to the GHGs, observed stratospheric aerosols (aerosol optical depth, AOD) have been steadily increasing since 2001 (Solomon et al., 2011) in the lower stratosphere (18–32 km) (Fig. 1e). This increase in stratospheric aerosol loading is attributed to a number of small volcanic eruptions and anthropogenically released aerosols transported into the stratosphere during the Asian Monsoon (Bourassa et al., 2012; Neely et al., 2013). An aerosol data set has been constructed for the CCMI project (ftp://iacftp.ethz.ch/pub_read/luo/ccmi/) and is similar to the data described by Solomon et al. (2011). The comparison of the two experiments with different AOD data sets will shed light on the stratospheric aerosol contribution to the observed temperature trend.

All natural and anthropogenic forcings will be discussed with respect to their contribution to the temperature variability in TTL in the following section.

3 Quantification of observed temperature variability

3.1 Observed temperature variability in the TTL

Figure 2 shows the latitude–height section of the linear temperature trends for the period 2001–2011 estimated from GPS-RO observations (see details of the GPS-RO data in Wang et al., 2013). A remarkable and statistically significant warming occurs around the TTL between about 20° south to north and from 16 to 21 km height. The warming in the TTL is 0.9 K decade^{-1} on average, with a maximum of about 1.8 K decade^{-1} directly at the tropical tropopause around 17 to 18 km. This figure is an extension of earlier work by Schmidt et al. (2010) and Wang et al. (2013) and shows an unexpected warming, despite the steady increase in GHGs. Therefore it is interesting to study whether this warming is simply a phenomenon of the past decade and the result of internal atmospheric variability, or whether it will persist for longer and therefore modify trace gas transport from the troposphere into the stratosphere.

Note that this decadal warming in the TTL may vary in magnitude when different end years are selected due to the relative short length of the time series. The warming is weaker if end years of 2012 or 2013 are chosen (see also Figs. S1 and S2 in the Supplement). In the following investigations, we keep the period from 2001 through 2011 to be most consistent with our stand-alone WACCM simulations (2001–2010). We will explain the temperature variability within a time period of about one decade. This decadal variability may change sign from decade to decade if it is mainly caused by natural/internal variability. However, it is

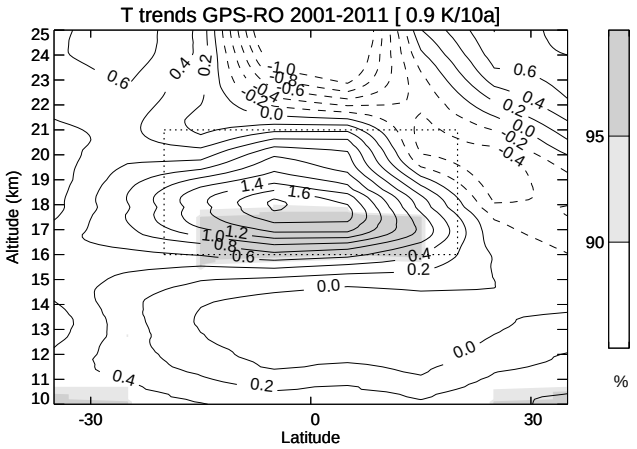

Figure 2. Latitude–height section of linear temperature trends over the past decade (2001–2011) from GPS-RO data over a height range from 10 to 25 km and 35° S to 35° N latitude; contour interval is 0.2 K decade^{-1}. Grey shading represents the statistical significance for the trends.

still very important to understand the reasons and mechanisms behind these internal variability modes as it might eventually enhance our decadal to multi-decadal predictive skills.

3.2 Contribution of solar variability

Figure 3a and b show the correlation between temperature differences (Natural – SolarMean) with solar forcing (TSI) in the Natural run over the whole simulation period from 1955 through 2099, as well as the estimated temperature trends during 2001 through 2011 related to a decreasing TSI. The correlation between temperature differences and TSI is relatively weak, amounts to less than 0.1 in the TTL region and is a little higher and more significant in the lower stratosphere. With such a weak positive correlation, the decreasing solar irradiance contributed to a cooling of about 0.2 K decade^{-1} in the TTL during 2001–2011.

3.3 Contribution of tropical SSTs

Figure 4 shows the correlation between temperature differences (Natural – FixedSST) with tropical (20°S–20°N) SSTs from the Natural run over the whole simulation period from 1955 through 2099, as well as the estimated temperature trends from 2001 through 2011 due to decreasing tropical SSTs. Temperature differences are closely correlated with tropical SSTs, which show strong positive correlations (up to 0.8) below and significant negative correlations (over 0.5) above the tropopause in the tropics. The strong correlation between tropical SSTs and atmospheric temperatures indicates that tropical SSTs have important impacts on the TTL temperature. A decrease in tropical SSTs contributes therefore to a statistically significant warming of 0.3 K decade^{-1}

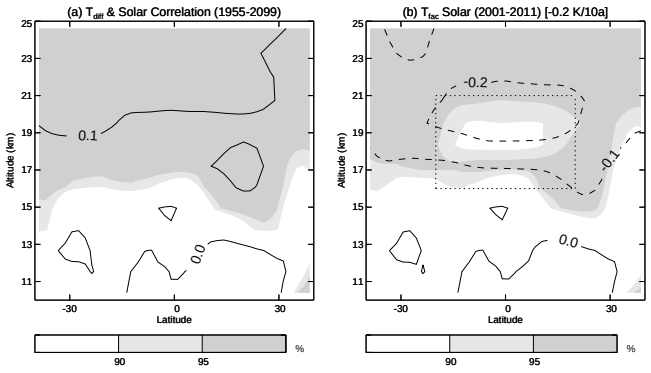

Figure 3. (a) Latitude–height sections of correlations between temperature differences (Natural – SolarMean) and solar TSI in the Natural run over the whole period (1955–2099); contour interval is 0.1; grey shading represents statistically significant correlations, with Student's *t* test. **(b)** The regressed contributions of solar TSI to the TTL temperature trends during 2001–2011 (Eq. 2); contour interval is 0.1 K decade^{-1}; grey shading represents statistically significant regressions. See text for details on the calculation of the regressed trend and the testing of the statistical significance. The decadal temperature trend in the title is the mean value from the dashed box.

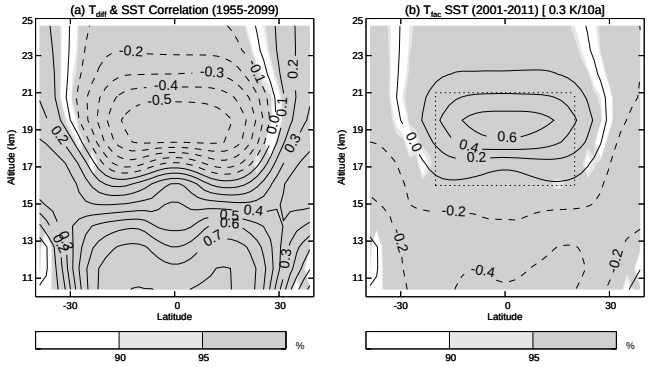

Figure 4. Same as Fig. 3 but for the impact of tropical SSTs by comparing the Natural and FixedSST runs. Contour interval is **(a)** 0.1 and **(b)** 0.2 K decade^{-1}.

on average (0.6 K decade^{-1} in maximum) in the TTL during 2001–2011 (Fig. 4c).

3.4 Contribution of the QBO

As described in Sect. 2.5, a pair of orthogonal time series of the QBO are used in the regression between temperature differences (Natural – NOQBO) and the QBO from the Natural run. Since the QBO1 mainly affects temperature in the middle and upper stratosphere, only the QBO2 correlation and impacts are shown in Fig. 5. QBO2 features a strong positive correlation in the TTL region, which amounts up to 0.6. An observed increase of QBO2 during 2001–2011, which means stronger westerlies, therefore contributes to a 0.2 K decade^{-1} warming on average (0.4 K decade^{-1} in maximum) in the

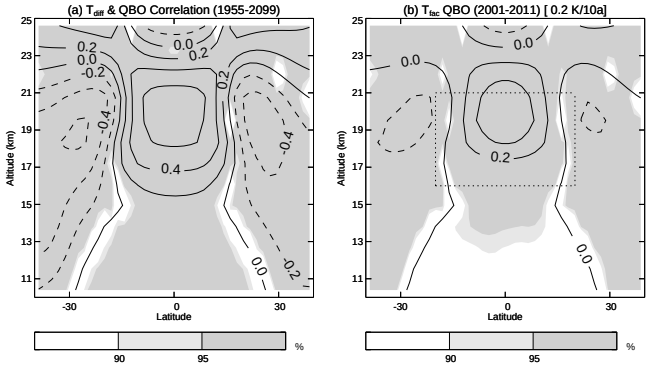

Figure 5. Same as Fig. 3 but for the impact of the QBO2 (see text for details) by comparing the Natural and the NOQBO experiments; contour interval is **(a)** 0.2 and **(b)** 0.2 K decade^{-1}.

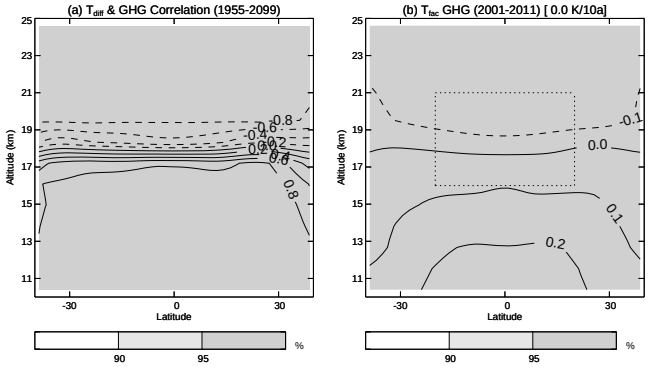

Figure 6. Same as Fig. 3 but for the impact of anthropogenic forcings (GHGs) by comparing the Natural and RCP85 experiments; contour interval is **(a)** 0.2 and **(b)** 0.1 K decade^{-1}.

TTL. Another effect of the QBO is the statistically significant cooling trend seen in the tropical middle stratosphere above 23 km. This QBO effect may help to explain the observed tropical cooling (see Fig. 2). However, CESM1.0 used for these simulations cannot generate a self-consistent QBO and hence uses wind nudging, which might cause problems when estimating QBO effects on temperature variability in the tropical lower stratosphere (Marsh et al., 2013; Morgenstern et al., 2010).

3.5 Contribution of GHGs

As expected, GHGs show strong positive correlations with temperatures in the troposphere and significant negative correlations with temperatures in the stratosphere, with a switch of sign near the tropopause (about 18 km, Fig. 6a). Increasing GHGs in the RCP85 experiment tend to cool the lower stratosphere and warm the upper troposphere, but have no evident contribution around the tropopause (with a change of correlation sign at about 18 km, Fig. 6b). This is consistence with previous studies (e.g. Kim et al., 2013), which confirmed a warming at 100 hPa (below the tropopause) and a cooling at 70 hPa (above the tropopause) due to the increase of GHGs in CMIP5 (Coupled Model Intercomparison Project Phase 5) simulations.

3.6 Contribution of stratospheric aerosols

The correlations between temperature differences (W_Aerosol – W_L103) with CCMI stratospheric aerosols, as well as the contributions of increasing stratospheric aerosols to the recent warming in the TTL are shown in Fig. 7a and b respectively. Weak but partly significant correlations of stratospheric aerosols to temperature in the TTL can be found in Fig. 7a, with a change of correlation sign below the tropopause (about 15 km) and up to 0.2 in the lower stratosphere. The effect of increasing stratospheric aerosols during 2001–2011 is estimated to be 0.2 K decade^{-1}

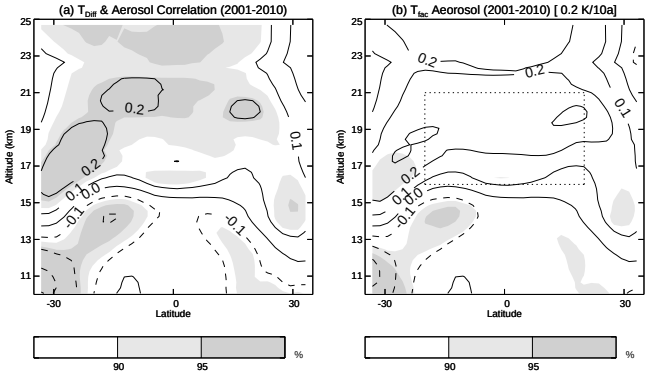

Figure 7. Same as Fig. 3 but for the impact of stratospheric aerosols by comparing the W_L103 and the W_Aerosol experiments. Contour interval is **(a)** 0.1 and **(b)** 0.1 K decade^{-1}. The temperatures in the W_L103 run were calculated from a three member ensemble mean.

warming in the TTL (Fig. 7b). Note that there may exist uncertainties for this result since we have only 10 years of simulations for the W_Aerosol run.

4 Effects of the vertical resolution

To estimate not only anthropogenic and natural contributions to the recent TTL temperature variability but also the effects of the vertical resolution in the model, Fig. 8 shows the temperature trends in both the standard (W_L66) and the high vertical resolution (W_L103) runs, as well as their differences. The W_L103 run (Fig. 8b) shows a statistically significant 0.5 K decade^{-1} warming on average over the past decade around the TTL, which maximizes at 1.2 K decade^{-1}. The standard W_L66 run (Fig. 8a) does not capture the warming. The only difference between the two experiments is the vertical resolution, meaning that a higher vertical resolution captures the warming in the TTL better than the standard vertical resolution, reaching up to 0.8 K decade^{-1}

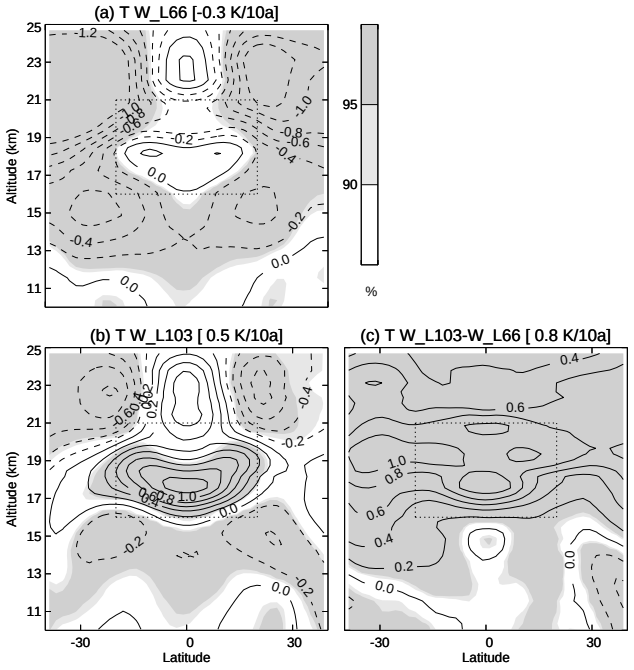

Figure 8. (a, b) Latitude–height sections of temperature trends over 2001–2010 from the W_L103 and W_L66 experiments respectively. **(c)** The differences between **(a)** and **(b)**. Contour interval is 0.2 K decade^{-1} and grey shading represents statistically significant trends. The temperature trends in the W_L103 and W_L66 runs are calculated by multiple linear regression for each three simulations.

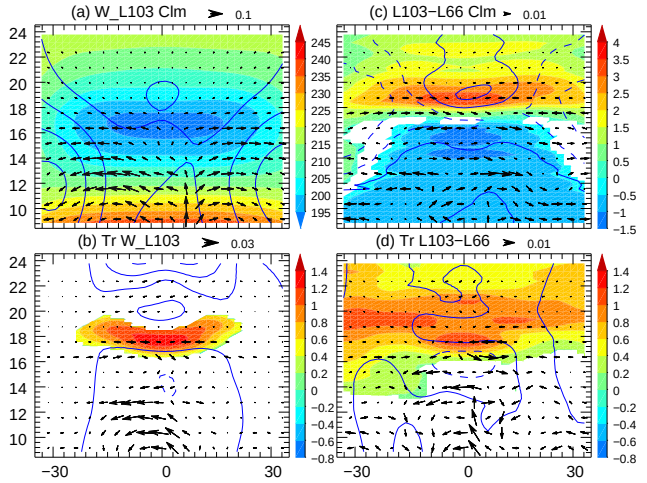

Figure 9. (a) Annual mean climatological zonal mean zonal wind (contours; contour interval is 10 m s^{-1}; dashed lines indicate easterly winds), BDC vector (arrows, scaled with the square root of pressure) and temperature (colour shadings) for the W_L103 experiment from 8 to 25 km and 35° S through 35° N. **(c)** Differences of the zonal mean zonal wind (contour interval 1.0 m s^{-1}), BDC vector and temperature (colour shadings indicate 95 % statistical significance) between the W_L103 and the W_L66 experiments. **(b)** and **(d)** are the same as **(a)** and **(c)** but for the linear trends from 2001 to 2010. The shadings in **(b)** and **(d)** indicate 95 % statistical significance. The contour intervals are 2 and 1 m s^{-1} in **(c)** and **(d)** respectively.

(Fig. 8c). Wang et al. (2013) showed that the tropical upwelling in the lower stratosphere has weakened over the past decade in the W_L103 run, while there is no significant upwelling trend in the standard vertical resolution (W_L66) run. The decreasing tropical upwelling in the W_L103 run might be the reason for the extra warming in the TTL compared to the W_L66 run, since dynamical changes would lead to adiabatic warming. More detailed investigations will be given in the following section.

4.1 Changes in the Brewer–Dobson circulation

To investigate dynamical differences between the two experiments with standard and higher vertical resolution in more detail, the transformed Eulerian mean diagnostic (Andrews et al., 1987) was applied to investigate differences in the wave propagation and BDC in the climatological mean as well as in the decadal trend.

Figure 9 shows the annual mean climatology of the BDC (arrows for the meridional and vertical wind components), the zonal mean zonal wind (blue contour lines) and the temperature (filled colours) from the W_L103 run (Fig. 9a), as well as the differences between the W_L103 and the W_L66 runs (Fig. 9c). The BDC shows an upwelling in the tropics and a downwelling through middle to high latitudes in the annual mean. With finer vertical resolution (W_L103) the model produces a stronger upwelling in the tropics (and a consistent cooling) up to the tropopause region, with westerly wind anomalies above. This strengthened tropical upwelling cannot continue further up because of the westerly wind anomalies which block the transport into the subtropics (Simpson et al., 2009; Flannaghan and Fueglistaler, 2013). Above the tropical tropopause there is less upwelling and in particular more transport from the subtropics into the tropical TTL, leading to a stronger warming around 19 km in the W_L103 experiment. These changes in the BDC indicate a strengthening of its lower branch and a weakening at upper levels in the lower stratosphere (Lin and Fu, 2013). This is consistent with a previous work by Bunzel and Schmidt (2013) which indicates a weaker upward mass flux around 70 hPa in a model experiment with higher vertical resolution.

The annual mean trends in the W_L103 experiment indicate a further strengthening of the BDC lower branch over the past decade in this simulation (Fig. 9b) and a statistically significant weakening in the lower stratosphere resulting in significant warming of 1 to 2 K decade^{-1} in the TTL. In particular the trends in the TTL are stronger in the W_L103 compared to the W_L66 experiment (Fig. 9d).

In summary, the finer vertical resolution can enhance the upward wave propagation from the tropics. This enhanced wave propagation speeds up the lower branch of the BDC in the upper troposphere and slows down the upper branch

Table 3. Summary of contributions from the varying factors to the observed TTL warming between 2001 and 2011, in the region 20° S–20° N latitude and 16–20 km.

Factors	Solar	SSTs	QBO	GHGs	Aerosols	Total
Contribution (K decade^{-1})	−0.2	0.3	0.2	0.0	0.2	0.5
Observation						0.9
Vertical resolution						0.8

of the BDC in the lower stratosphere. These changes in the BDC and corresponding wave–mean flow interactions (not shown) finally result in the statistically significant warming in the TTL.

Bunzel and Schmidt (2013) attributed the differences in the BDC to different vertical resolutions which tend to reduce the numerical diffusion through the tropopause and the secondary meridional circulation. Our results show that the strong warming and subsequent enhanced static stability (not shown) above the tropopause may also influence wave dissipation and propagation around the tropopause. Oberländer et al. (2013) point out that an increase of tropical SSTs enhances the BDC. This is consistent with our results, which show a weakening of the BDC in the lower stratosphere following a decrease in tropical SSTs. At the same time, this response of the stratosphere to the surface can be better represented by a model with finer vertical resolution.

5 Summary and discussion

Based on a series of sensitivity simulations with NCAR's CESM-WACCM model, the relationships between different natural (solar, QBO, tropical SSTs) and anthropogenic (GHGs, ODS) factors and temperatures around TTL, as well as their contributions to the observed warming of the TTL over the past decade from 2001 through 2011, have been studied. By regressing the temperature differences between model experiments to the respective factors for the whole simulation periods between 1955 and 2099 and projecting the regressed coefficients onto the observed trends of the respective factor during 2001–2011, the contribution of each factor has been quantified in order to explain the causes of the observed recent decadal variability seen in GPS-RO data.

The SSTs show strong significant negative correlation (−0.5) with temperatures in the TTL, while the QBO2 shows a reversed pattern (0.6). The TSI and stratospheric aerosols result in weak positive correlations (0.1–0.2) with TTL temperatures. GHGs show positive correlations with temperatures in the troposphere and negative correlations with temperatures in the stratosphere, while there is no significant correlation around the tropopause.

A decrease in tropical SSTs, an increase in stratospheric aerosol loading and stronger QBO westerlies contribute each about 0.3, 0.2 and 0.2 K decade^{-1} to this warming respectively, resulting in a total 0.7 K decade^{-1} warming, while the delay and smaller amplitude of the current solar maximum contribute about 0.2 K decade^{-1} to cooling. Adding all natural and anthropogenic factors, we estimate a total modelled warming of 0.5 K decade^{-1} around the TTL (Table 3), which is less than the observed 0.9 K decade^{-1} warming from GPS-RO data. One possible reason of this weak estimate is the relative low vertical resolution of the model, which strongly influences the TTL response to the surface mainly via dynamical changes, i.e. an enhancement of the lower branch of the BDC and a decrease of the upper branch in the lower stratosphere in response to decreasing tropical SSTs. This leads to a 0.8 K decade^{-1} extra warming in the TTL in the finer vertical resolution experiment as compared to the standard vertical resolution. However, in reality non-linear interactions between the different factors occur which we did not take into account in our first-order linear approach. The comprehensive impact of all factors on the recent TTL warming can be estimated by the W_Aerosol run. The W_Aerosol run, with almost all observed forcings considered in this study, can be seen as the most realistic simulation. The TTL warming in the W_Aerosol run is on average 0.9 K decade^{-1} and maximum 1.6 K decade^{-1} (Fig. 7b), both of which are very close to the observed trend.

According to our experiments, one of the primary factors contributing to the recent warming in the TTL is the natural variability in tropical SSTs. However, the mechanism of the TTL response to SSTs awaits further investigation. One key issue is how much improvement we can expect from using a fully coupled ocean–atmosphere model instead of atmosphere-only model with prescribed SSTs. Our W_L66 and W_L103 simulations indicate that the atmosphere-only model may not correctly reproduce the response of TTL variability to SST, but can be improved with finer vertical resolution.

Another important factor in contributing to the recent warming in the TTL is the QBO. The QBO is closely related to the tropical upwelling Flury et al. (2013). A regression of temperature differences onto the differences in the vertical component of BDC between the Natural and NOQBO run shows a very similar result than the regression of temperature differences onto the QBO time series (not shown). The QBO may influence the TTL temperature by modifying the BDC.

Figure S3 clearly shows decadal to multidecadal fluctuations in TTL temperatures from both the Modern

Era Retrospective-analysis for Research and Applications (MERRA) reanalysis data and our Natural and RCP85 runs, which provide strong support to the internal variability dominated TTL warming over the past decade.

The external forcings (solar, GHGs, ODS) contribute relatively little to the temperature variability in the TTL, except for the stratospheric aerosols. Internal variability, i.e. the QBO and tropical SSTs, seem to be mainly responsible for the recent TTL warming.

The Supplement related to this article is available online at doi:10.5194/acp-15-5815-2015-supplement.

Acknowledgements. W. Wang is supported by a fellowship of the China Scholarship Council (CSC) at FU Berlin. This work was also performed within the Helmholtz University Young Investigators Group NATHAN, funded by the Helmholtz Association through the president's Initiative and Networking Fund and the GEOMAR – Helmholtz-Zentrum für Ozeanforschung in Kiel. The model calculations have been performed at the Deutsche Klimarechenzentrum (DKRZ) in Hamburg, Germany. We thank F. Hansen, C. Petrick, R. Thiéblemont and S. Wahl for carrying out some of the simulations. We appreciate discussions about the statistical methods with D. Maraun and the help with grammar checking from L. Neef.

The article processing charges for this open-access publication were covered by a Research Centre of the Helmholtz Association.

Edited by: P. Haynes

References

Andrews, D. G.: An Introduction to Atmospheric Physics, Cambridge University Press, New York, 248 pp., 2010.

Andrews, D. G., Holton, J. R., and Leovy, C. B.: Middle Atmosphere Dynamics, vol. 40, Academic Press, San Diego, 489 pp., 1987.

Baldwin, M. P., Gray, L. J., Dunkerton, T. J., Hamilton, K., Haynes, P. H., Randel, W. J., Holton, J. R., Alexander, M. J., Hirota, I., Horinouchi, T., Jones, D. B. A., Kinnersley, J. S., Marquardt, C., Sato, K., and Takahashi, M.: The quasi-biennial oscillation, Rev. Geophys., 39, 179–229, doi:10.1029/1999RG000073, 2001.

Bourassa, A. E., Robock, A., Randel, W. J., Deshler, T., Rieger, L. A., Lloyd, N. D., Llewellyn, E. T., and Degenstein, D. A.: Large volcanic aerosol load in the stratosphere linked to Asian monsoon transport, Science, 337, 78–81, doi:10.1126/science.1219371, 2012.

Bunzel, F. and Schmidt, H.: The Brewer–Dobson circulation in a changing climate: impact of the model configuration, J. Atmos. Sci., 70, 1437–1455, doi:10.1175/JAS-D-12-0215.1, 2013.

Butchart, N.: The Brewer–Dobson circulation, Rev. Geophys., 52, 157–184, doi:10.1002/2013RG000448, 2014.

Butchart, N., Cionni, I., Eyring, V., Shepherd, T. G., Waugh, D. W., Akiyoshi, H., Austin, J., Bruhl, C., Chipperfield, M. P., Cordero, E., Dameris, M., Deckert, R., Dhomse, S., Frith, S. M., Garcia, R. R., Gettelman, A., Giorgetta, M. A., Kinnison, D. E., Li, F., Mancini, E., McLandress, C., Pawson, S., Pitari, G., Plummer, D. A., Rozanov, E., Sassi, F., Scinocca, J. F., Shibata, K., and Tian, W.: Chemistry-climate model simulations of twenty-first century stratospheric climate and circulation changes, J. Climate, 23, 5349–5374, doi:10.1175/2010JCLI3404.1, 2010.

Dessler, A. E., Schoeberl, M. R., Wang, T., Davis, S. M., and Rosenlof, K. H.: Stratospheric water vapor feedback, P. Natl. Acad. Sci. USA, 110, 18087–18091, doi:10.1073/pnas.1310344110, 2013.

Dessler, A., Schoeberl, M., Wang, T., Davis, S., Rosenlof, K., and Vernier, J.-P.: Variations of stratospheric water vapor over the past three decades, J. Geophys. Res., 119, 12–588, doi:10.1002/2014JD021712, 2014.

Engel, A., Mobius, T., Bonisch, H., Schmidt, U., Heinz, R., Levin, I., Atlas, E., Aoki, S., Nakazawa, T., Sugawara, S., Moore, F., Hurst, D., Elkins, J., Schauffler, S., Andrews, A., and Boering, K.: Age of stratospheric air unchanged within uncertainties over the past 30 years, Nat. Geosci., 2, 28–31, doi:10.1038/ngeo388, 2009.

Flannaghan, T. and Fueglistaler, S.: The importance of the tropical tropopause layer for equatorial Kelvin wave propagation, J. Geophys. Res., 118, 5160–5175, doi:10.1002/jgrd.50418, 2013.

Flury, T., Wu, D. L., and Read, W. G.: Variability in the speed of the Brewer–Dobson circulation as observed by Aura/MLS, Atmos. Chem. Phys., 13, 4563–4575, doi:10.5194/acp-13-4563-2013, 2013.

Fueglistaler, S., Dessler, A., Dunkerton, T., Folkins, I., Fu, Q., and Mote, P. W.: Tropical tropopause layer, Rev. Geophys., 47, 1004, doi:10.1029/2008RG000267, 2009.

Fueglistaler, S., Liu, Y., Flannaghan, T., Haynes, P., Dee, D., Read, W., Remsberg, E., Thomason, L., Hurst, D., Lanzante, J., and Bernath, P. F.: The relation between atmospheric humidity and temperature trends for stratospheric water, J. Geophys. Res., 118, 1052–1074, doi:10.1002/jgrd.50157, 2013.

Gettelman, A. and Birner, T.: Insights into tropical tropopause layer processes using global models, J. Geophys. Res., 112, D23104, doi:10.1029/2007JD008945, 2007.

Gettelman, A. and Forster, P. D. F.: A climatology of the tropical tropopause layer, J. Meteor. Soc. Jpn., 80, 911–924, doi:10.2151/jmsj.80.911, 2002.

Gettelman, A., Birner, T., Eyring, V., Akiyoshi, H., Bekki, S., Brühl, C., Dameris, M., Kinnison, D. E., Lefevre, F., Lott, F., Mancini, E., Pitari, G., Plummer, D. A., Rozanov, E., Shibata, K., Stenke, A., Struthers, H., and Tian, W.: The Tropical Tropopause Layer 1960–2100, Atmos. Chem. Phys., 9, 1621–1637, doi:10.5194/acp-9-1621-2009, 2009.

Gray, L. J., Beer, J., Geller, M., Haigh, J. D., Lockwood, M., Matthes, K., Cubasch, U., Fleitmann, D., Harrison, G., Hood, L., Luterbacher, J., Meehl, G. A., Shindell, D., van Geel, B., and White, W.: Solar influences on climate, Rev. Geophys., 48, RG4001, doi:10.1029/2009RG000282, 2010.

Grise, K. M. and Thompson, D. W.: Equatorial planetary waves and their signature in atmospheric variability, J. Atmos. Sci., 69, 857–874, doi:10.1175/JAS-D-11-0123.1, 2012.

Grise, K. M. and Thompson, D. W.: On the signatures of equatorial and extratropical wave forcing in tropical tropopause layer temperatures, J. Atmos. Sci., 70, 1084–1102, doi:10.1175/JAS-D-12-0163.1, 2013.

Hansen, F., Matthes, K., and Gray, L.: Sensitivity of stratospheric dynamics and chemistry to QBO nudging width in the chemistry-climate model WACCM, J. Geophys. Res., 118, 10–464, doi:10.1002/jgrd.50812, 2013.

Kawatani, Y. and Hamilton, K.: Weakened stratospheric quasibiennial oscillation driven by increased tropical mean upwelling, Nature, 497, 478–481, doi:10.1038/nature12140, 2013.

Kim, J., Grise, K. M., and Son, S.: Thermal characteristics of the cold-point tropopause region in CMIP5 models, J. Geophys. Res., 118, 8827–8841, doi:10.1002/jgrd.50649, 2013.

Lean, J., Rottman, G., Harder, J., and Kopp, G.: SORCE contributions to new understanding of global change and solar variability, Sol. Phys., 230, 27–53, doi:10.1007/s11207-005-1527-2, 2005.

Li, F., Austin, J., and Wilson, J.: The strength of the Brewer–Dobson circulation in a changing climate: coupled chemistry-climate model simulations, J. Climate, 21, 40–57, doi:10.1175/2007JCLI1663.1, 2008.

Lin, P. and Fu, Q.: Changes in various branches of the Brewer–Dobson circulation from an ensemble of chemistry climate models, J. Geophys. Res., 118, 73–84, doi:10.1029/2012JD018813, 2013.

Marsh, D. R., Mills, M. J., Kinnison, D. E., Lamarque, J.-F., Calvo, N., and Polvani, L. M.: Climate change from 1850 to 2005 simulated in CESM1 (WACCM), J. Climate, 26, 7372–7391, doi:10.1175/JCLI-D-12-00558.1, 2013.

Matthes, K., Marsh, D. R., Garcia, R. R., Kinnison, D. E., Sassi, F., and Walters, S.: Role of the QBO in modulating the influence of the 11 year solar cycle on the atmosphere using constant forcings, J. Geophys. Res., 115, 18110, doi:10.1029/2009JD013020, 2010.

Meehl, G. A., Washington, W. M., Arblaster, J. M., Hu, A., Teng, H., Tebaldi, C., Sanderson, B. N., Lamarque, J.-F., Conley, A., Strand, W. G., and White, J. B.: Climate system response to external forcings and climate change projections in CCSM4, J. Climate, 25, 3661–3683, doi:10.1175/JCLI-D-11-00240.1, 2012.

Meinshausen, M., Smith, S. J., Calvin, K., Daniel, J. S., Kainuma, M. L. T., Lamarque, J.-F., Matsumoto, K., Montzka, S., Raper, S., Riahi, K., Thomson, A., Velders, G. J. M., and van Vuuren, D. P.: The RCP greenhouse gas concentrations and their extensions from 1765 to 2300, Climatic Change, 109, 213–241, doi:10.1007/s10584-011-0156-z, 2011.

Morgenstern, O., Giorgetta, M. A., Shibata, K., Eyring, V., Waugh, D. W., Shepherd, T. G., Akiyoshi, H., Austin, J., Baumgaertner, A. J. G., Bekki, S., Braesicke, P., Brühl, C., Chipperfield, M. P., Cugnet, D., Dameris, M., Dhomse, S., Frith, S. M., Garny, H., Gettelman, A., Hardiman, S. C., Hegglin, M. I., Jöckel, P., Kinnison, D. E., Lamarque, J.-F., Mancini, E., Manzini, E., Marchand, M., Michou, M., Nakamura, T., Nielsen, J. E., Olivié, D., Pitari, G., Plummer, D. A., Rozanov, E., Scinocca, J. F., Smale, D., Teyssèdre, H., Toohey, M., Tian, W., and Yamashita, Y.: Review of the formulation of present-generation stratospheric chemistry-climate models and associated external forcings, J. Geophys. Res., 115, D00M02, doi:10.1029/2009JD013728, 2010.

Neely, R. R., Toon, O. B., Solomon, S., Vernier, J. P., Alvarez, C., English, J. M., Rosenlof, K. H., Mills, M. J., Bardeen, C. G., Daniel, J. S., and Thayer, J. P.: Recent anthropogenic increases in SO_2 from Asia have minimal impact on stratospheric aerosol, Geophys. Res. Lett., 40, 999–1004, doi:10.1002/grl.50263, 2013.

Oberländer, S., Langematz, U., and Meul, S.: Unraveling impact factors for future changes in the Brewer–Dobson circulation, J. Geophys. Res., 118, 10–296, doi:10.1002/jgrd.50775, 2013.

Randel, W. J. and Jensen, E. J.: Physical processes in the tropical tropopause layer and their roles in a changing climate, Nat. Geosci., 6, 169–176, doi:10.1038/ngeo1733, 2013.

Randel, W. J., Shine, K. P., Austin, J., Barnett, J., Claud, C., Gillett, N. P., Keckhut, P., Langematz, U., Lin, R., Long, C., Mears, C., Miller, A., Nash, J., Seidel, D. J., Thompson, D. W. J., Wu, F., and Yoden, S.: An update of observed stratospheric temperature trends, J. Geophys. Res., 114, D02107, doi:10.1029/2008JD010421, 2009.

Richter, J. H., Solomon, A., and Bacmeister, J. T.: On the simulation of the quasi-biennial oscillation in the Community Atmosphere Model, version 5, J. Geophys. Res.-Atmos., 119, 3045–3062, doi:10.1002/2013JD021122, 2014.

Schmidt, T., Wickert, J., and Haser, A.: Variability of the upper troposphere and lower stratosphere observed with GPS radio occultation bending angles and temperatures, Adv. Space. Res., 46, 150–161, doi:10.1016/j.asr.2010.01.021, 2010.

Shepherd, T. G. and McLandress, C.: A robust mechanism for strengthening of the Brewer–Dobson circulation in response to climate change: critical-layer control of subtropical wave breaking, J. Atmos. Sci., 68, 784–797, doi:10.1175/2010JAS3608.1, 2011.

Simpson, I. R., Blackburn, M., and Haigh, J. D.: The role of eddies in driving the tropospheric response to stratospheric heating perturbations, J. Atmos. Sci., 66, 1347–1365, doi:10.1175/2008JAS2758.1, 2009.

Solomon, S., Rosenlof, K. H., Portmann, R. W., Daniel, J. S., Davis, S. M., Sanford, T. J., and Plattner, G.-K.: Contributions of stratospheric water vapor to decadal changes in the rate of global warming, Science, 327, 1219–1223, doi:10.1126/science.1182488, 2010.

Solomon, S., Daniel, J., Neely, R., Vernier, J.-P., Dutton, E., and Thomason, L.: The persistently variable "background" stratospheric aerosol layer and global climate change, Science, 333, 866–870, doi:10.1126/science.1206027, 2011.

SPARC-CCMVal: SPARC Report on the Evaluation of Chemistry-Climate Models, SPARC Report 5, WCRP-132, WMO/TD-1526, 2010.

Stiller, G. P., von Clarmann, T., Haenel, F., Funke, B., Glatthor, N., Grabowski, U., Kellmann, S., Kiefer, M., Linden, A., Lossow, S., and López-Puertas, M.: Observed temporal evolution of global mean age of stratospheric air for the 2002 to 2010 period, Atmos. Chem. Phys., 12, 3311–3331, doi:10.5194/acp-12-3311-2012, 2012.

Wang, J. S., Seidel, D. J., and Free, M.: How well do we know recent climate trends at the tropical tropopause?, J. Geophys. Res., 117, D09118, doi:10.1029/2012JD017444, 2012.

Wang, W., Matthes, K., Schmidt, T., and Neef, L.: Recent variability of the tropical tropopause inversion layer, Geophys. Res. Lett., 40, 6308–6313, doi:10.1002/2013GL058350, 2013.

Wigley, T.: Appendix A: Statistical issues regarding trends, in: Temperature Trends in the Lower Atmosphere: Steps for Understanding and Reconciling Differences, edited by: Karl, T. R., Hassol, S. J., Miller, C. D., and Murray, W. L., A Report by Climate Change Science Program and the Subcommittee on Global Change Research, Washington, DC, USA, UNT Digital Library, 129–139, 2006.

Zhou, X.-L., Geller, M. A., and Zhang, M.: Cooling trend of the tropical cold point tropopause temperatures and its implications, J. Geophys. Res., 106, 1511–1522, doi:10.1029/2000JD900472, 2001.

Supplement of Atmos. Chem. Phys., 15, 5815–5826, 2015
http://www.atmos-chem-phys.net/15/5815/2015/
doi:10.5194/acp-15-5815-2015-supplement

Atmospheric Chemistry and Physics Open Access

Supplement of

Quantifying contributions to the recent temperature variability in the tropical tropopause layer

W. Wang et al.

Correspondence to: W. Wang (wuke.wang@fu-berlin.de)

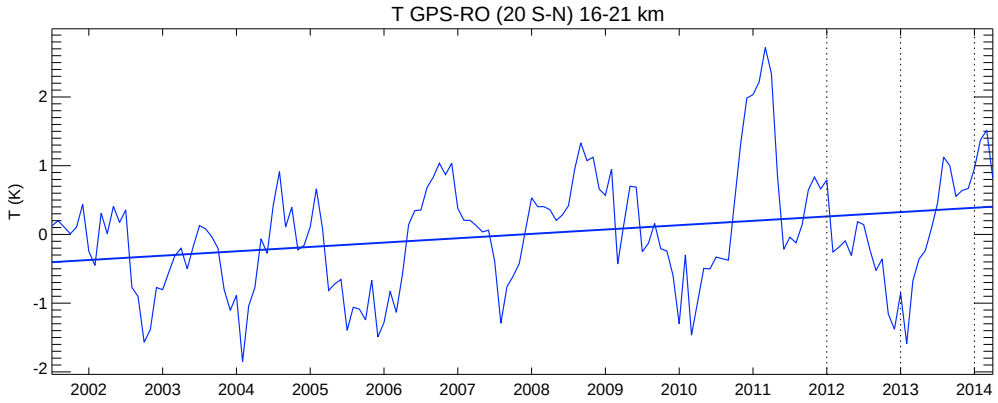

Figure S1: Deseasonalized time series of temperature anomalies from observations (GPS-RO data), averaged between $20^{\circ}S$ and $20^{\circ}N$ latitude and between 16 and 21 km height. This figure shows large interannual temperature fluctuations. From this time series alone, the future development of temperatures in the TTL is not clear (see also Fig. S3 for a longer time series. Vertical lines indicate different end dates for the trend estimates in Fig. S2.

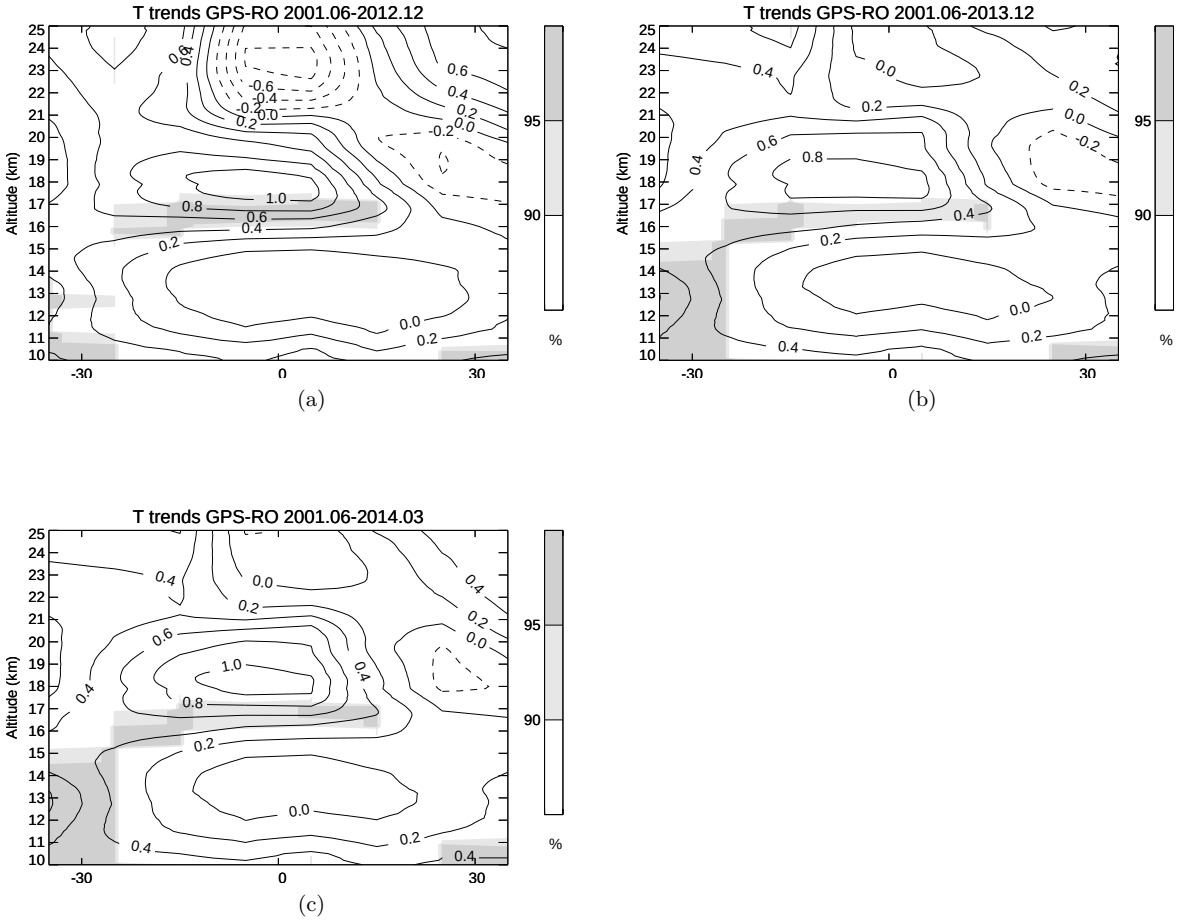

Figure S2: Same as in Fig. 2, but with different ending dates: (a) 31 December 2012; (b) 31 December 2013 and (c) 31 March 2014 (most recent data available). The trend calculations are sensitive to the ending date of the time series.

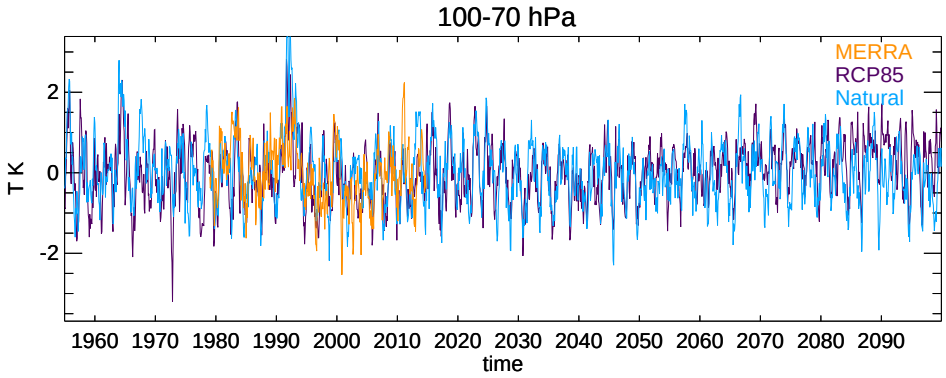

Figure S3: Deseasonalized time series of temperature anomalies from the Natural and RCP85 runs as well as the MERRA reanalysis data, averaged between $20^{\circ}S$ and $20^{\circ}N$ in latitude and between 100 and 70 hPa. Also over a longer time period than shown in Fig. S1, the TTL temperatures show large interannual variability from both model simulations and reanalysis data. The long-term temperature time series from the model simulations show a clear decadal to multidecadel signal.

Chapter 4

Multidecadal variability of tropical tropopause temperature and its relation to the Pacific Decadal Oscillation

4.1 Introduction

As described in Chapter 1, the TTL has important impacts on both the stratosphere and the surface climate. Fundamental understanding of long-term variability and trends of tropopause temperatures and its links to tropospheric and stratospheric circulation is still lacking (*Fueglistaler et al.*, 2009; *Randel and Wu*, 2015). So far a long-term cooling in the lower stratosphere has been reported from the 1970s to 2000s, although there are large differences between different data sets (*Fueglistaler et al.*, 2013; *Randel et al.*, 2009; *Wang et al.*, 2012). The recent TTL warming as shown in Chapter 2 is different from historical trends and might indicate a climate change signal, with possible important impacts on stratospheric climate, e.g., tropical tropopause temperatures dominate the amount of water vapour entering the stratosphere (*Dessler et al.*, 2014, 2013; *Gettelman et al.*, 2009; *Randel and Jensen*, 2013; *Solomon et al.*, 2010). From Chapter 3, this recent warming in the TTL is likely due to internal variability (*Wang et al.*, 2015a) such as SST variations. Which processes dominate this multidecadal internal variability, and how important are they in estimating the long-term trend of TPTs are still not clear. In this chapter, the multidecadal variability of TPTs, as well as the controlling processes and possible physical mechanisms are investigated.

4.2 Data and methods

4.2.1 MERRA tropopause temperature

The MERRA tropopause data are downloaded from the single-level diagnostics products (http://disc.sci.gsfc.nasa.gov/mdisc/data-holdings/merra/merra_products_nonjs.shtml). Fig. 4.1 shows the very good agreement between MERRA and GPS-RO data for the time period 2001-2014. The tropopause temperatures are based on the lapse rate tropopause, following the World Meteorological Organization (WMO) definition (*WMO*, 1957). GPS-RO data described above are not assimilated into MERRA reanalysis.

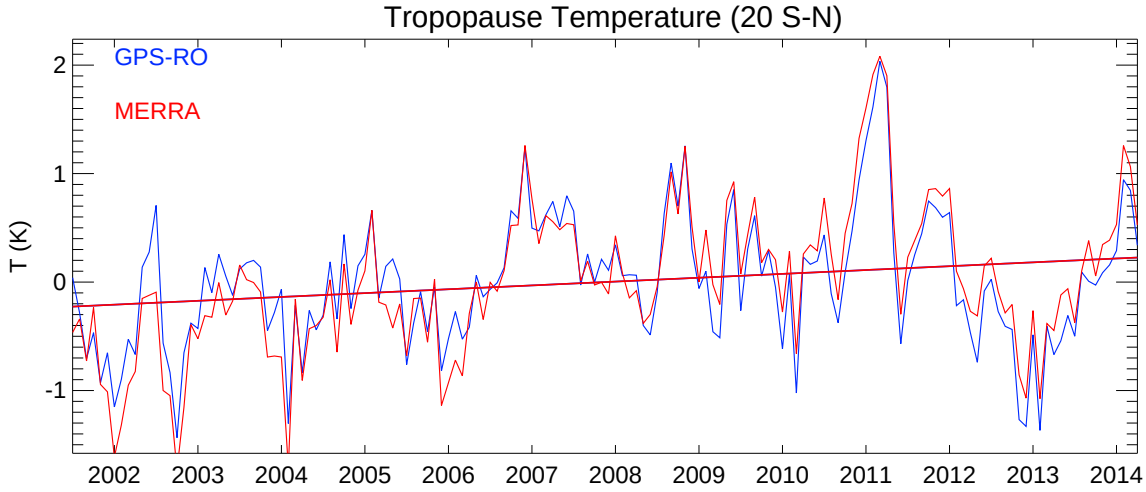

Fig. 4.1 Deseasonalized anomalies of tropical tropopause temperatures from GPS-RO (blue) and MERRA (red) data, from June 2001 through March 2014. The straight lines are linear trends, which are 95% statistically significant. Note that MERRA data do not assimilate GPS-RO data, whereas ERA-interim does.

4.2.2 Model and simulations

The CESM Natural and SolarMean runs, which cover the period from 1955 to 2099 as listed in Chapter 3, are analyzed in this chapter. The Natural run employs all natural forcing agents including spectrally resolved solar variability, a fully interactive ocean, volcanic aerosols and a nudged QBO, while the SolarMean run uses constant solar irradiance values averaged over the past 4 observed solar cycles. An overview of all CESM simulations and details of all external forcings can be found in Chapter 3. The tropopause temperature is a direct output of the model, using a standard WMO definition (*WMO*, 1957).

4.2.3 Maximum Covariance Analysis (MCA)

The MCA is useful for exploring relationships between two time varying fields, although physical interpretations of the MCA modes require additional physical knowledge (*Wilks*, 2011). The MCA between tropical (30°S-30°N) SSTs and TPTs is achieved by singular value decomposition of the temporal covariance matrix, using equal area weighting (square root of cosine of latitude). The pairs of singular vectors describe the spatial patterns of each field. The Principal Components (PCs) of SST and TPT (Fig. 4.5) are obtained by projections of SST and TPT fields on these spatial patterns correspondingly, and the global patterns shown in Figs. 4.3 a-b are regressions of SST and TPT anomalies on the first pair of TPT and SST PCs, respectively. Please note that, the data are low-pass filtered (15 years), since we focus on decadal variability, and influences from volcanic aerosols are removed by linear regression before applying the MCA. Without a low-pass filter, the PDO is the third mode, while the first mode is the ENSO and the second mode is the QBO.

4.2.4 Regression of recent TPT trends on PDO

A linear regression (see an instruction in Chapter 3) is used to estimate the link of the TPT to the PDO. By regressing TPT time series from MERRA on the observed PDO index (Fig. 4.4), coefficients at each longitude and latitude are obtained. During 2001-2014, a decreasing PDO index is seen in the HadISST data (Fig. 4.4). The regression coefficients times the linear trend of the PDO, then yields the corresponding contribution of the PDO to the TPT trends during 2001-2014 (Fig. 4.3f).

4.3 Analyses and results

4.3.1 Multidecadal variability of the tropical tropopause temperature

Deseasonalized tropical tropopause temperature anomalies during 1979-2014 from MERRA reanalysis data (orange line in Fig. 4.2a) exhibit strong interannual variability, which is primarily related to the El-Niño Southern Oscillation (ENSO) and the Quasi-Biennial Oscillation (QBO) (*Randel and Wu*, 2015; *Wang et al.*, 2013). Multidecadal variability is also prominent, with gradual cooling between 1979 and 2000 and an opposite trend thereafter. While greenhouse gases (GHGs) have been increasing monotonically during the whole period, the lack of a sustained long-term trend and the existence of multidecadal variability suggests that tropical tropopause temperatures are strongly influenced by internal climate variability. However, since the reliable observational data sets are very short, and an accurate statistical assessment of natural variability is very difficult, long simulations with a state-of-the-art model were additionally analyzed.

Also shown in Fig. 4.2a is a simulation (grey line) with the CESM-WACCM model. This model captures the variability of the Upper Troposphere-Lower Stratosphere (UTLS) temperatures reasonably well (*Gettelman et al.*, 2010). The model was integrated in fully coupled mode for 145 years (1955-2099), i.e. with an interactive ocean and interactive atmospheric chemistry. It was driven with natural external forcing (solar irradiance and volcanic aerosols) only, and additionally employed a nudged QBO. GHG concentrations were kept constant at 1960 values throughout the integration. This experiment will be named "Natural" hereafter (see Methods and Table 4.1). The model nicely captures the interannual and decadal variations of tropical tropopause temperatures seen in MERRA and GPS-RO data (Fig. 4.2a and Fig. 4.1).

4.3.2 Connections to Sea Surface Temperatures (SSTs)

MCA between SST and TPT anomalies simulated in the CESM-WACCM Natural run was performed to understand possible relations (see details in Methods). Figs. 4.3a and 4.3b show the regressed patterns of SST and TPT anomalies on the corresponding time series of the first MCA mode (Fig. 4.5). The SST anomalies are reminiscent of a negative PDO phase, with cold SST anomalies in the tropical Pacific and warm SST anomalies in the North Pacific. In fact, the pattern correlation with the PDO derived from observed SSTs amounts to 0.81 (the PDO pattern can be obtained by an Empirical Orthogonal Function (EOF) analysis of SST anomalies in the North Pacific (20°N-70°N, as suggested by *Deser et al.* (2010)), see Fig. 4.4). This PDO-like pattern is accompanied with tropopause warming over the tropical

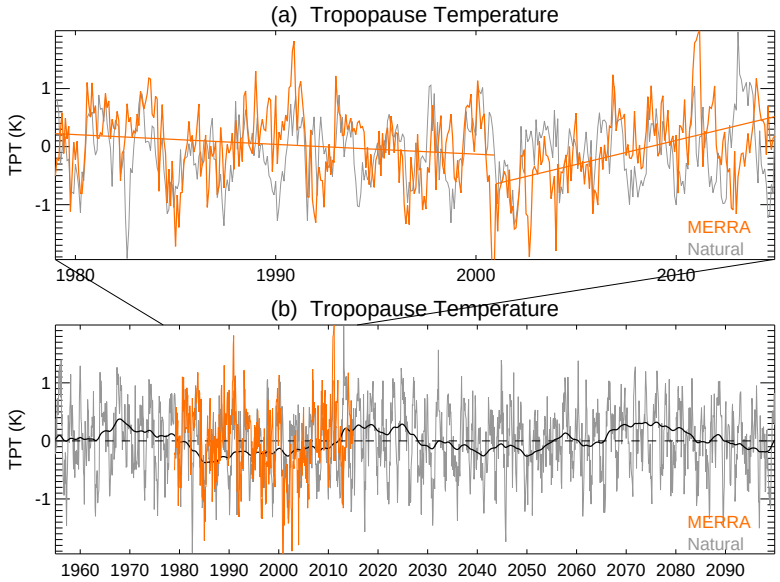

Fig. 4.2 Deseasonalized anomalies of tropical (20°S-20°N) tropopause temperatures from the MERRA data (orange) and the CESM Natural simulation (grey). **a**, Recent decades (1979-2014). The orange straight lines are the linear trends of MERRA data over the period 1979-2000 and 2001-2014. **b**, Long-term (1955-2099) variations. The thick black line is low-pass filtered (15 years) data of the CESM Natural run. Influences from volcanic aerosols have been removed by a linear regression.

and subtropical east and central Pacific and tropopause cooling in the midlatitudes of both hemispheres in CESM-WACCM.

The PDO pattern, which is obtained using the same method as suggested by *Deser et al.* (2010), from the observed SSTs (Hadley Centre SST, HadISST (*Rayner et al.*, 2003)) can be seen in Fig. 4.4. Also shown in Fig. 4.4 is the PDO index, which is the first PC of the corresponding EOF analysis. As addressed by previous studies (*Deser et al.*, 2010, and references therein), the PDO index shows prominent multidecadal variability. Recently, since the late 1970s, positive PDO-phases dominated until the end of the 20th century (around 1998), whereas the PDO turned into its negative phase afterwards (see Fig. 4.4).

Fig. 4.5 shows the corresponding time series of the first pair of PCs from the MCA analysis. Both of the PCs show prominent multidecadal variations. As expected by a MCA analysis, this pair of PCs are closely related to each other, with a correlation of 0.9. At the

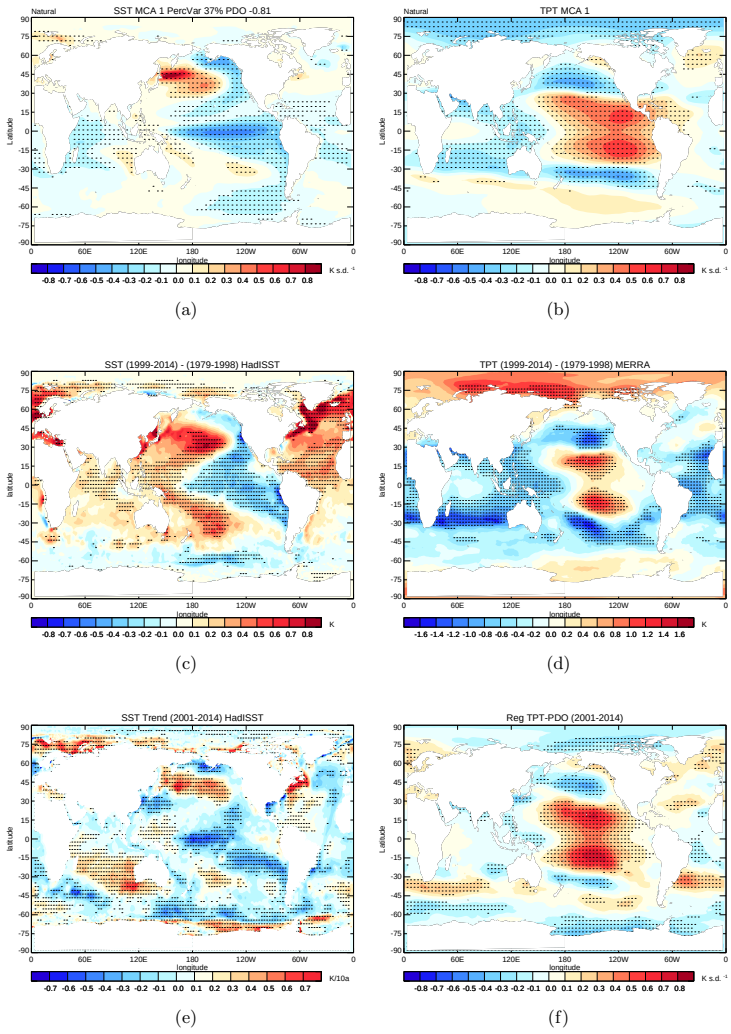

Fig. 4.3 **(top)** Regression of global SST and TPT anomalies on the first MCA-PCs (details in Methods). **a**, SSTs. The percentage (%) is the amount of the first MCA mode that accounts for the squared covariance between SSTs and TPTs, the number on the right-hand side is the pattern correlation between the MCA-PC regressed SSTs with the observed PDO pattern (Fig. 4.4). **b**, TPTs. **(middle)** Differences between 1999-2014 and 1979-1998 in SSTs from the HadISST data (**c**) and TPTs from MERRA data (**d**). **(bottom) e**, Spatial distribution of linear trends (2001-2014) in SSTs from the HadISST data. **f**, Regressed MERRA TPT trends during 2001-2014 (details in Methods) on the observed PDO index (Fig. 4.4b). Stippling indicates the 95% significance level.

same time, both of them are closely linked to the PDO index in the Natural run (Fig. 4.6). The close relationship between the pair of PCs as well as between each of them and the simulated ENSO and PDO index indicate that, SSTs and TPTs are closely related to each

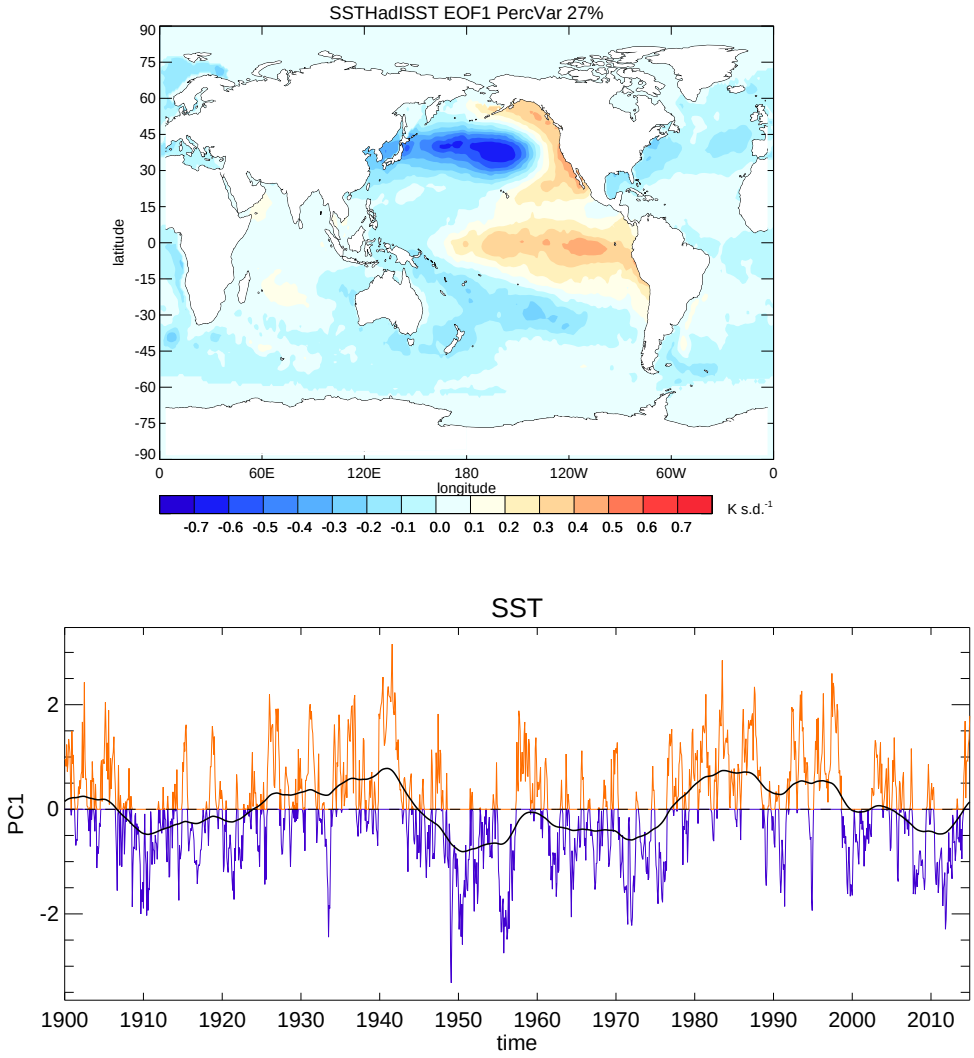

Fig. 4.4 PDO pattern and time series based on an EOF analysis of observed SST anomalies (HadISST), with the global mean removed from 1900 to 2014 between 20°-70°N, and 110°E-100°W region of the North Pacific, which explains 27% of the variance. The principal component time series, given below in normalized units, is regressed on global SST anomalies to provide the map in the top panel. The red and blue colours in the lower part depict the positive and negative PDO-phases. The black curve provides the low-pass (15 years) filtered time series.

other. In particular, the close correlation between both TPT and SST PCs and the simulated index indicate an important role of PDO in the connection between SSTs and TPTs.

The regressed SST anomalies from an EOF analysis, using the same method as suggested by *Deser et al.* (2010) for observations, are applied to simulated SSTs from the Natural run. As shown in Fig. 4.6a, the CESM model captures the PDO pattern relatively well, with a

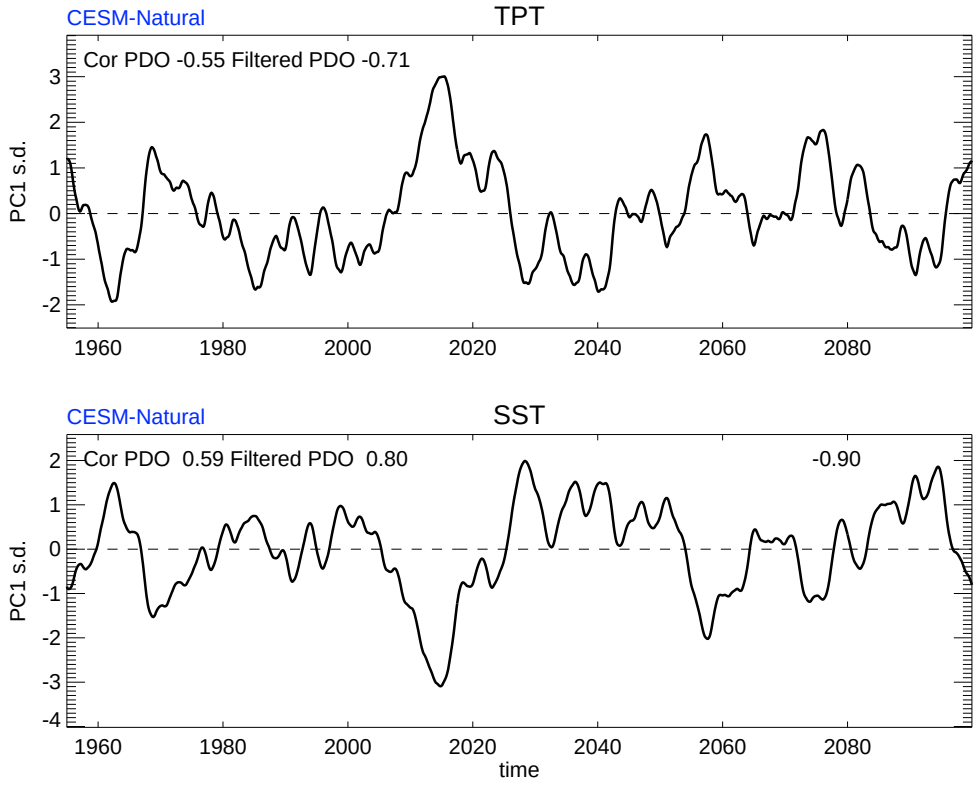

Fig. 4.5 The first pair of PCs from the MCA analysis between tropical (30°S-30°N) tropopause temperatures (**top**) and SSTs (**bottom**). Left side numbers show the correlation between the MCA PCs and the PDO time series as shown in **Fig. 4.6b**. The right side number in the bottom panel indicates the correlation between **a** and **b**.

pattern correlation of 0.72 with the observed PDO pattern (Fig. 4.4). Also shown in Fig. 4.6b is the corresponding EOF PC for the regressed SST pattern as shown in Fig. 4.6a. Again, multidecadal variability can be seen evidently from the time series. This provides confidence for our models simulations in analyzing the relationship between SSTs and TPTs as shown in Fig. 4.3.

A similar link between the two variables is noticed during recent decades when using the observed SSTs (HadISST (*Rayner et al.*, 2003)) and the TPTs from MERRA (Figs. 4.3 c-f). While the period 1979-1998 was characterized by a positive PDO-phase, the period 1999-2014 featured a negative PDO-phase (Fig. 4.4 and *Trenberth et al.* (2014)). The differences between these two time periods (Figs. 4.3 c-d) compare favorably with the patterns extracted from our Natural model run (Figs. 4.3 a-b).

The response of tropopause temperatures to the phase shift of the PDO towards negative conditions could well explain the observed warming of the tropopause since the beginning of

the 21st century (*Wang et al.*, 2013). This is supported by the trends in the observed SSTs and the corresponding MERRA TPTs (Figs. 4.3 e-f). During 2001-2014, the SST showed a negative PDO-like trend pattern, with a very similar TPT pattern as that in Fig. 4.3b. This consistency between observations/reanalysis and model integration suggests that tropical SSTs strongly affect tropical tropopause temperatures. In particular, the recent warming trend observed in tropical TPTs may be a consequence of the PDO-phase change at the end of last century.

To further understand the relationship between the PDO and tropical TPTs, a wavelet analysis (*Torrence and Compo*, 1998) was applied to the first pair of MCA-PCs (Fig. 4.5) that have been used in the above regression analyses. Both, the tropical SSTs and TPTs depict significant decadal to multidecadal variability with periods of 21 and 50 years (Fig. 4.7). These periods are consistent with the well known periodicities of the PDO (*Deser et al.*, 2010). The short observational and model records, however, introduce uncertainty concerning in particular multidecadal timescales.

4.3.3 Mechanism

To elucidate the mechanism for the connection between tropical TPTs and SSTs, a composite analysis of selected variables was performed based on positive and negative PDO-phases from the Natural model run (see PDO-phases in Fig. 4.6). During the negative PDO-phase, near surface (850 hPa) winds are enhanced and indicate a strengthening of the Walker Circulation over the equatorial Pacific, which is associated with anomalously cold equatorial Pacific SSTs due to enhanced equatorial upwelling of water from subsurface levels. The stronger Walker Circulation results in less frequent deep convection in the tropical central Pacific and more frequent deep convection in the Western Pacific (Fig. 4.8b). At the same time, anomalously warm SSTs and anticyclonic low-level circulation anomalies appear over the North Pacific (Fig. 4.8a). Along with the weakened Aleutian low in the North Pacific (Fig. 4.8c), there is less deep convection in the Northeast and enhanced deep convection in the Northwest Pacific (Fig. 4.8b).

The weaker Aleutian low generally interferes negatively with the climatological, stationary wave structure and weakens the climatological-mean stationary waves. Such negative interference dampens the upward and poleward planetary wave propagation into the high-latitude extratropical stratosphere (see the composite differences in the Eliassen-Palm flux (E-P flux), Fig. 4.9). This in turn leads to a less wave-disturbed and stronger polar vortex (Fig. 4.8c) (*Hurwitz et al.*, 2012; *Ineson and Scaife*, 2009). The strengthened polar vortex contributes to a weaker lower-stratosphere Brewer-Dobson circulation (Fig. 4.8d), according to the momentum budget (*Andrews et al.*, 1987). The reduced vertical motion shown in Fig.

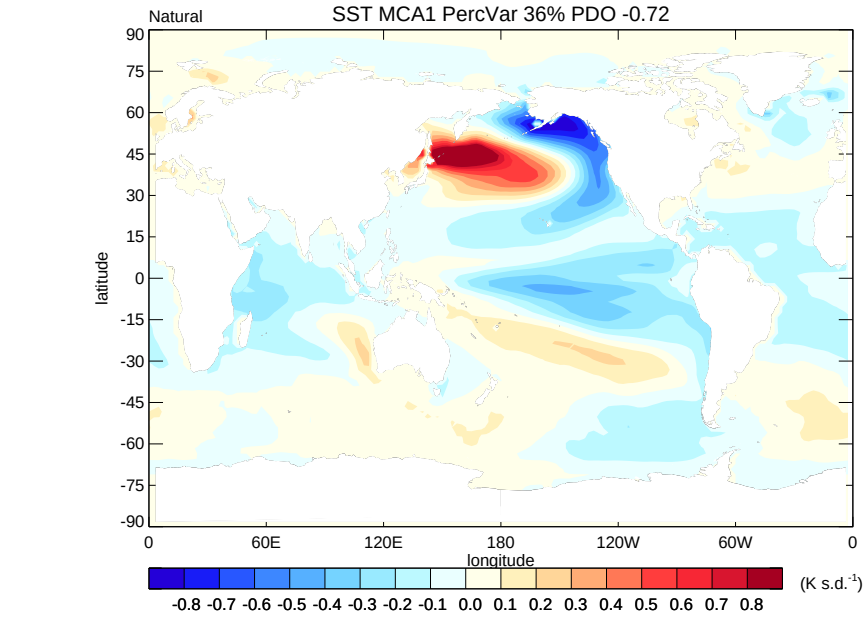

(a)

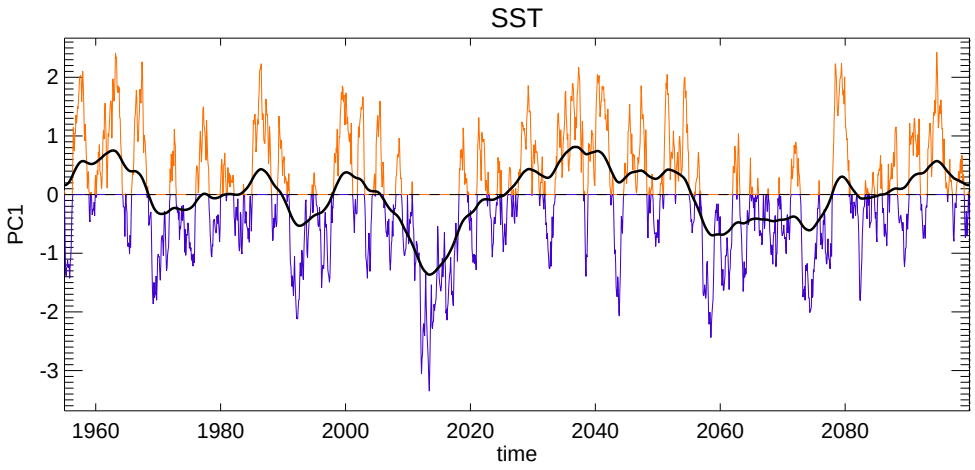

(b)

Fig. 4.6 PDO pattern and time series from EOF analysis as in Fig. 4.4, but for the Natural model experiment. The PDO accounts for 36% of the SST variances in the model, and its correlation with the PDO pattern in HadISST (Fig. 4.4a) is 0.72.

4.8d in the equatorial upper troposphere and lower stratosphere indicates a weaker Hadley circulation in the upper tropical troposphere, and also a result combined with the weaker Brewer-Dobson circulation in the tropical lower stratosphere. Recall to the thermodynamic balance equation (1.2) in Chapter 1, the reduced vertical motion leads to the warming around

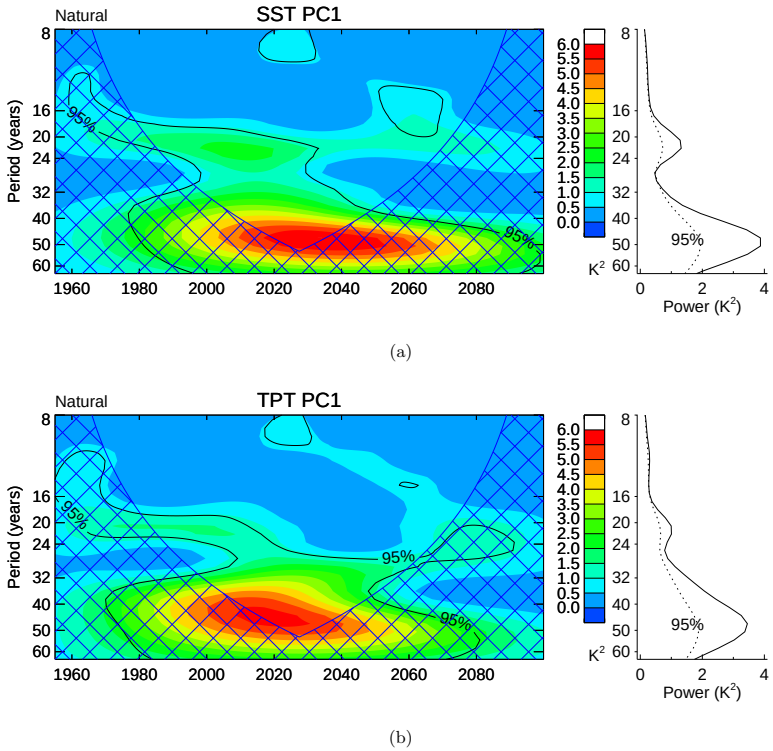

Fig. 4.7 Wavelet analysis of the first pair of MCA-PCs from the Natural run (see time series of MCA-PCs in Fig. 4.5). **a**, SSTs. **left**, Power distribution due to time and periods. The black contour line indicates the regions above 95% confidence, Cross-hatched regions on either end indicate the "cone of influence", where edge effects become important. **right**, The time-averaged power with different periods. The dotted line indicates the 95% level of confidence. **b**, As in **a**, but for TPTs.

the tropical tropopause at around 18 km, which is strongest between 15°N and 15°S (Fig. 4.8d).

The different analyses described above are based on one single run with the CESM-WACCM including a repeating 11-year solar cycle. Since such external forcing can produce or enhance decadal to multidecadal variability in climate models (*Park and Latif*, 2012), we repeated the analysis with data from a companion simulation in which solar forcing was set constant (SolarMean, see a detailed description in Chapter 3). The results from the SolarMean experiment are in very good agreement with the above results from the Natural run. This especially applies to the MCA of SST with TPT anomalies as shown in Fig. 4.10. Only the multidecadal peaks in the wavelet spectra of leading MCA-PCs are shifted to slightly longer periods (24 and 60 years), which may indicate the involvement of solar

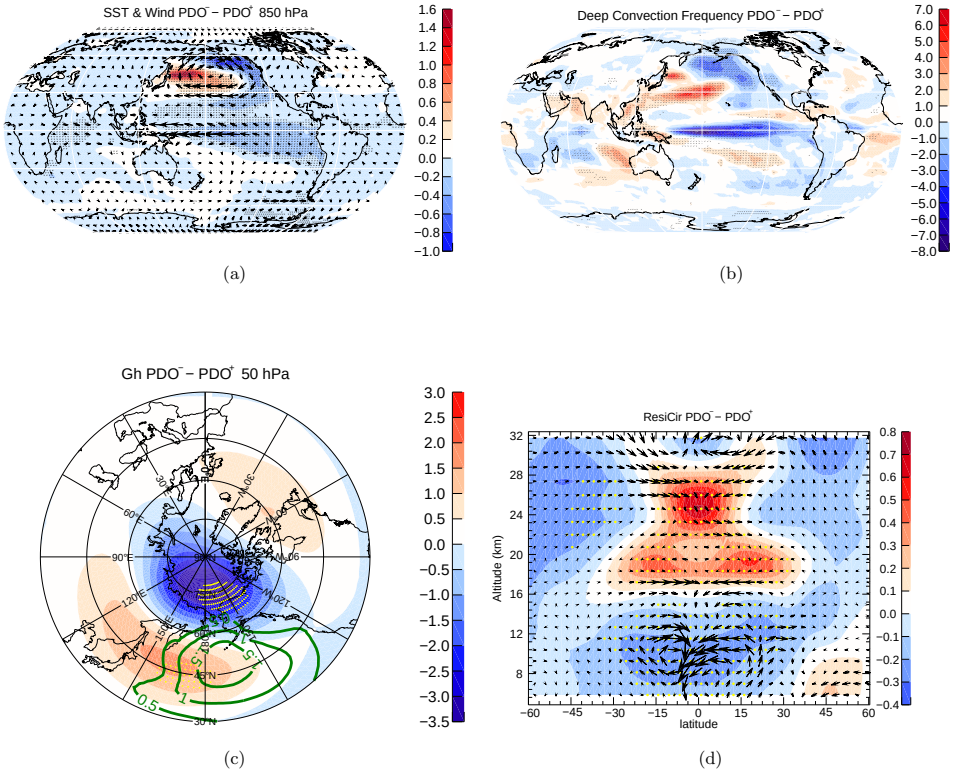

Fig. 4.8 Composite differences between negative and positive PDO-phases from the Natural run. **a**, Mean differences for SSTs (colours) and near surface (850hPa) wind speeds (arrows). **b**, Mean differences for fractions of deep convection. **c**, Mean differences for sea level pressures (green contour lines) and geopotential heights (colours) in the middle stratosphere (50 hPa) in the northern hemisphere (30°-90°N). **d**, Latitude-altitude cross section for differences in the residual mean meridional circulation (arrows, scaled with the square root of pressure, a direct diagnosis of meridional transport which combines contributions of eddy and mean transport, calculated from the Transformed Eulerian Mean (TEM) diagnostics) and temperature differences (colours). Stippling in **a-d** indicates 95% significance level.

forcing in modulating the time scales of the coupled ocean-atmosphere interaction, but this does not affect the mechanism for PDO-TPT influences.

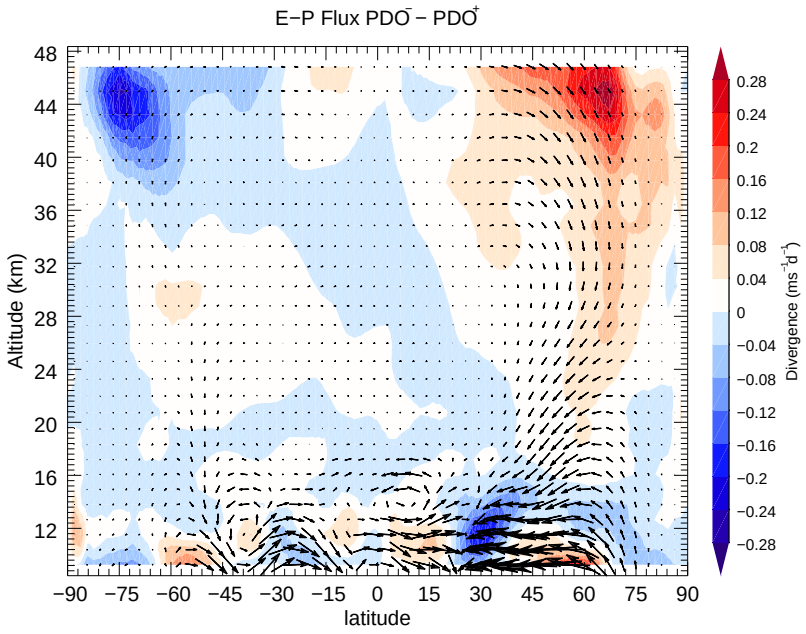

Fig. 4.9 Latitude-altitude cross section for differences between negative and positive PDO-phases in the E-P flux (arrows, scaled with the square root of pressure) as well as its divergence (colours). The EP flux vector describes the strength and propagation direction of planetary waves, while its divergence describes the interaction of planetary waves with the mean flow.

4.4 Conclusions and outlook

In summary, recent trends in tropical tropopause temperatures between 1979 and 2014 show a slight decrease between 1979 and 2000, and a statistically significant increase since 2001. We attribute this multidecadal variability in TPTs to the shift of the Pacific Decadal Oscillation from its positive to its negative phase (Fig. 4.4). This PDO-phase shift around the turn of the millennium has also been confirmed in other studies, both at the surface, e.g., as expressed by the global warming hiatus (*England et al.*, 2014; *Trenberth et al.*, 2014) and in the lower stratosphere, e.g. as the hiatus in the acceleration of the Brewer-Dobson circulation (*Aschmann et al.*, 2014). Recent studies with short data sets (*Dessler et al.*, 2014; *Hegglin et al.*, 2014) cannot detect significant long-term trends in stratospheric water vapour, but find clear decadal variability in agreement with the results from our model experiments (Fig. 4.11).

We suggest that tropical tropopause temperatures, which have a control on stratospheric water vapour, are influenced by decadal to multidecadal variability in Pacific SSTs. The

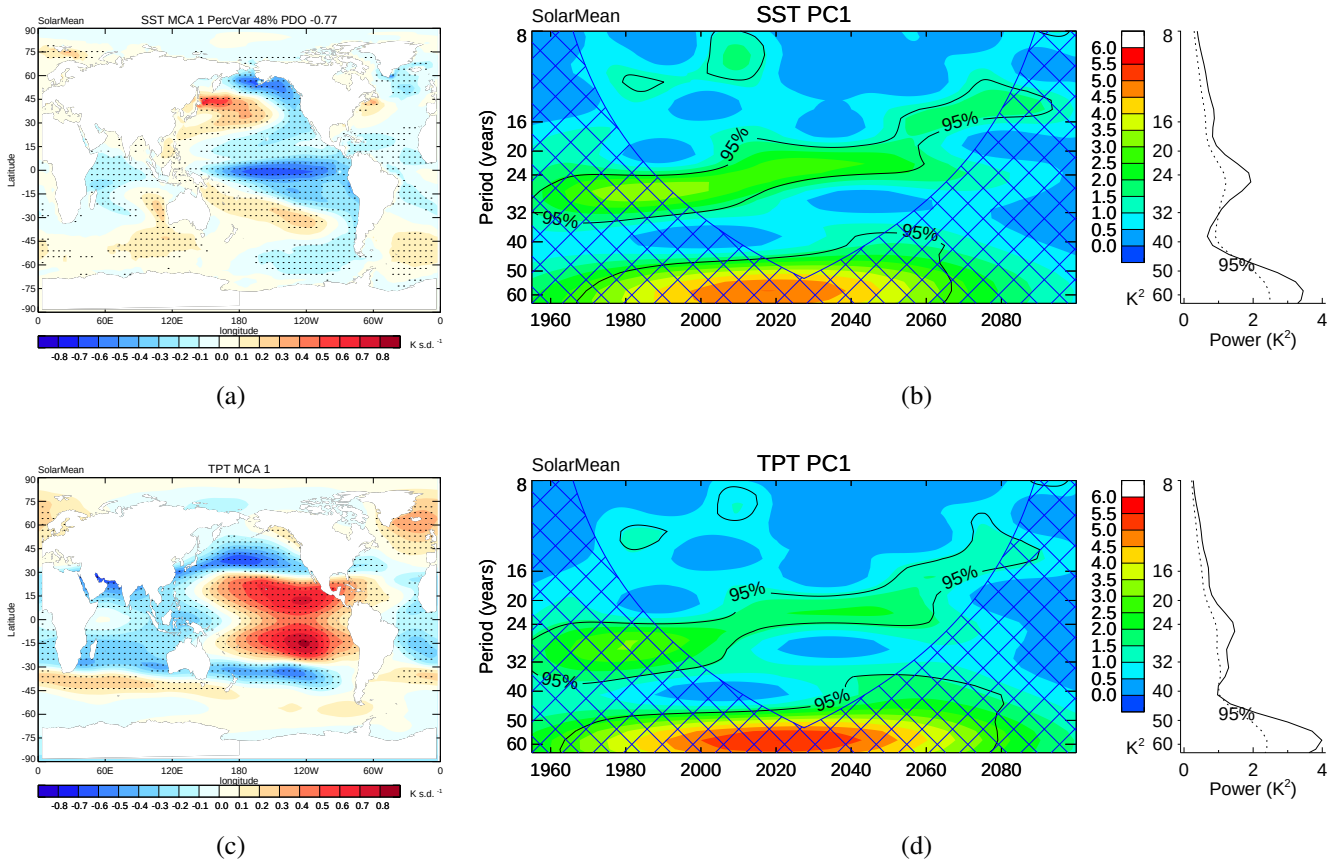

Fig. 4.10 MCA and wavelet analysis of tropical SSTs and TPTs. **a, c**, same as in **Figs. 4.3a, 4.3b**, but for the **SolarMean** model experiment. **b, d**, same as in **Figs. 4.7a, 4.7b**, but for the **SolarMean** model experiment.

PDO-like SST patterns modulate tropical tropopause temperatures via Walker, Hadley, and Brewer-Dobson circulation changes. The PDO-phase may therefore provide a useful indicator for tropopause and lower stratosphere decadal to multidecadal temperature and water vapour variability. Further, there is also evidence of multidecadal modulation in stratospheric circulation variability (e.g. the strength of the polar vortex) by the Atlantic Multidecadal Variability (*Omrani et al.*, 2014). The importance of such "bottom-up" mechanisms for stratospheric dynamics and chemistry is still controversially discussed. Whether and how these stratospheric changes feed back to the ocean awaits further studies.

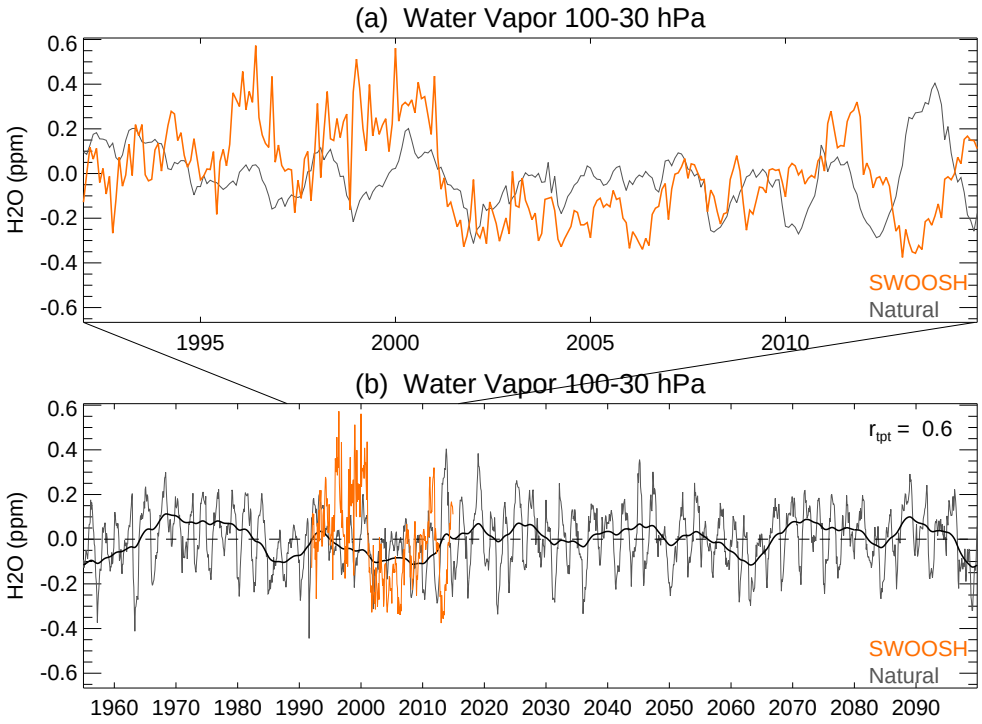

Fig. 4.11 Deseasonalized anomalies of tropical (20°S-20°N) lower stratospheric water vapour from the SWOOSH (Stratospheric Water and Ozone Satellite Homogenized data set, http://www.esrl.noaa.gov/csd/groups/csd8/swoosh/) data (orange) and the Natural simu-lation (grey). **a**, Recent decades (1992-2014), and **b**, Long-term (1955-2099) variations. The thick black line in **b** is low-pass filtered (15 years) data of the Natural run. Influences from volcanic aerosols have been removed by a linear regression. $r_{tpt} = 0.6$ is the corre-lation between the low-pass filtered lower stratospheric water vapour and tropical tropopause temperature (Fig. 4.2b) from the Natural run.

Chapter 5

Decadal variability of lower stratospheric water vapour: links to the solar cycle and sea surface temperatures

5.1 Introduction

As described in Chapter 1, water vapour is one of the most important stratospheric trace gases. The long-term trends in lower stratospheric (LS) water vapour are of great interest but have not been understood and quantified to date. Clear decadal variability in LS water vapour has been noticed from both model and observational studies (*Dessler et al.*, 2014; *Fueglistaler et al.*, 2013; *Hurst et al.*, 2011). Recently, this decadal variability in LS water vapour has been linked to the 11-year solar cycle (*Schieferdecker et al.*, 2015) with a time lag of about 2 years. An explanation for this behavior and its physical mechanism, however, is still not well understood.

LS water vapour is mainly controlled by the CPT, since it freeze-dries while crossing the tropopause (*Fueglistaler et al.*, 2009; *Randel and Jensen*, 2013). Chapter 4 shows an evidence of the decadal to multidecadal variability in the tropical TPTs and connected this decadal to multidecadal variability to the PDO. While the atmosphere has only a relatively short memory, long-term variations of the climate system are mostly related to the ocean which has a long-term memory due to its large heat capacity. This implies that SSTs may play an important role in modulating the decadal to multidecadal variability of water vapour in the lower stratosphere.

This chapter is a direct extension to Chapter 4, which investigates the decadal variability of LS water vapour by using merged-satellite observations and reanalysis data as well as

model simulations. A special focus of this chapter is to link LS water vapour to the 11-year solar cycle and modes of sea surface temperatures (SSTs), i.e., the variability in combination with ENSO and PDO.

5.2 Data, model simulations and methods

5.2.1 SWOOSH and MERRA water vapour data

The Stratospheric Water and OzOne Satellite Homogenized (SWOOSH) data set is a merged record of stratospheric ozone and water vapour measurements taken by a number of limb sounding and solar occultation satellites over the previous 30 years. The SWOOSH record spans the period from 1984 to 2014 and comprises data from the SAGE-II/III, UARS HALOE, UARS MLS, and Aura MLS instruments, with large amount of missing values in the data before 1991 (since 1991 the HALOE data is available). The vertical pressure range of SWOOSH data for H2O has 31 pressure levels, from 316 to 1 hPa. The measurements are homogenized by applying corrections that are calculated from data taken during time periods of instrument overlap. For further details, see http://www.esrl.noaa.gov/csd/groups/csd8/swoosh/usersguide.pdf.

The Modern Era Retrospective-Analysis for Research and Applications (MERRA) reanalysis water vapour data, with full vertical resolution (72 vertical levels, about 1 km resolution in the upper troposphere and lower stratosphere (UTLS)), is used as well (*Rienecker et al.*, 2011). The MERRA temperature data is in good agreement with observations in the UTLS, and has been widely used in trajectory simulations for stratospheric water vapour (*Fueglistaler et al.*, 2013; *Schoeberl and Dessler*, 2011; *Schoeberl et al.*, 2012). MERRA assimilates water vapour data from both, the HALOE and the MLS instruments (*Rienecker et al.*, 2011). However, the MERRA stratospheric water vapour data has been rarely used in previous studies. We start with a short validation of the MERRA water vapour data by comparison with the SWOOSH data in section 5.3.

5.2.2 Model simulations

Same as in Chapter 4, the CESM Natural and SolarMean runs, which cover the period from 1955 to 2099 as listed in Chapter 3, are analyzed in this chapter. The Natural run employs all natural forcing agents including spectrally resolved solar variability, a fully interactive ocean, volcanic aerosols and a nudged QBO, while the SolarMean run uses constant solar irradiance values averaged over the past 4 observed solar cycles. An overview of all CESM simulations and details of all external forcings can be found in Chapter 3.

5.2.3 Canonical correlation analysis (CCA)

The CCA is useful for exploring relationships between two time varying fields and for finding projections of the data onto coherent patterns with maximum correlation. Although physical interpretation of the CCA modes requires additional physical knowledge (*Wilks*, 2011). The CCA between tropical (30°S-30°N) lower stratospheric (85 hPa) water vapour and SSTs is achieved by singular value decomposition of the temporal correlation matrix, using equal area weighting (square root of cosine of latitude). The pairs of singular vectors describe the spatial patterns of each field. The PCs of water vapour and SST are obtained by projections on the corresponding patterns. The global pattern of SSTs and water vapour, can be obtained by regressions on the PCs of water vapour and SST, respectively. Note that the data are low-pass filtered (6 years), since we focus on decadal to multidecadal variability, and influences from volcanic aerosols are removed by a linear regression before applying the CCA.

5.3 Recent variability of LS water vapour

As discussed in previous studies, MERRA data shows high quality temperatures around the tropical tropopause, in both its climatological values and its interannual variability (*Schoeberl et al.*, 2012; *Wang et al.*, 2015b). However, MERRA water vapour data, especially in the stratosphere to our knowledge has not been evaluated so far. Fig. 5.1a shows the normalized time series of tropical (20°S-20°N) LS water vapour anomalies from both SWOOSH (1984-2014) and MERRA (1979-2014) data. In general, the MERRA data shows relative good agreement with the SWOOSH data with respect to the interannual variability of LS water vapour, as well as in the decadal variability, i.e. an evident drop around 2001 and an increase thereafter. Without normalization, LS water vapour variations in MERRA are less than in the SWOOSH data (not shown, with discrepancies larger at higher levels), which might be due to the slower tropical upward motion of the Brewer-Dobson circulation (BDC) in MERRA compared to other observations (*Schoeberl et al.*, 2012). Despite the differences in absolute values between MERRA and SWOOSH data, MERRA provides a useful data set of LS water vapour, with high horizontal and vertical resolution and relatively long time span from 1979 to 2014, which allows us to investigate decadal variability of LS water vapour.

Fig. 5.1b also gives the power spectrum of MERRA tropical LS water vapour anomalies for the period of 1979-2014, which is computed by a FFT. Tropical LS water vapour shows strong interannual variability with two significant peaks at about 2-3 years, which is related to interannual ENSO and QBO variability. Another statistically significant peak can be found at around 10 years, which indicates decadal variability in tropical LS water vapour in agreement with previous studies (*Dessler et al.*, 2014; *Fueglistaler et al.*, 2013; *Hurst et al.*, 2011).

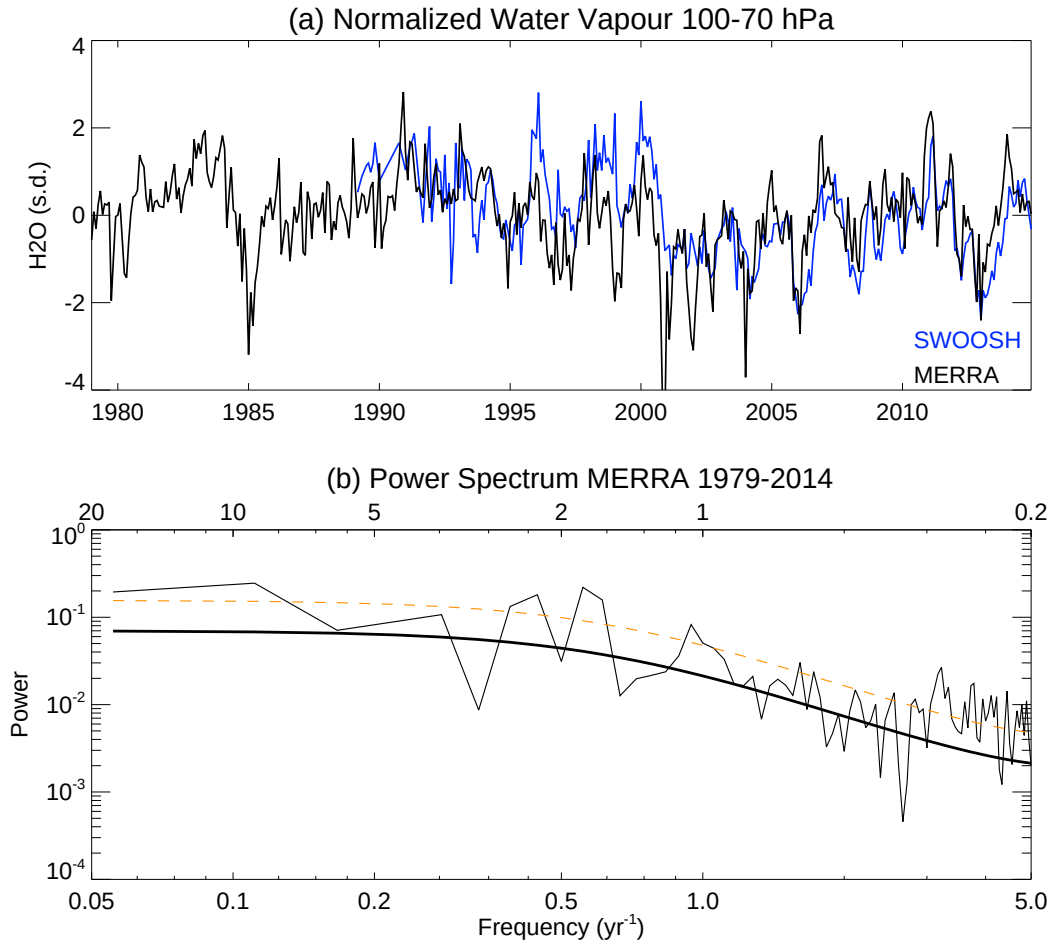

Fig. 5.1 **a**, Time series of normalized tropical LS water vapour anomalies from SWOOSH (1984-2014, blue) and MERRA (1979-2014, black) data. The seasonal cycle has been removed. **b**, Power spectrum of the MERRA water vapour time series in **a**, by a Fast Fourier Transform (FFT) approach. Thick black line indicates the best fit based on a first-order autoregressive model, and dashed red line indicates the 95% confidence level.

Beside the zonal mean, the spatial distribution of LS water vapour is also important, since it is strongly controlled by the spatial structure of the tropopause temperature and therefore a useful indicator for the LS response to the surface (*Fu*, 2013; *Garfinkel et al.*, 2013a). Fig. 5.2 shows the spatial distribution of the LS (85 hPa) water vapour climatology and standard deviations of monthly anomalies (1992-2014) from data of SWOOSH, MERRA, as well as our two CESM-WACCM simulations (Natural and SolarMean). The lowest water vapour concentration together with the highest standard deviations in the tropics appear over

the Indo-Pacific warm pool (IPWP), where the strongest convection and coldest tropopause temperatures can be found. Such zonal asymmetry of LS water vapour as well as its standard deviation can be seen in both SWOOSH and MERRA data, and also in our model simulations. While the CESM model simulates comparable standard deviations with the SWOOSH data, MERRA data shows less standard deviations, which is consistent with weak interannual variability in MERRA as described above. Though there are some biases in both MERRA and model simulations compared with the SWOOSH data, e.g. the low LS water vapour belt in the tropics is too narrow in MERRA (might also be due to the weak BDC in MERRA), MERRA and our model can generally capture the spatial pattern in the tropics and are suitable to study LS water vapour variability.

As described above, there are also zonal asymmetries in tropopause temperature and LS water vapour variability (*Fu*, 2013; *Garfinkel et al.*, 2013a). A zonal average diminishes the anomalies within different areas and may not be the best indicator of LS water vapour variability, especially while quantifying the relative contributions due to different processes. Here we applied an Empirical Orthogonal Function (EOF) analysis to the tropical (30°S-30°N) water vapour deseasonalized anomalies at 85 hPa. The data has been area weighted by the square root of cosine of latitude. As shown in Fig. 5.3a, there are two negative areas over the IPWP and South America in the 1st EOF pattern, which is similar to the climatological distribution of LS water vapour and its standard deviations (Fig. 5.2). Different to the 1st EOF, the second EOF shows obvious zonal asymmetry (Fig. 5.3b). While a positive pattern exists over the central Pacific, the Indian Ocean shows two negative belts in the tropics. This zonal asymmetry pattern may be related to the redistribution of sea surface temperatures (SSTs) and subsequent atmospheric circulation changes, which will be further discussed in section 5.4.1.

The corresponding PCs for the two modes above are shown in Fig. 5.3c and 5.3d. PC1 represents the most of tropical LS water vapour variability over recent decades (Fig. 5.1a), while PC2 contributes to some of the aspects. In particular, clear decadal to multidecadal variability can be seen in both PCs after applying a low-pass (6 years) filter. Because we are focusing on the decadal variability in this study, another EOF analysis was applied to the low-pass (6 years) filtered tropical LS water vapour. The results (not shown), in both the EOF patterns and PCs, are quite similar to what we show in Fig. 5.3. Hereafter, without any special notice, we will do further analyses based on low-pass (6 years) filtered data.

Multiple linear regression (MLR) has been widely used to explain LS water vapour variability (e.g. *Dessler et al.*, 2014; *Schieferdecker et al.*, 2015). Here we apply the MLR to the first 2 EOF-PCs of the tropical LS water vapour. Before applying the MLR, lagged correlations were calculated to identify possible connections between different predictors and

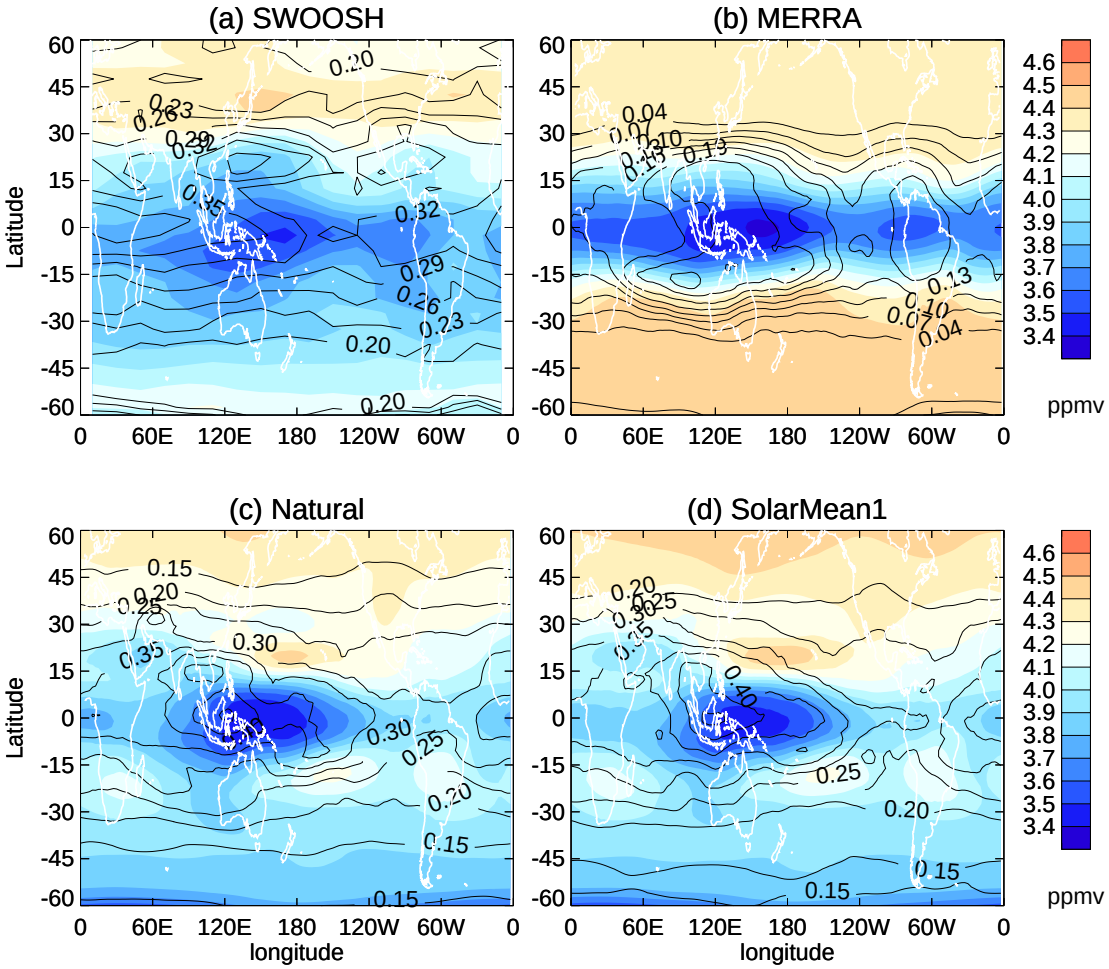

Fig. 5.2 Spatial distribution of the 85 hPa water vapour climatology (colour) and standard deviations (black contour lines) for the period of 1992-2014. Standard deviations are calculated from deseasonalized monthly anomalies. **a**, SWOOSH; **b**, MERRA; **c**, CESM Natural run and **d**, SolarMean run.

LS water vapour, and to investigate possible time lags for the different factors. The predictors we considered include the ENSO, the QBO, the vertical velocity ($\overline{w}^*$) of the BDC at 100 hPa, solar cycle variability (Solar) and stratospheric aerosols (SAD) as suggested by previous studies (e.g. *Dessler et al.*, 2014; *Randel and Wu*, 2015; *Schieferdecker et al.*, 2015), as well as the PDO index which may have strong influences on decadal to multidecadal variability of tropopause temperatures (*Wang et al.*, 2015b).

The ENSO index is the 1st EOF-PC of monthly global sea surface temperature (SST) anomalies (deseasonalized and detrended) as suggested by *Deser et al.* (2010). The observed SSTs used in this study are the Hadley Centre SSTs (HadISST, 1900-2014 for this study)

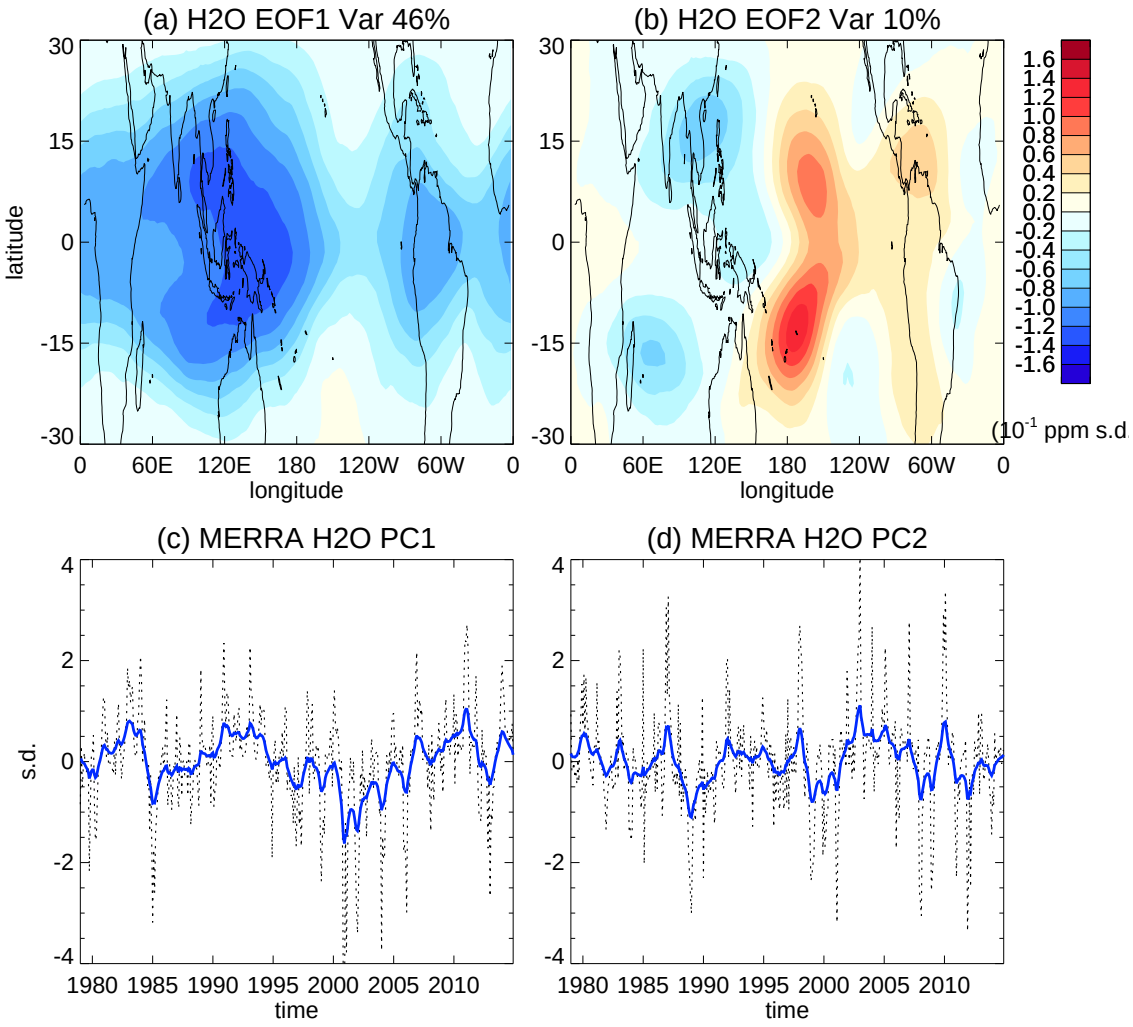

Fig. 5.3 **(Top)** Regression of tropical (30°S-30°N) water vapour anomalies at 85 hPa on the first 2 EOF-PCs (bottom) from the MERRA data. **(Bottom)** The first two PCs (dotted black lines) of an EOF analysis for the tropical (30°S-30°N) water vapour anomalies at 85 hPa. The long-term trend and the annual cycle have been removed before the EOF analysis. Thick blue curves indicate the low-pass (6 years) filtered time series.

(*Rayner et al.*, 2003). The QBO variations are usually represented by a pair of orthogonal time series QBO1 and QBO2, which can be constructed by an EOF analysis of the equatorial zonal winds over 70-10 hPa (*Randel et al.*, 2009). We use the observed QBO2 (data from the FU Berlin: http://www.geo.fu-berlin.de/en/met/ag/strat/produkte/qbo/index.html) in this study, which is the dominant mode of the QBO in the tropical lower stratosphere. The vertical component of the BDC is calculated from the Transformed Eulerian Mean (TEM) diagnostics (*Andrews et al.*, 1987) from MERRA data. The solar cycle is based on monthly values of the F10.7 index (10.7 cm solar radio flux) from National Oceanic and Atmospheric

Administration (NOAA)'s Space Environment Center (www.sec.noaa.gov). We use the aerosol data set which has been constructed for the CCMI project (ftp://iacftp.ethz.ch/pub_read/luo/ccmi/) and is similar to the data described by *Solomon et al.* (2011). The PDO index is the 1st EOF-PC of North Pacific (20°-70°N) SST anomalies (deseasonalized, detrended and with global mean extracted) as suggested by *Deser et al.* (2010). All factors described above are available for the period 1979-2014.

Fig. 5.4a shows lagged correlations between different factors and the first PC of LS water vapour with different time lags. As addressed in the introduction, LS water vapour is controlled by TPTs. TPTs show a very high correlation of 0.9 with the 1st EOF-PC of LS water vapour. SAD and $\overline{w}^*$ show also both relative large correlations with the 1st PC, which are 0.52 and -0.47, respectively. ENSO and QBO2 show relative low correlations (about 0.2) with time lags of 5 and 2 months (this means ENSO and QBO are leading LS water vapour of 5 and 2 months, not shown), respectively. These time lags are in general consistent with previous studies (*Marsh and Garcia*, 2007, e.g.). Note that LS water vapour has been low-pass filtered before applying the EOF analysis (see above), which is the reason of the relative low correlations of ENSO and QBO . Without any low-pass filter, the correlations of ENSO and QBO are a little higher (about 0.3). Solar and PDO show very low correlations with the first PC (less than 0.1, not shown) at any time lags.

The lagged correlations between different factors and PC2 of LS water vapour are also shown in Fig. 5.4b. Different from PC1, PC2 shows high correlations of -0.63, -0.57 and -0.48 with Solar, ENSO and PDO, respectively. This indicates that PC2 is mainly an indicator of decadal variability of tropical LS water vapour. It is very interesting that the Solar is leading the LS water vapour by about 3 years. This confirms the results by *Schieferdecker et al.* (2015), which also find a time lag between solar cycle and LS water vapour. However, the time lag of about 3 years we found is a little different with their results of about 25 months. This difference in time lag may be due to our EOF analysis instead of using zonal mean water vapour in *Schieferdecker et al.* (2015). Additionally, the relative short time observations (36 years in our study and 22 years in *Schieferdecker et al.* (2015)) may cause uncertainties in estimating the exact time lag. Also interesting is the correlation with the PDO. As discussed by *Wang et al.* (2015b), a positive PDO-phase indicates warmer SSTs in the equatorial Pacific associated with a weaker Walker Circulation, which leads to more convection and colder tropopause temperatures over the central Pacific, and therefore results in less water vapour transport across the tropopause. However, this negative correlation between PDO and LS water vapour achieves its maximum while the water vapour is leading the PDO of several months. This gives a hint for potential feedback of LS water vapour to surface climate.

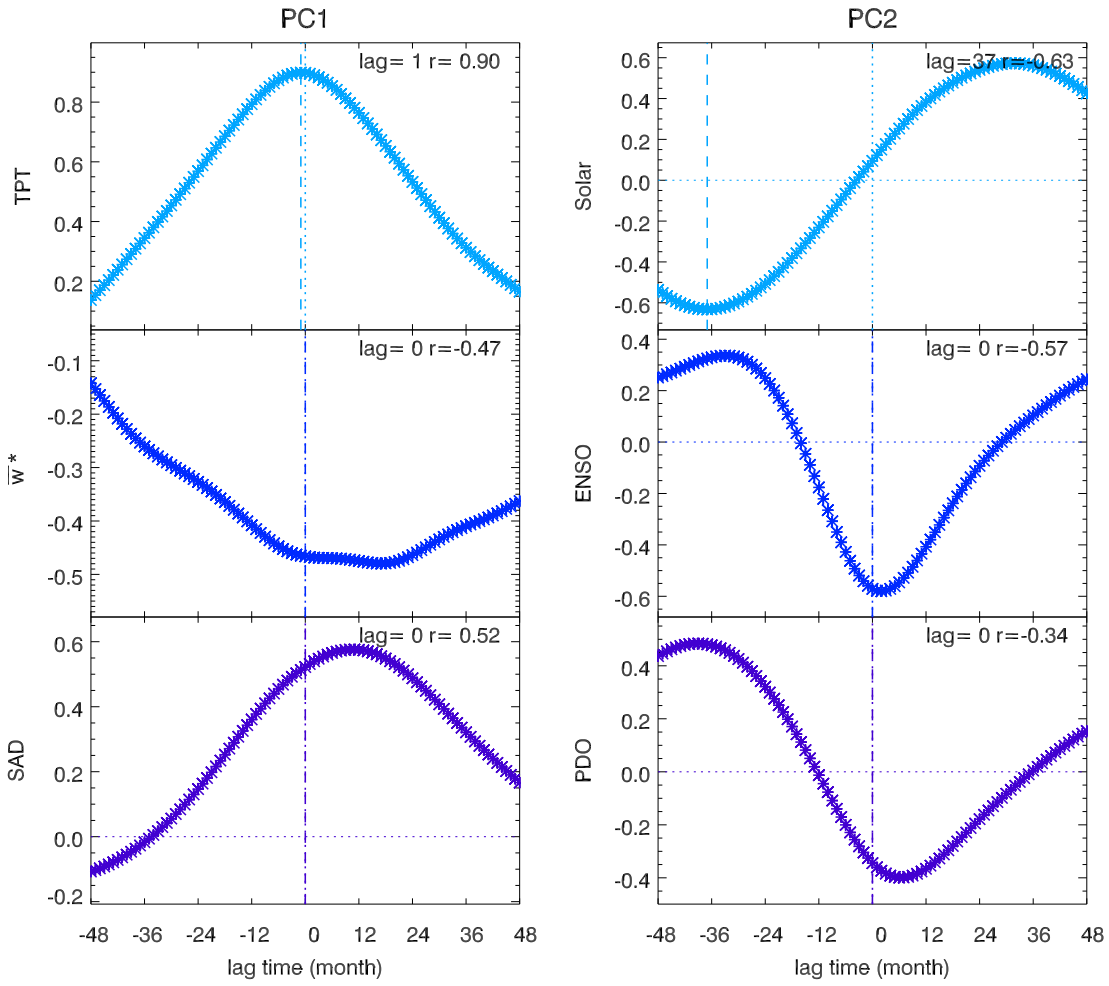

Fig. 5.4 Lag correlations between different predictors and the first 2 EOF-PCs of MERRA LS water vapour with different time lags. The LS water vapour before the EOF and the time series of predictors before doing the correlation have been low-pass (6 years) filtered. **a**, TPT, $\overline{w}^*$ and SAD with PC1. **b**, Sloar, ENSO and PDO with PC2. Negative lag times mean the factors are leading the PCs. The time lag as well as the value of the maximal correlation are marked on the top right corner of each panel. The horizontal and vertical pointed lines indicate the zero correlation and zero time lag lines, respectively. The vertical dashed lines mark the time lag of each maximal correlations. Since this study is mainly attribute LS water vapour variations to different predictors, the maximal corrections are only marked while the predictors are leading the LS water vapour.

Now we start to attribute the 1st PC of tropical LS water vapour variability to different predictors in a MLR. Fig. 5.5a shows time series of the 1st PC of tropical LS water vapour, the regressed contributions by different factors, as well as the residuals. Proper time lags

were used for each factor based on the lagged correlations in Fig. 5.4. Five and two month lags were used for ENSO and QBO2, respectively, while no time lag were used for $\overline{w}^*$ and SAD. The solar signal has been tested with different time lags (0-22 months), which has little contribution. Here we only present the result without the solar term for PC1.

The 1st PC shows obvious decadal to multidecadal variability beside the interannual variability, i.e. a slight drop around 1985, a peak around 1991 due to the Pinatubo eruption, a deep drop around 2001 and an increase afterwards. This is consistent with previous studies (*Dessler et al.*, 2014; *Hegglin et al.*, 2014; *Schieferdecker et al.*, 2015), though they used different LS water vapour data sets. This confirms the suitability of the MERRA data for studying the LS water vapour and our low-pass filtered EOF analysis to investigate the decadal variability.

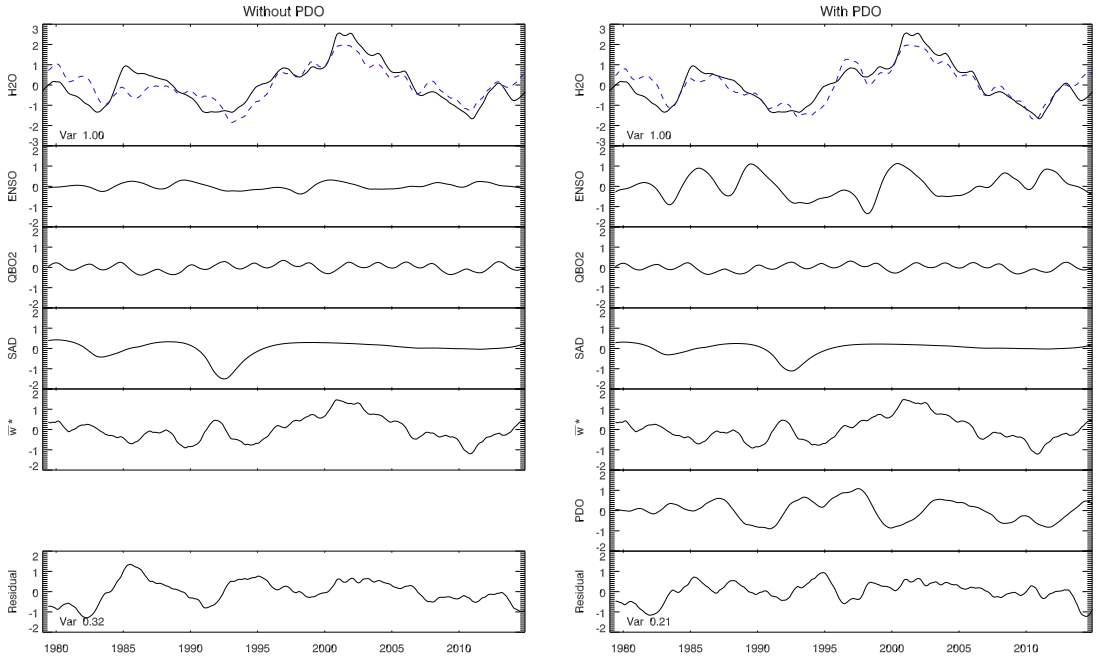

(a) (b)

Fig. 5.5 Time series of the 1st EOF-PC of low-pass (6 years) filtered tropical LS water vapour from MERRA data (top, black line), the regressed water vapour with all factors (top, dashed blue line), contributions of different factors, as well as the residuals (bottom). **a**, Without PDO and **b**, with PDO included. The whole regression and the regression for each factor are all over 95% significance.

The high values after 1991 are closely related to the Pinatubo eruption as seen in the regressed SAD term. The steep drop around 2001 can be relatively well explained by ENSO and $\overline{w}^*$, and the increase after 2001 can be partly explained by $\overline{w}^*$. However, the drop around

1985 can not be well regressed by these factors, which can be clearly seen in the residual. The variance of the residual is relatively small, which means that the MLR with ENSO, QBO2, $\overline{w}^*$, SAD and solar can generally well explain the decadal to multidecadal variability in LS water vapour except the negative anomalies around 1985. Fig. 5.5b shows a similar regression but with the PDO as regressor included. This time the drop around 1985 and the increase after 2001 can be better reconstructed, and the residual is significantly reduced. This indicates that the PDO plays an important role for multidecadal variability of LS water vapour.

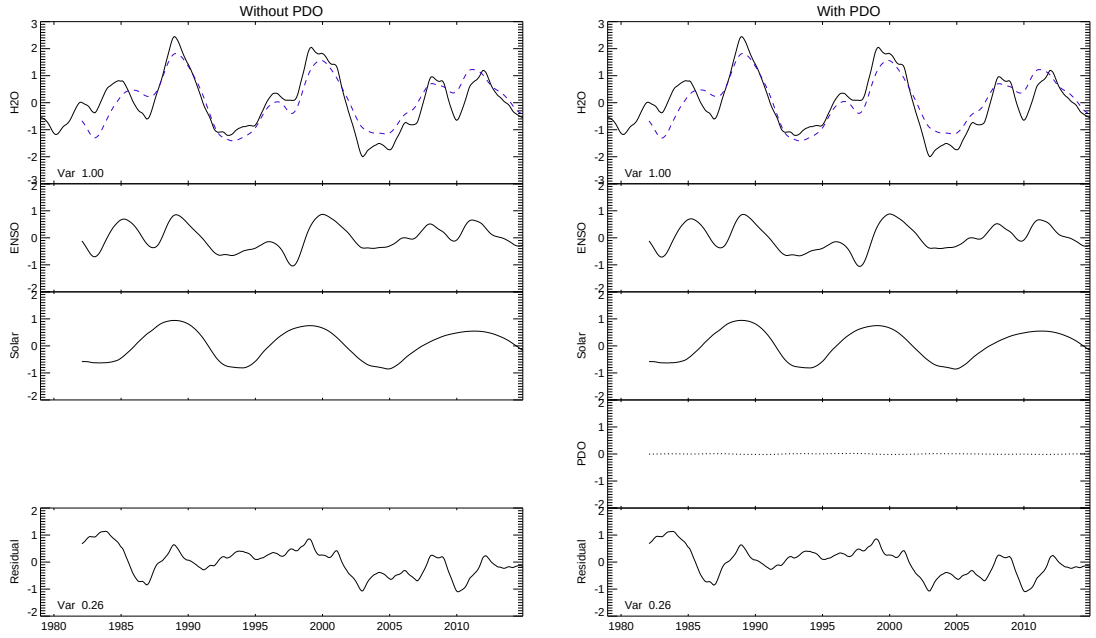

(a) (b)

Fig. 5.6 Same as Fig. 5.5, but for PC2. The regression of PDO in **b** is not significant (shown as dotted line).

Fig. 5.6 shows the MLR analysis for the 2nd PC. In contrast to PC1, PC2 shows a clear decadal variability. The 2nd PC can be well explained by ENSO and the solar cycle, with a time lag of 37 months for the solar term. Note that, as discussed above, the time lag between solar and LS water vapour is different from previous studies (*Schieferdecker et al.*, 2015). A similar result can be found when taking a time lag of 25 months in the solar term for the MLR. The variance of the residuals will be 0.33 with a lag of 25 months compared to a 0.26 of variance with a lag of 37 months (not shown). The short observational time period (36 years in our study and 22 years in *Schieferdecker et al.* (2015)), makes it very difficult to detect the exact time lag between the solar cycle and LS water vapour.

In summary, the 1st PC of LS water vapour, which is a mixture of interannual to multidecadal variability, is mainly dominated by a combined effect of SAD, $\overline{w}^*$, ENSO and PDO. Whereas the 2nd PC depicts decadal variability of LS water vapour, and is determined by decadal variability of ENSO and the 11-year solar cycle.

5.4 Links to the solar cycle, SSTs and tropopause temperatures

5.4.1 Links to SSTs

From the discussions above, it is obvious that there is decadal to multidecadal variability in tropical LS water vapour. Since the atmosphere has only a short memory, it performs small decadal to multidecadal variability due to internal processes. And therefore, an atmosphere-ocean coupling is needed to explain the decadal to multidecadal variability. The CCA, as described in section 5.2.3, was used to detect possible connections between LS water vapour and SSTs.

Figs. 5.7a and 5.7b show the regressed patterns of observed SST and MERRA LS water vapour anomalies on the corresponding time series of the first CCA mode (Figs. 5.7c and 5.7d). The SST anomalies are reminiscent of the negative ENSO/PDO phase, with cold SST anomalies in the tropical Pacific and warm SST anomalies in the North Pacific. The pattern correlation with the ENSO/PDO derived from observed SSTs amounts to -0.69/-0.47 (see observed ENSO/PDO patterns *Deser et al.*, 2010). This ENSO/PDO like pattern is accompanied with more water vapour over the tropical and subtropical east and central Pacific and less over the Indian Ocean, especially over the IPWP region.

The corresponding pair of CCA-PCs is shown in Fig. 5.7c and 5.7d. The 1st CCA-PC of water vapour is a clear combination of the first two EOF-PCs as shown in Fig. 5.3c and 5.3d. It is closely correlated to the 1st SST CCA-PC, with a correlation of 0.66. This confirms again the important impacts of SSTs on LS water vapour. The 1st SST CCA-PC further indicates that it is closely related to both ENSO and PDO, with a correlation of 0.74 and 0.42, respectively. A combination of ENSO and PDO (blue curve in Fig. 5.7d) can well represent the 1st CCA-PC of SST, and therefore well explains the 1st CCA-PC and the recent decadal variability of tropical LS water vapour.

LS water vapour pattern shown as in Fig. 5.7b is consistent with the ENSO/PDO regressed pattern as in Figs. 5.8a and 5.8b, and also similar to the 2nd EOF shown in Fig. 5.3b. Fig. 5.8a shows the regressed MERRA LS water vapour (85 hPa) anomalies on the observed ENSO index (negative) from the HadISST. During La Niña (negative ENSO) events, which

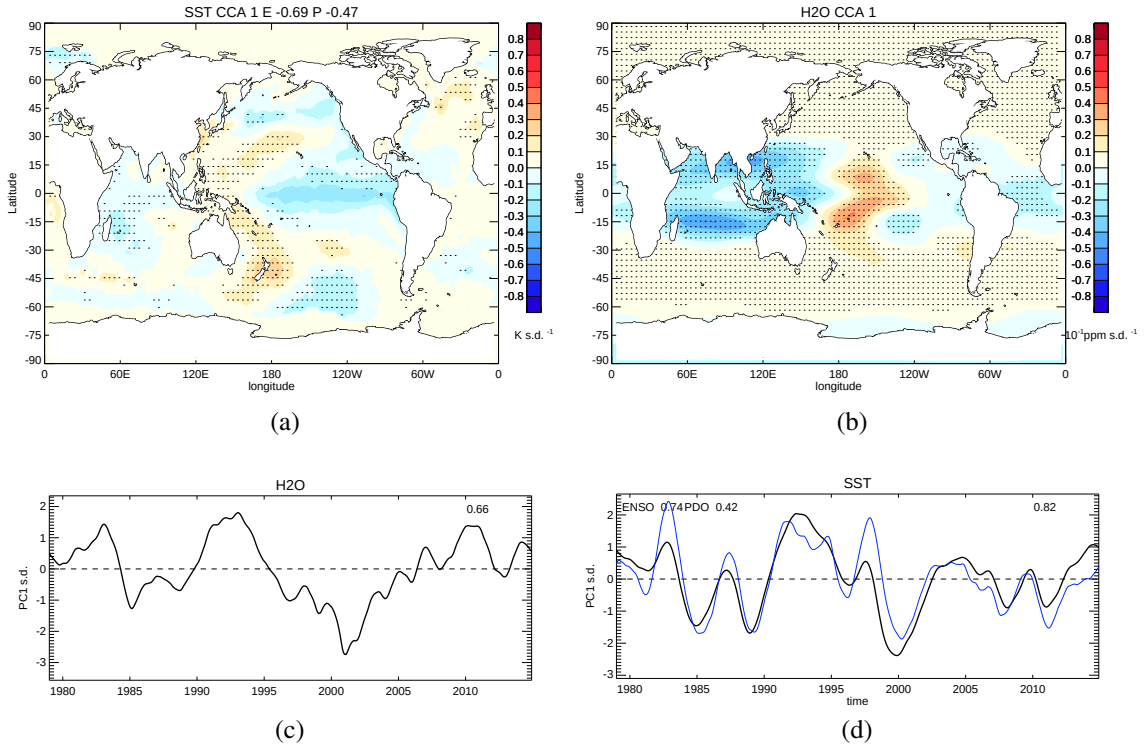

Fig. 5.7 **(top)** Regression of global observed SST (HadISST) and LS (85 hPa) water vapour anomalies (MERRA) on the first pair of CCA-PCs (Figs. 5.7 c-d). **a**, H2O and **b**, SSTs. The percentage (%) is the amount of the first CCA mode that accounts for the squared covariance between SSTs and water vapour, the number on the right-hand side is the pattern correlation between the CCA-PC regressed SSTs with the observed ENSO and PDO pattern. Stippling indicates the 95% significance level, with autocorrelation effects considered. **(bottom)** The first pair of PCs from the CCA analysis between MERRA tropical (30°S-30°N) LS water vapour and HadISST SSTs (details in Methods). The right side number in **c** indicates the correlation between **c** and **d**. Left side numbers in **d** show the correlation between the 1st CCA-PC of SST and the observed ENSO and PDO time series from EOF analyses (see details in the text). The blue curve is a regression of the black curve from observed ENSO and PDO time series, with a correlation shown at the right corner.

means cold SST anomalies in the equatorial Pacific, there are positive LS water vapour anomalies over the central Pacific. At the same time, associated with colder SSTs in the central and eastern Pacific, the Walker Circulation over the Western Pacific is enhanced and result in stronger convection over the IPWP region. The stronger and deeper convection leads to a colder tropopause and therefore contributes to more dehydration and less water vapour transport across the tropopause. This results in negative water vapour anomalies shown over the Indian Ocean.

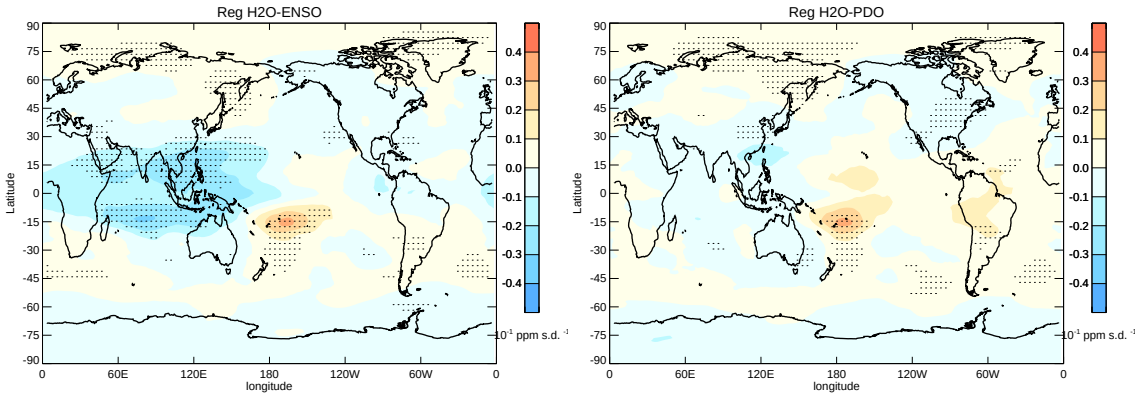

(a) (b)

Fig. 5.8 Regression of global observed SST (HadISST) and LS (85 hPa) water vapour anomalies (MERRA) on observed ENSO and PDO indexes for the period 1979-2014. **a**, ENSO and **b**, PDO. Stippling indicates the 95% significance level.

Fig. 5.8b shows the regressed MERRA LS water vapour anomalies at 85 hPa on the observed PDO index (negative) from the HadISST. A negative PDO, with also cold SST anomalies in the equatorial Pacific, shares a similar mechanism to a La Niña event, which leads to positive anomalies over the central Pacific and negative anomalies over the IPWP of LS water vapour. In addition, with stronger warm SST anomalies in the North Pacific, a negative PDO results in anticyclonic low-level circulation anomalies, which indicates a weaker Aleutian low. The weaker Aleutian low generally interferes negatively with the average wave structure and weakens the climatological mean stationary waves. Such negative interference damps the upward and poleward planetary wave propagation into the high-latitude extratropical stratosphere (*Wang et al.*, 2015b). This leads to a wave-induced strengthening of the polar vortex (*Hurwitz et al.*, 2012; *Ineson and Scaife*, 2009) and thus contributes to a weaker lower-stratosphere BDC, according to the momentum budget (*Andrews et al.*, 1987). The reduced vertical motion in the equatorial lower stratosphere due to a slower BDC, leads to a warmer tropical tropopause and more LS water vapour. Different to a La Niña event, the regressed negative anomalies over the Indian Ocean are not as strong, while the positive anomalies over the Central Pacific are much stronger. These ENSO and PDO regressed patterns are quite similar to both the CCA pattern above and the 2nd EOF shown in Fig. 5.3b, which indicates that the LS water vapour is closely related to ENSO or PDO, or a combination of both.

Although we used relative long period of reanalysis data, 36 years of MERRA data is still too short to provide conclusive connections of LS water vapour with the PDO on decadal to multidecadal time scales. To confirm the connection between the PDO and LS water vapour,

two model simulations for 145 years with NCAR's CESM-WACCM model were analyzed. This model captures the variability of the UTLS temperatures and water vapour reasonably well (*Gettelman et al.*, 2010; *Wang et al.*, 2015b).

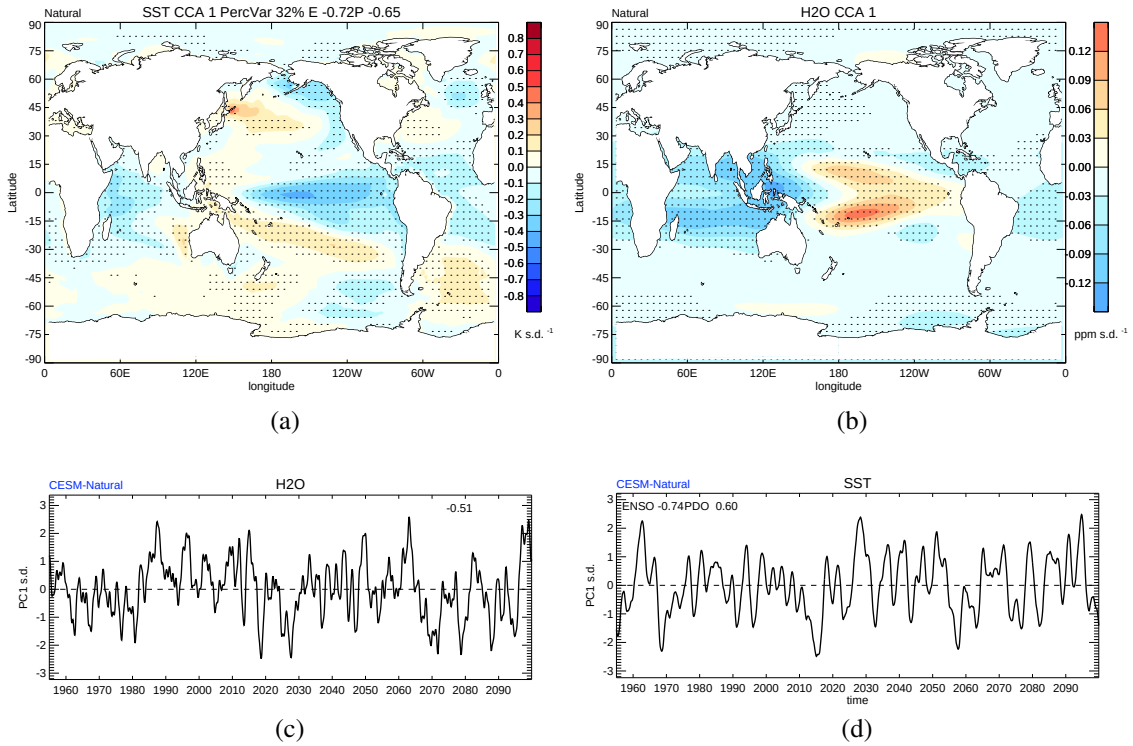

Fig. 5.9 (**top**) Regression of model simulated (Natural run) global SST and LS (85 hPa) water vapour anomalies on the first pair of CCA-PCs. **a**, H2O and **b**, SSTs. The percentage (%) is the amount of the first CCA mode that accounts for the squared covariance between SSTs and water vapour, the number on the right-hand side is the pattern correlation between the CCA-PC regressed SSTs with the observed ENSO and PDO pattern. Stippling indicates the 95% significance level, with autocorrelation effects considered. **(bottom)** The first pair of PCs from the CCA analysis between tropical (30°S-30°N) LS water vapour and SSTs from the CESM Natural run. The right side number in the top panel indicates the correlation between **c** and **d**. Left side numbers in the bottom panel show the correlations between **d** and modeled ENSO and PDO time series from EOF analyses (see details in the text).

Figs. 5.9a and 5.9b show the regressed patterns of SST and LS water vapour anomalies on the corresponding time series of the first CCA mode (Figs. 5.9c and 5.9d). The SST anomalies are again similar to ENSO/PDO phase, with pattern correlation of -0.75/-0.66 with observed ENSO/PDO pattern, while the corresponding LS water vapour anomalies are quite similar as shown in Fig. 5.7b. The first pair of CCA-PCs of LS water vapour and SSTs, as shown in Figs. 5.9 c-d, are closely related to each other, with a correlation of -0.51. The

corresponding SST PC is closely correlated the modeled ENSO/PDO time series (based on the EOF analysis as suggested by *Deser et al.* (2010) for the Natural run), with correlations of 0.74/0.60. This consistency between observations/reanalysis and model integration suggests that the variations of SSTs, such as ENSO and PDO, strongly affect the tropical LS water vapour.

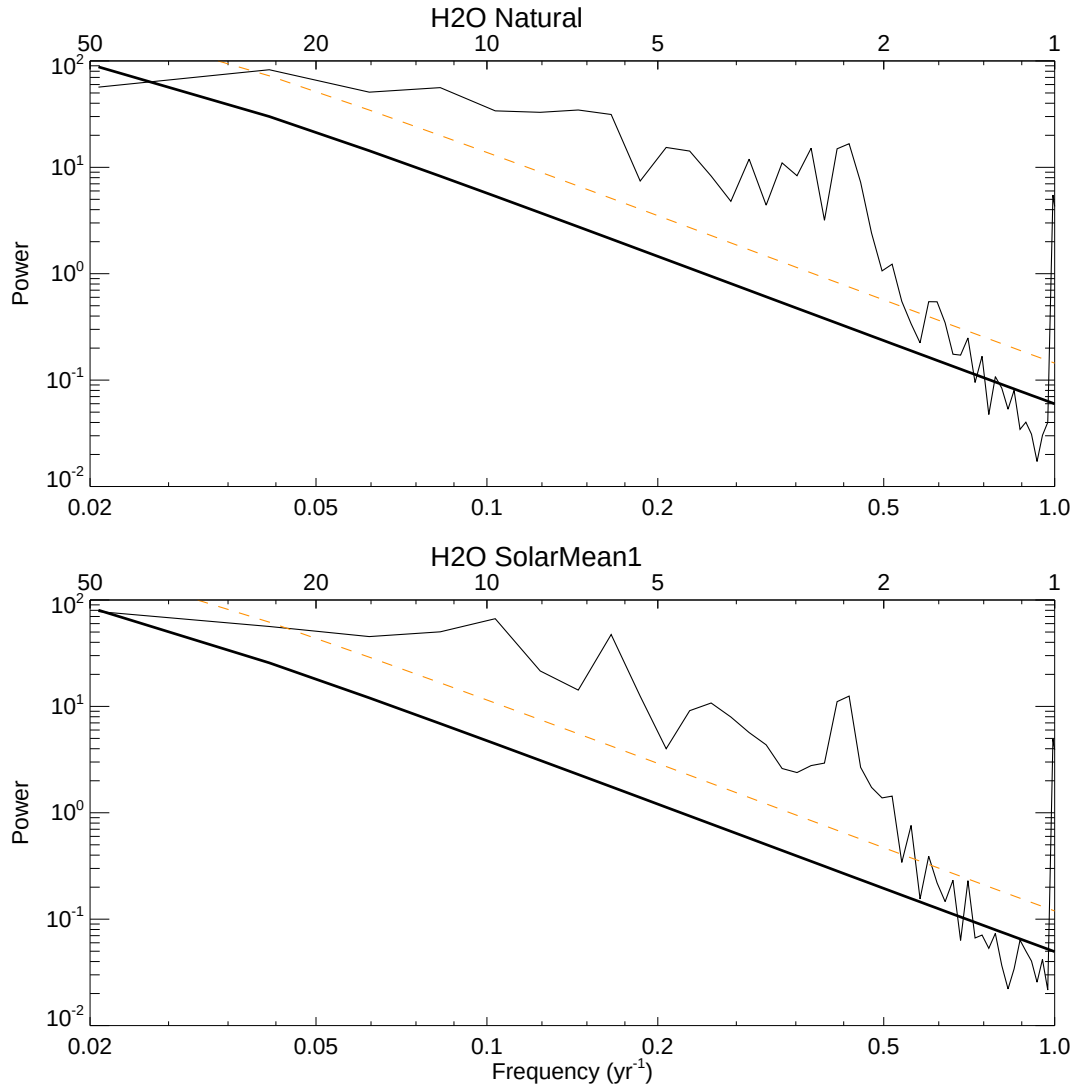

Fig. 5.10 Power spectrum of corresponding CCA-PCs of LS water vapour from Natural (top) and SolarMean (bottom) runs. Thick black lines indicates the best fit based on a first-order autoregressive model, and dashed red lines indicates the 95% confidence level.

To further understand the decadal to multidecadal variability of tropical LS water vapour, a power spectrum analysis was applied to the corresponding 1st CCA-PC of water vapour (Fig. 5.9c) for the whole integrated period from 1955 to 2099. The tropical LS water vapour

depicts significant decadal to multidecadal variability with periods of about 6, 11 and 24 years (Fig. 5.10a). The 11-year period can be confirmed to be related to the 11-year solar cycle by the SolarMean simulation. The SolarMean simulation shows similar results (not shown) from a CCA analysis as shown in Fig. 5.9 for the Natural run. However, without the 11-year solar cycle, the peak around 11-year is shifted to about 9 year in the SolarMean run (Fig. 5.10b). The 6-year period may be due to the multi-year variability of ENSO, while the 24-year period may be related to the PDO. This can be supported by the power spectrum of the observed ENSO and PDO time series as shown in Fig. 5.11.

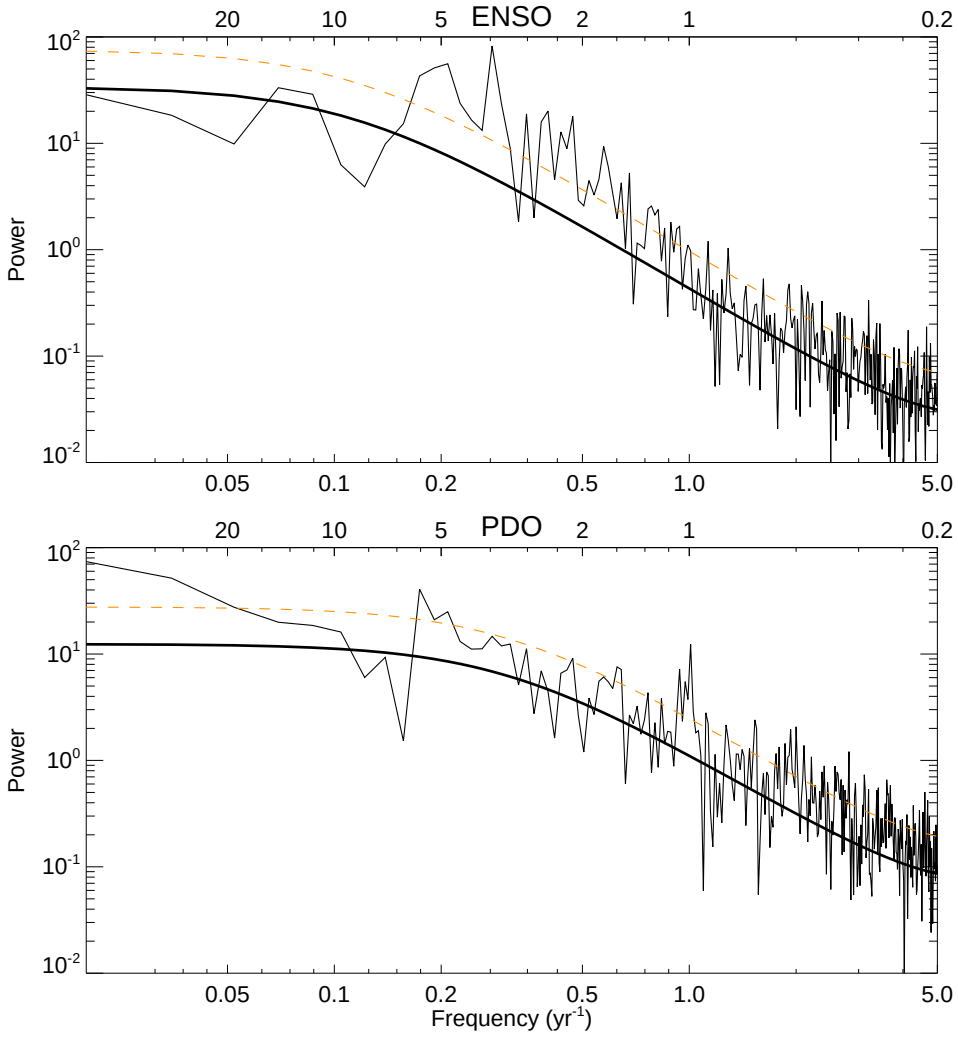

Fig. 5.11 Power spectrum of observed (HadISST) ENSO and PDO time series from EOF analyses (see details in the text). Thick black lines indicates the best fit based on a first-order autoregressive model, and dashed red lines indicates the 95% confidence level.

5.4.2 Solar influences on SSTs

From analyses above, the decadal variability of LS water vapour is evident and its connection with the 11-year solar cycle has been confirmed from both observations and model simulations. One remaining question is the time lag of 2-3 years between the 11-year solar cycle and LS water vapour as addressed by *Schieferdecker et al.* (2015) and also discussed above.

As discussed in previous studies, the irradiance anomalies of the 11-year solar cycle may be amplified and produce ENSO-like SST anomalies in the Pacific (e.g. *Meehl et al.*, 2009; *van Loon and Meehl*, 2014). Further, though the mechanism is not clear, a lagged response in SSTs to the solar cycle has been discussed in both the North Atlantic (*Gray et al.*, 2013; *Scaife et al.*, 2013; *Thieblemont et al.*, 2015) and the North Pacific (*Hood et al.*, 2013; *Meehl and Arblaster*, 2009; *Roy and Haigh*, 2012). This indicates a potential mechanism for the delayed solar signal in LS water vapour as pointed out by *Schieferdecker et al.* (2015).

Fig. 5.12 shows regressed SST anomalies on the monthly solar f10.7 fluxes with different time lags for the period of 1950-2014. A clear evolution of ENSO- or PDO-like pattern can be seen. Without time lag, there are only weak positive/negative SST anomalies in the Indian/Atlantic Ocean, and warm/cold SST anomalies in the northeastern/central Pacific. Note that our analysis is a little different to previous studies (e.g. *Meehl et al.*, 2009). We regressed SST anomalies (after subtract the global mean time series) directly onto the solar f10.7 monthly time series, while they applied a composite of winter SST anomalies due to solar maximum and solar minimum years. This may be one reason why our pattern looks different from their results. Another reason might be due to the time period selected for regression. We chose the period of 1950-2014, when the solar f10.7 observations are available, while they used the sunspot numbers from 1870 to 2002. With longer time delay, the signals become stronger in the Pacific, i.e. warmer anomalies in the equatorial Pacific, colder anomalies over North Pacific. After about 2 years, an ENSO- or PDO-like pattern can be seen clearly. Our results confirm *Meehl and Arblaster* (2009), which showed a warm ENSO event after about two years of the solar maximum. It also happens in the North Atlantic (*Gray et al.*, 2013; *Scaife et al.*, 2013; *Thieblemont et al.*, 2015). After about two years, a positive NAO-like pattern can be seen in the SST anomalies over the North Atlantic.

The ENSO- or PDO-like pattern evolution can also be seen from areas with significant SST anomalies. At lag 0-month, when the solar forcing is maximum, significant warm SST anomalies mainly exist over the Indian Ocean Warm Pool area and part of the western tropical Pacific. The warm SST anomalies over the western Pacific further develop and extend to the central and eastern tropical Pacific as the lag longer. Finally, at lag 20-month, significant warm SST anomalies prevail over the most of the tropical Pacific, of which pattern is El Niño-like. We therefore hypothesize that solar forcing initially warms the Indian Ocean and

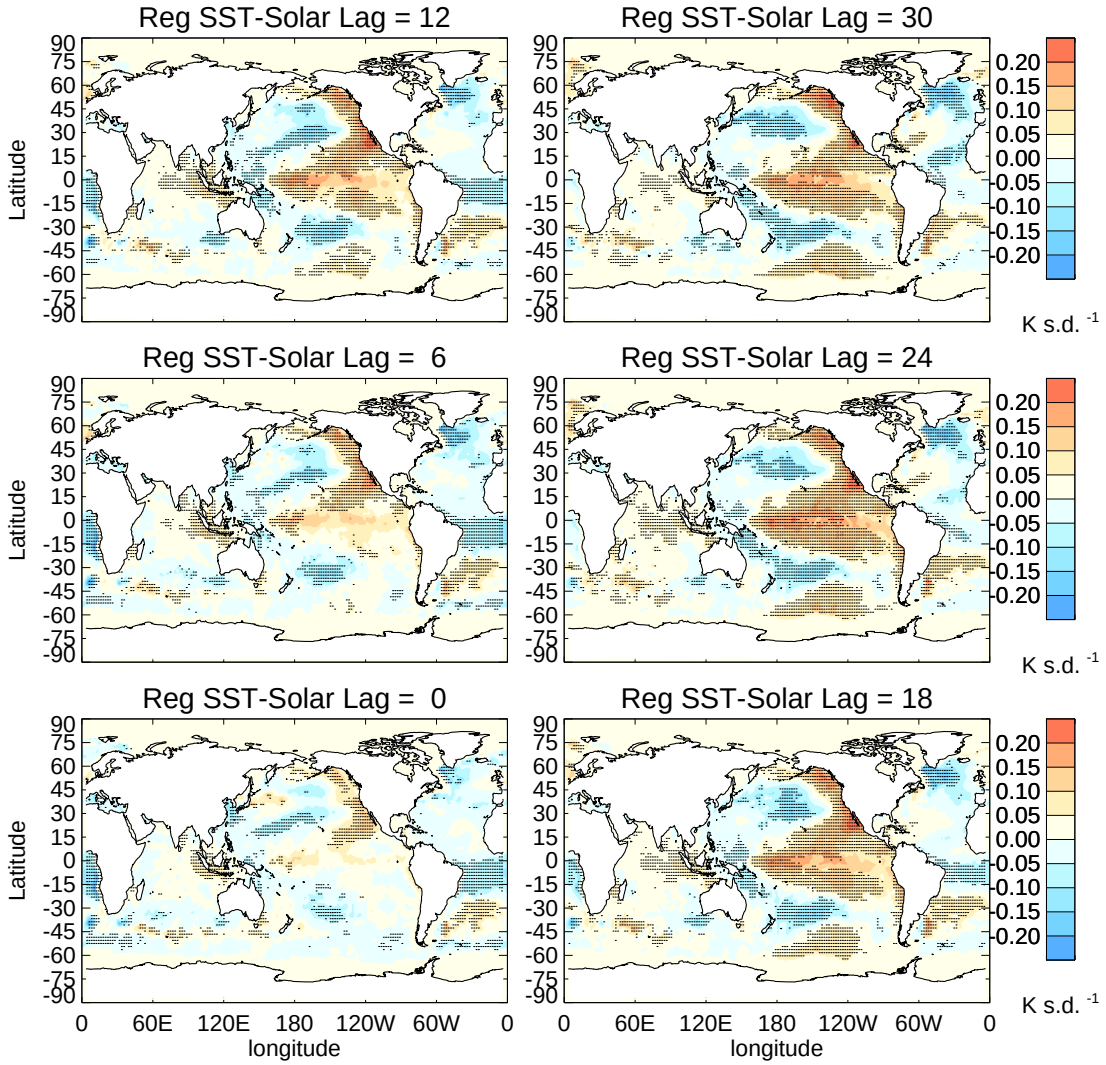

Fig. 5.12 Regressed SST anomalies from HadISST due to observed solar F10.7 time series (NOAA) for the period 1950-2014, with different time lags of 0-30 months. Stippling indicates the 95% significance level, with autocorrelation effects considered.

western Pacific Ocean radiatively, and propagation of these SST anomalies are important to generate El Niño-like pattern at the end. The mechanism of the SST development and propagation need further investigation though involvement of Walker circulation seems important such that positive feedback between the El Niño-like SST anomalies and Walker Circulation weakening. Resulting El Niño-like pattern then influences the North Pacific through the atmospheric teleconnections, e.g. the atmospheric bridge (*Alexander*, 2013), and produces PDO-like SST anomalies maximum at about lag 30-month. It is noteworthy that

SST anomalies in the North Pacific start to develop significantly when El Niño-like pattern is being matured at lag 18-month.

Beside the interannual variability of 3-8 years, ENSO also has decadal variability (*Deser et al.*, 2010), which can be seen in Fig. 5.11. Fig. 5.13 shows the band-pass filtered (9-13 year) time series of the f10.7 solar flux (black), as well as the observed ENSO and PDO index (blue) from the HadISST. Solar is leading the decadal ENSO of 20 months obviously, and is leading the PDO of about 30 months. This confirms the ENSO-to-PDO evolution of the regressed SST pattern with different time lags shown in Fig. 5.12. The larger time lag of PDO compared with ENSO is consistent with previous studies (e.g. *Newman et al.*, 2003), which indicated that the PDO may be somehow driven by the ENSO. The delay of 20 months between Solar and decadal ENSO might be due to the atmosphere-ocean interactions, which has been discussed by previous studies for the lag response of NAO to the solar cycle (*Gray et al.*, 2013; *Scaife et al.*, 2013; *Thieblemont et al.*, 2015). This is reminiscent of the 'bottom-up' mechanism of amplifying responses of the troposphere and stratosphere to the solar signal. The 'bottom-up' mechanism magnifies responses to a small initial solar forcing by involving air-sea coupling (e.g. *Gray et al.*, 2010; *Meehl et al.*, 2009), which may take a couple of years (*Meehl and Arblaster*, 2009; *White and Liu*, 2008).

In summary, with a lag of 20/31 months from Solar to ENSO- or PDO-like SST pattern, plus the links between LS water vapour and SSTs by modulating TPTs as addressed above, a link between the solar cycle, ocean variability, tropopause temperatures and finally the LS water vapour is established. This confirms and explains the results of *Schieferdecker et al.* (2015).

5.5 Conclusions and discussion

The MERRA data are suitable for investigating the LS water vapour variations over the past decades (1979-2014). Obvious decadal to multidecadal variability in tropical LS water vapour has been confirmed by both merged satellite observations (SWOOSH) and MERRA reanalysis data. Beside the zonal mean, LS water vapour also shows an asymmetry in its spatial distribution, i.e. low concentrations over the IPWP and high concentrations over the central Pacific. An EOF analysis was applied to the MERRA water vapour data at 85 hPa. The 1st mode shows a similar pattern as its climatology, which indicates large variations of LS water vapour over the IPWP. The 2nd mode shows a dipole pattern in LS water vapour, i.e., positive anomalies over the central Pacific and negative anomalies over the Indian Ocean.

The 1st PC of LS water vapour can be explained by the combined contributions from ENSO, QBO, $\overline{w}^*$, SAD and PDO, which indicates that PC1 depicts mixed variations from

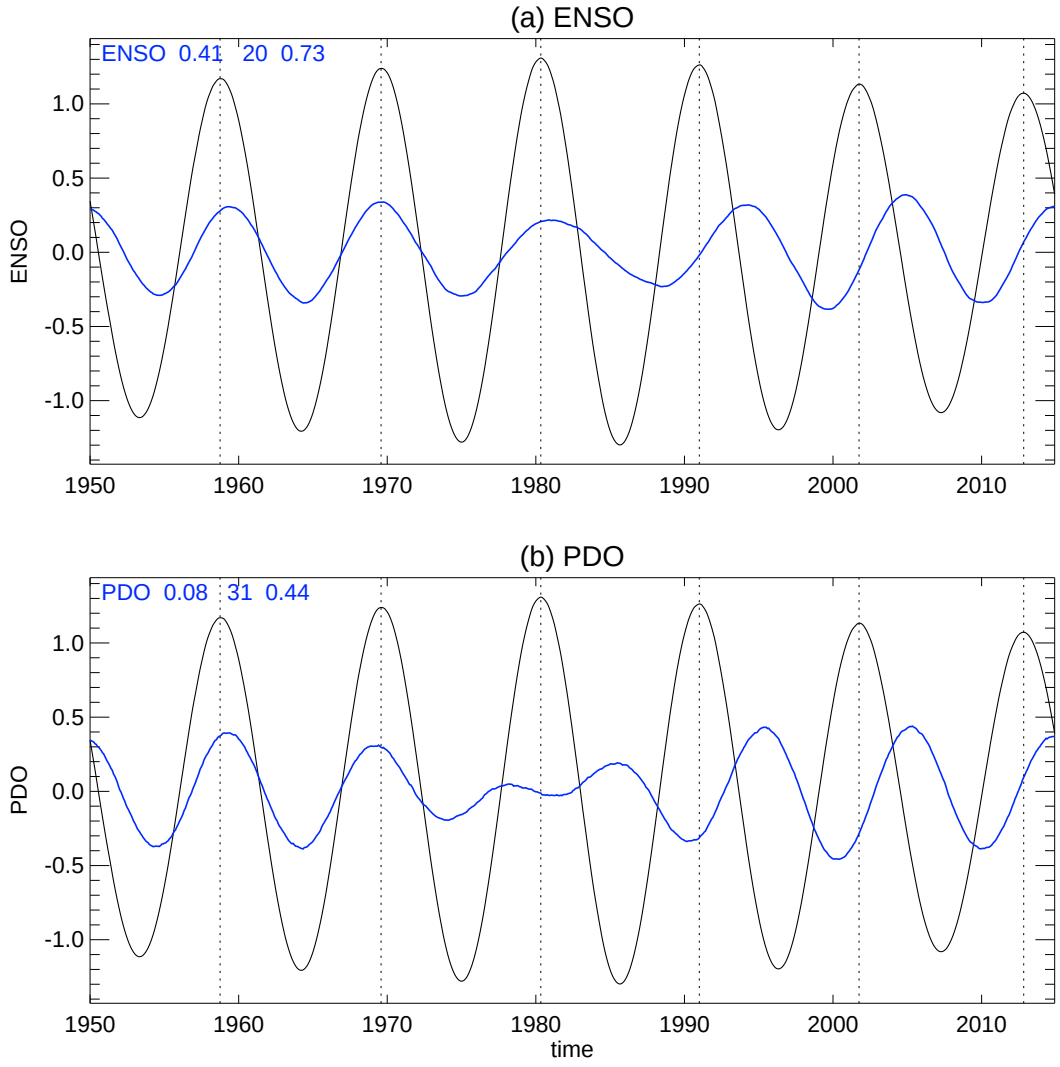

Fig. 5.13 Band-pass filtered (9-13 year) observed solar f10.7 flux time series (NOAA), as well as ENSO **(a)** and PDO **(b)** indexes from EOF analyses on HadISST.

interannual to multidecadal time scale. The ENSO, QBO and PDO influence LS water vapour by modulating the TPT and the $\overline{w}^*$. The 2nd PC, which depicts decadal variability of LS water vapour, is dominated by ENSO and the 11-year solar cycle. A time lag between solar cycle and LS water vapour, has been confirmed, though the exact timing of the lag needs further investigations.

The connection between LS water vapour and SSTs is evident from observed SSTs and MERRA reanalysis, based on a CCA analysis. SSTs affect LS water vapour by modulating convection, TPTs and dynamical circulations in both the troposphere and the stratosphere.

This could be confirmed by long-term fully-coupled model simulations. A power spectrum analysis indicates that the variability of LS water vapour peaks at periods of 6, 11 and 24 years from our mode simulations, which are potentially related to ENSO, solar cycle, and PDO, respectively.

A link for the solar signal in the LS water vapour over ocean variability and tropopause temperatures has been established. From observed solar f10.7 fluxes and SSTs, the solar 11-year cycle is leading the decadal variability of ENSO of about 20 months. Solar maximum conditions lead to positive SST anomalies over the western tropical Pacific and these SST anomalies propagates east to the central and eastern Pacific producing El Niño-like SST anomalies. These warm SST anomalies in the central and eastern Pacific further lead to a weaker Walker Circulation. This results in stronger and deeper convection over the central Pacific and weaker and shallower convections over the IPWP, and therefore colder TPTs and less water vapour over the central Pacific, and warmer TPTs and more water vapour over the IPWP in the lower stratosphere.

However, though there are some discussions by previous studies, the mechanism of the time lag between the 11-year solar cycle and ENSO or PDO is still not clear (*Gray et al.*, 2010). The exact period of lag needs further investigations because of the relative short time measurements. Or, the lag of time may depend on the background climate and may be different under different conditions (*Roy and Haigh*, 2012).

As a powerful greenhouse gas, water vapour has important feedbacks to the surface climate. The decadal to multidecadal variability in LS water vapour provides a potential way in driving the surface climate or influencing air-sea interactions. This study demonstrates that it is of paramount importance to pay attention to decadal to multidecadal variability of the LS water vapour, in order to understand interactions with the surface climate.

Chapter 6

Summary and outlook

In this thesis, the detailed thermal structure of the TTL, i.e. the tropopause inversion layer (TIL), has been studied in high accuracy and high vertical resolution GPS-RO observations, and in model simulations with high vertical resolution. The recent variability of the strength of the TIL since 2001 has been investigated for the first time, in both observations and model simulations.

An exceptional set of long (about 150 years) model simulations with NCAR's CESM-WACCM model, which includes an interactive ocean, an interactive chemistry, and a well-resolved stratosphere, has been used to explain the observed TTL variability. These experiments were designed to specifically quantify the contributions from both natural and anthropogenic factors, including solar variability, SSTs, the QBO, stratospheric aerosols and GHGs. The importance of the vertical resolution in climate models has also been evaluated in reproducing the observed TTL variability.

The observations and model simulations together provide, for the first time, evidence of a connection between the TTL decadal to multidecadal variability and the PDO. Such a connection is vital to explain the observed long-term variability of the TTL temperature, and implies potential improvements in the decadal predictability of the TTL. This work has also investigated possible links between the decadal to multidecadal variability of lower stratospheric water vapour and SSTs, as well as the 11-year solar cycle.

6.1 Conclusions

Here, the questions raised in the introductory chapter of this thesis shall be revisited, and the answers to them obtained in the different chapters will be summarized.

- **What is the recent TTL temperature variability measured by the GPS-RO data? How well can the WACCM model capture this variability?**
  - A decrease in the strength of the tropical TIL of 0.4 K, and an increase in tropical tropopause temperature of 1 K over the last decade, were found in the GPS-RO data.
  - The increase of tropical tropopause temperature and the decline in the strength of TIL can only be simulated in the WACCM with high vertical resolution (~300 m in the TTL) but not in the standard WACCM simulation (~1 km).
  - The decrease of the strength of TIL and the increase of the tropopause temperature are directly related to each other and are a combination of both dynamical and radiative processes. Weaker upwelling might lead to a warmer tropopause and less cooling or even warming of the lower stratosphere.

- **How do different natural and anthropogenic factors contribute to the recent TTL temperature variability? How important is the vertical resolution of a climate model for reproducing the TTL variability?**
  - Internal variability, i.e. a decrease in tropical sea surface temperatures and stronger QBO associated westerlies are main drivers of the recent warming of the TTL, contributing about 0.3 and 0.2 $Kdecade^{-1}$, respectively. Increased stratospheric aerosols also contribute 0.2 $Kdecade^{-1}$ warming, while the delayed and relatively weak current solar maximum contributes a cooling of about 0.2 $Kdecade^{-1}$.
  - The vertical resolution of the model influences the TTL response to the surface strongly, via dynamical changes, e.g., the lower and upper branches of the BDC. This leads to a 0.8 $Kdecade^{-1}$ extra warming in the TTL in the finer vertical resolution experiment as compared to the standard vertical resolution.

- **How important is decadal to multidecadal variability in estimating the long-term trend of the tropical tropopause temperature, and which processes control it?**
  - Instead of a sustained long-term trend, tropopause temperatures performed evident multidecadal variability during recent decades, i.e., a slight decrease between 1979 and 2000, and a statistically significant increase since 2001.
  - We present for the first time evidence that multi-decadal variability in tropical tropopause temperature is tightly linked to the Pacific Decadal Oscillation (PDO).

A negative PDO phase is linked to anomalously cold sea surface temperatures in the tropical Pacific and warm sea surface temperatures in the North Pacific. This drives a stronger Walker Circulation in the equatorial Pacific and a weaker Hadley Circulation in the troposphere, and a slower Brewer-Dobson circulation in the stratosphere. The subsequent weaker tropical upwelling from the troposphere to the lower stratosphere then warms the tropical tropopause. The reverse is true for the positive phase of the PDO.

– The multidecadal variability in the tropical tropopause temperatures over the recent three decades can be attributed to the shift of the PDO from its positive to its negative phase. This shift, which happened around the turn of the millennium, has also been confirmed in other studies, both at the surface, e.g., as expressed by the so-called global warming hiatus (*England et al.*, 2014; *Trenberth et al.*, 2014) and in the lower stratosphere, e.g. as the hiatus in the acceleration of the Brewer-Dobson circulation (*Aschmann et al.*, 2014).

- **Can we explain the recent variability of lower stratospheric water vapour? Which processes determine its decadal to multidecadal variability?**

  – Decadal to multidecadal variations in lower stratospheric water vapour from 1979-2014 are found to be mainly due to the 11-year solar cycle, decadal ENSO variations and the PDO.

  – An EOF analysis indicates that, the first principal component of lower stratospheric water vapour can be explained by the combined contributions from ENSO, QBO, the Brewer-Dobson circulation, stratospheric aerosols and the PDO, while the second principal component is dominated by ENSO and the 11-year solar cycle.

  – The 11-year solar cycle leads an ENSO-like SST pattern by about 2-3 years, which in turn influences the atmospheric circulations in both the troposphere and the stratosphere. It particularly modulates tropical tropopause temperatures and thereby determines lower stratospheric water vapour.

  – A link between the solar cycle, decadal ENSO variations and tropopause temperature variability provides a potential way to improve decadal predictability of lower stratospheric water vapour, which may have important feedbacks on surface climate due to its strong radiative effects.

6.2 Discussion and outlook

In this thesis, long-term variations in the strength of the TIL, a recently discovered aspect of the tropopause, has been investigated for the first time. This illuminated the mechanisms for TIL formation and maintenance, which are currently still under debate. However, the exact impacts of the TIL on both the stratosphere and troposphere are still not well understood. Modeling key aspects of the TIL was improved using a climate model with a high vertical resolution, the main features of the TIL are still difficult to reproduce, e.g., the maximum of N^2 (Buoyancy Frequency) is still not simulated at the correct height. This indicates that, beside the vertical resolution, other improvements, e.g., a proper representation of gravity waves, are likely needed.

Three short (10-year) simulations indicate that WACCM with a higher vertical resolution simulates a more realistic response of the TTL region to prescribed SST changes. This suggests that, without a proper vertical resolution, atmosphere-only simulations with prescribed SSTs may provide unrealistic surface-forced upper atmosphere variability. For example, the disagreement among CCMs in the BDC trend (e.g., *Butchart*, 2014; *Engel et al.*, 2009; *Oberländer et al.*, 2013; *SPARC-CCMVal*, 2010) may be due to unrealistic responses to SST forcing caused by the coarse vertical resolution of most CCMs. This indicates the need for further studies with long-term model simulations to estimate the importance of the vertical resolution.

This thesis has found for the first time a connection between the tropical tropopause temperatures and the decadal to multidecadal variability in Pacific SSTs (PDO), evident in both observations and model simulations. However, details about the proper mechanism are still unclear. For example, it remains to be seen how the PDO works together with ENSO in modulating the tropospheric and stratospheric circulations, subsequently influencing the tropopause temperature. Distinguishing the individual effects of the decadal variability in ENSO and the PDO remains a challenge. At the same time, there is evidence for multidecadal modulation in stratospheric circulation variability (e.g. the strength of the polar vortex) by the Atlantic Multidecadal Variability (*Omrani et al.*, 2014), which indicates also a "bottom-up" mechanism. However, the importance of such "bottom-up" effects for stratospheric dynamics and chemistry is still controversial. Whether and how these stratospheric changes feedback on the ocean awaits further studies.

A link between the 11-year solar cycle and decadal lower stratospheric water vapour variability has been established through air-sea interactions. However, the mechanism of lagged solar signals in SST anomalies is still lacking. As a powerful greenhouse gas, water vapour may provide an amplification mechanism for solar effects on the surface.

The GPS-RO observations are only available since 2001. Even relatively high quality reanalysis data, e.g. MERRA, are only available since 1979. These short time observation or observation-based data sets limit the certainty that we can currently have in long-term trends or even multidecadal variations in the TTL. It is hoped that the findings presented in this thesis, which are based on limited observations and simulations with one model, will trigger new research with other climate models on the decadal to multidecadal variability of the stratosphere, especially its connections to the surface.

References

Abalos, M., W. Randel, D. Kinnison, and E. Serrano (2013), Quantifying tracer transport in the tropical lower stratosphere using waccm, *Atmos. Chem. Phys*, *13*(10), 591–10, doi:10.5194/acp-13-10591-2013.

Abalos, M., W. J. Randel, and E. Serrano (2014), Dynamical forcing of subseasonal variability in the tropical brewer–dobson circulation, *J. Atmos. Sci.*, *71*(9), 3439–3453, doi:http://dx.doi.org/10.1175/JAS-D-13-0366.1.

Alexander, M. (2013), *Extratropical Air-Sea Interaction, Sea Surface Temperature Variability, and the Pacific Decadal Oscillation*, pp. 123–148, American Geophysical Union, doi:10.1029/2008GM000794.

Alexander, M., et al. (2010), Recent developments in gravity-wave effects in climate models and the global distribution of gravity-wave momentum flux from observations and models, *Quart. J. Roy. Meteor. Soc.*, *136*(650), 1103–1124, doi:10.1002/qj.637.

Andrews, D. G., J. R. Holton, and C. B. Leovy (1987), *Middle atmosphere dynamics*, vol. 40, Academic press.

Aschmann, J., J. Burrows, C. Gebhardt, A. Rozanov, R. Hommel, M. Weber, and A. Thompson (2014), On the hiatus in the acceleration of tropical upwelling since the beginning of the 21st century, *Atmos. Chem. Phys.*, *14*(23), 12,803–12,814, doi:10.5194/acp-14-12803-2014.

Austin, J., et al. (2008), Coupled chemistry climate model simulations of the solar cycle in ozone and temperature, *J. Geophys. Res.*, *113*(D11), doi:10.1029/2007JD009391.

Ayarzagüena, B., U. Langematz, S. Meul, S. Oberländer, J. Abalichin, and A. Kubin (2013), The role of climate change and ozone recovery for the future timing of major stratospheric warmings, *Geophys. Res. Lett.*, *40*(10), 2460–2465, doi:10.1002/grl.50477.

Baldwin, M. P., et al. (2001), The quasi-biennial oscillation, *Rev. Geophys.*, *39*(2), 179–229, doi:10.1029/1999RG000073.

Barsugli, J. J., and D. S. Battisti (1998), The basic effects of atmosphere-ocean thermal coupling on midlatitude variability, *Journal of the Atmospheric Sciences*, *55*(4), 477–493, doi:http://dx.doi.org/10.1175/1520-0469(1998)055<0477:TBEOAO>2.0.CO;2.

Birner, T. (2006), Fine-scale structure of the extratropical tropopause region, *J. Geophys. Res.*, *111*(D4), D04,104, doi:10.1029/2005JD006301.

Birner, T. (2010), Residual circulation and tropopause structure, *J. Atmos. Sci.*, *67*(8), 2582–2600, doi:10.1175/2010JAS3287.1.

Birner, T., A. Dörnbrack, and U. Schumann (2002), How sharp is the tropopause at midlatitudes?, *Geophys. Res. Lett.*, *29*(14), 45–1–45–4, doi:10.1029/2002GL015142.

Birner, T., D. Sankey, and T. Shepherd (2006), The tropopause inversion layer in models and analyses, *Geophys. Res. Lett.*, *33*(14), L14,804, doi:10.1029/2006GL026549.

Bunzel, F., and H. Schmidt (2013), The brewer–dobson circulation in a changing climate: Impact of the model configuration, *J. Atmos. Sci.*, *70*(5), 1437–1455, doi:http://dx.doi.org/10.1175/JAS-D-12-0215.1.

Butchart, N. (2014), The brewer-dobson circulation, *Rev. Geophys.*, *52*(2), 157–184, doi:10.1002/2013RG000448.

Butchart, N., et al. (2010), Chemistry-climate model simulations of twenty-first century stratospheric climate and circulation changes, *J. Climate*, *23*(20), 5349–5374, doi:http://dx.doi.org/10.1175/2010JCLI3404.1.

Butler, A. H., L. M. Polvani, and C. Deser (2014), Separating the stratospheric and tropospheric pathways of el niño–southern oscillation teleconnections, *Environ. Res. Lett.*, *9*(2), 024,014, doi:10.1088/1748-9326/9/2/024014.

Cagnazzo, C., et al. (2009), Northern winter stratospheric temperature and ozone responses to enso inferred from an ensemble of chemistry climate models, *Atmos. Chem. Phys.*, *9*(22), 8935–8948, doi:10.5194/acp-9-8935-2009.

Calvo, N., R. Garcia, W. Randel, and D. Marsh (2010), Dynamical mechanism for the increase in tropical upwelling in the lowermost tropical stratosphere during warm enso events, *J. Atmos. Sci.*, *67*(7), 2331–2340, doi:10.1175/2010JAS3433.1.

Deser, C., M. A. Alexander, S.-P. Xie, and A. S. Phillips (2010), Sea surface temperature variability: Patterns and mechanisms, *Annual Review of Marine Science*, *2*(1), 115–143, doi:10.1146/annurev-marine-120408-151453.

Dessler, A., M. Schoeberl, T. Wang, S. Davis, K. Rosenlof, and J.-P. Vernier (2014), Variations of stratospheric water vapor over the past three decades, *J. Geophys. Res.*, *119*(22), 12–588, doi:10.1002/2014JD021712.

Dessler, a. E., M. R. Schoeberl, T. Wang, S. M. Davis, and K. H. Rosenlof (2013), Stratospheric water vapor feedback., *Proc. Natl. Acad. Sci. U. S. A.*, *110*(45), 18,087–91, doi:10.1073/pnas.1310344110.

Engel, A., et al. (2009), Age of stratospheric air unchanged within uncertainties over the past 30 years, *Nature Geoscience*, *2*(1), 28–31, doi:10.1038/ngeo388.

England, M. H., et al. (2014), Recent intensification of wind-driven circulation in the pacific and the ongoing warming hiatus, *Nature Clim. Change*, *4*(3), doi:10.1038/nclimate2106.

Eyring, V., et al. (2006), Assessment of temperature, trace species, and ozone in chemistry-climate model simulations of the recent past, *J. Geophys. Res.*, *111*(D22), doi:10.1029/2006JD007327.

Eyring, V., et al. (2007), Multimodel projections of stratospheric ozone in the 21st century, *J. Geophys. Res.*, *112*(D16), doi:10.1029/2006JD008332.

Flannaghan, T., and S. Fueglistaler (2013), The importance of the tropical tropopause layer for equatorial kelvin wave propagation, *J. Geophys. Res.*, *118*(11), 5160–5175, doi:10.1002/jgrd.50418.

Flato, G., et al. (2014), Evaluation of climate models, in *Climate Change 2013 - The Physical Science Basis. Contribution of Working Group I to the Fifth Assessment Report of the Intergovernmental Panel on Climate Change [Stocker, T.F., D. Qin, G.-K. Plattner, M. Tignor, S.K. Allen, J. Boschung, A. Nauels, Y. Xia, V. Bex and P.M. Midgley (eds.)]*, pp. 741–866, Cambridge University Press, Cambridge, United Kingdom and New York, NY, USA.

Flury, T., D. L. Wu, and W. G. Read (2013), Variability in the speed of the Brewer–Dobson circulation as observed by Aura/MLS, *Atmos. Chem. Phys.*, *13*(9), 4563–4575, doi:10.5194/acp-13-4563-2013.

Force, N. A. (1976), National oceanic and atmospheric administration, *National Aeronautics and Space Administration, United States Air Force, Washington, DC*.

Fritts, D. C., and M. J. Alexander (2003), Gravity wave dynamics and effects in the middle atmosphere, *Rev. Geophys.*, *41*(1), 1003, doi:10.1029/2001RG000106.

Fu, Q. (2013), Ocean-atmosphere interactions: Bottom up in the tropics, *Nature Clim. Change*, *3*(11), 957–958, doi:10.1038/nclimate2039.

Fueglistaler, S., A. Dessler, T. Dunkerton, I. Folkins, Q. Fu, and P. W. Mote (2009), Tropical tropopause layer, *Rev. Geophys.*, *47*(1), 1004, doi:10.1029/2008RG000267.

Fueglistaler, S., P. Haynes, and P. Forster (2011), The annual cycle in lower stratospheric temperatures revisited, *Atmos. Chem. Phys.*, *11*(8), 3701–3711.

Fueglistaler, S., et al. (2013), The relation between atmospheric humidity and temperature trends for stratospheric water, *J. Geophys. Res.*, *118*(2), 1052–1074, doi:10.1002/jgrd.50157.

Garcia, R., D. Marsh, D. Kinnison, B. Boville, and F. Sassi (2007), Simulation of secular trends in the middle atmosphere, 1950–2003, *J. Geophys. Res.*, *112*(D9), D09,301, doi:10.1029/2006JD007485.

Garfinkel, C., D. Waugh, L. Oman, L. Wang, and M. Hurwitz (2013a), Temperature trends in the tropical upper troposphere and lower stratosphere: Connections with sea surface temperatures and implications for water vapor and ozone, *J. Geophys. Res.*, *118*(17), 9658–9672, doi:10.1002/jgrd.50772.

Garfinkel, C. I., M. M. Hurwitz, L. D. Oman, and D. W. Waugh (2013b), Contrasting effects of central pacific and eastern pacific el niño on stratospheric water vapor, *Geophys. Res. Lett.*, *40*(15), 4115–4120, doi:10.1002/grl.50677.

Gettelman, A., and T. Birner (2007), Insights into tropical tropopause layer processes using global models, *J. Geophys. Res.*, *112*(D23), D23,104, doi:10.1029/2007JD008945.

Gettelman, A., and P. D. F. Forster (2002), A climatology of the tropical tropopause layer, *J. Meteor. Soc. Japan.*, *80*(4B), 911–924, doi:http://dx.doi.org/10.2151/jmsj.80.911.

Gettelman, A., et al. (2009), The tropical tropopause layer 1960–2100, *Atmos. Chem. Phys.*, *9*(5), 1621–1637, doi:10.5194/acp-9-1621-2009.

Gettelman, A., et al. (2010), Multimodel assessment of the upper troposphere and lower stratosphere: Tropics and global trends, *J. Geophys. Res.*, *115*(D3), doi:10.1029/2009JD013638.

Giorgetta, M. A., E. Manzini, and E. Roeckner (2002), Forcing of the quasi-biennial oscillation from a broad spectrum of atmospheric waves, *Geophys. Res. Lett.*, *29*(8), 86–1, doi:10.1029/2002GL014756.

Gray, L. J., et al. (2010), SOLAR INFLUENCES ON CLIMATE, *Rev. Geophys.*, *48*(4), doi:10.1029/2009RG000282.

Gray, L. J., et al. (2013), A lagged response to the 11 year solar cycle in observed winter atlantic/european weather patterns, *J. Geophys. Res.*, *118*(24), 13–405, doi:10.1002/2013JD020062.

Grise, K. M., and D. W. Thompson (2012), Equatorial planetary waves and their signature in atmospheric variability, *J. Atmos. Sci.*, *69*(3), 857–874, doi:http://dx.doi.org/10.1175/JAS-D-11-0123.1.

Grise, K. M., and D. W. Thompson (2013), On the signatures of equatorial and extratropical wave forcing in tropical tropopause layer temperatures., *J. Atmos. Sci.*, *70*(4), 1084–1102, doi:http://dx.doi.org/10.1175/JAS-D-12-0163.1.

Grise, K. M., D. W. Thompson, and T. Birner (2010), A global survey of static stability in the stratosphere and upper troposphere, *J. Climate*, *23*(9), 2275–2292, doi:10.1175/2009JCLI3369.1.

Hansen, F., K. Matthes, and L. Gray (2013), Sensitivity of stratospheric dynamics and chemistry to qbo nudging width in the chemistry–climate model waccm, *J. Geophys. Res.*, *118*(18), 10–464, doi:10.1002/jgrd.50812.

Hansen, F., K. Matthes, C. Petrick, and W. Wang (2014), The influence of natural and anthropogenic factors on major stratospheric sudden warmings, *J. Geophys. Res.*, *119*(13), 8117–8136, doi:10.1002/2013JD021397.

Hegglin, M., C. Boone, G. Manney, and K. Walker (2009), A global view of the extratropical tropopause transition layer from atmospheric chemistry experiment fourier transform spectrometer o3, h2o, and co, *J. Geophys. Res.*, *114*(D7), D00B11, doi:10.1029/2008JD009984.

Hegglin, M., et al. (2014), Vertical structure of stratospheric water vapour trends derived from merged satellite data, *Nature Geoscience*, *7*(10), 768–776, doi:10.1038/NGEO2236.

Highwood, E. J., and B. J. Hoskins (1998), The tropical tropopause, *Quart. J. Roy. Meteor. Soc.*, *124*(549), 1579–1604, doi:10.1002/qj.49712454911.

Hood, L., S. Schimanke, T. Spangehl, S. Bal, and U. Cubasch (2013), The surface climate response to 11-yr solar forcing during northern winter: Observational analyses and comparisons with gcm simulations, *26*(19), 7489–7506, doi:10.1175/JCLI-D-12-00843.1.

Hurst, D. F., S. J. Oltmans, H. Vömel, K. H. Rosenlof, S. M. Davis, E. A. Ray, E. G. Hall, and A. F. Jordan (2011), Stratospheric water vapor trends over boulder, colorado: Analysis of the 30 year boulder record, *J. Geophys. Res.*, *116*(D2), D02,306, doi:10.1029/2010JD015065.

Hurwitz, M. M., P. A. Newman, and C. I. Garfinkel (2012), On the influence of north pacific sea surface temperature on the arctic winter climate, *J. Geophys. Res.*, *117*(D19), n/a–n/a, doi:10.1029/2012JD017819.

Ineson, S., and A. Scaife (2009), The role of the stratosphere in the european climate response to el niño, *Nature Geoscience*, *2*(1), 32–36, doi:10.1038/ngeo381.

Jung, T., et al. (2012), High-resolution global climate simulations with the ecmwf model in project athena: Experimental design, model climate, and seasonal forecast skill, *J. Climate*, *25*(9), 3155–3172, doi:http://dx.doi.org/10.1175/JCLI-D-11-00265.1.

Kamae, Y., H. Shiogama, M. Watanabe, M. Ishii, H. Ueda, and M. Kimoto (2015), Recent slowdown of tropical upper-tropospheric warming associated with pacific climate variability, *Geophys. Res. Lett.*, pp. n/a–n/a, doi:10.1002/2015GL063608.

Kim, J., K. M. Grise, and S. Son (2013), Thermal characteristics of the cold-point tropopause region in CMIP5 models, *J. Geophys. Res.*, *118*(16), 8827–8841, doi:10.1002/jgrd.50649.

Kim, J.-E., and M. J. Alexander (2015), Direct impacts of waves on tropical cold point tropopause temperature, *Geophys. Res. Lett.*, pp. n/a–n/a, doi:10.1002/2014GL062737.

Kunz, A., P. Konopka, R. Müller, L. Pan, C. Schiller, and F. Rohrer (2009), High static stability in the mixing layer above the extratropical tropopause, *J. Geophys. Res.*, *114*(D16), 16,305, doi:10.1029/2009JD011840.

Li, F., J. Austin, and J. Wilson (2008), The strength of the brewer-dobson circulation in a changing climate: Coupled chemistry-climate model simulations, *J. Climate*, *21*(1), 40–57, doi:10.1175/2007JCLI1663.1.

Manzini, E., M. Giorgetta, M. Esch, L. Kornblueh, and E. Roeckner (2006), The influence of sea surface temperatures on the northern winter stratosphere: Ensemble simulations with the maecham5 model, *Journal of climate*, *19*(16), 3863–3881, doi:http://dx.doi.org/10.1175/JCLI3826.1.

Marsh, D. R., and R. R. Garcia (2007), Attribution of decadal variability in lower-stratospheric tropical ozone, *Geophys. Res. Lett.*, *34*(21), 21,807, doi:10.1029/2007GL030935.

Marsh, D. R., M. J. Mills, D. E. Kinnison, J.-F. Lamarque, N. Calvo, and L. M. Polvani (2013), Climate change from 1850 to 2005 simulated in cesm1 (waccm), *J. Climate*, *26*, 7372–7391, doi:10.1175/JCLI-D-12-00558.1.

Matthes, K., D. R. Marsh, R. R. Garcia, D. E. Kinnison, F. Sassi, and S. Walters (2010), Role of the qbo in modulating the influence of the 11 year solar cycle on the atmosphere using constant forcings, *J. Geophys. Res.*, *115*(D18), 18,110, doi:10.1029/2009JD013020.

Matthes, K., K. Kodera, R. R. Garcia, Y. Kuroda, D. R. Marsh, and K. Labitzke (2013), The importance of time-varying forcing for qbo modulation of the atmospheric 11 year solar cycle signal, *J. Geophys. Res.*, *118*(10), 4435–4447, doi:10.1002/jgrd.50424.

Meehl, G. A., and J. M. Arblaster (2009), A lagged warm event-like response to peaks in solar forcing in the pacific region, *22*(13), 3647–3660, doi:10.1175/2009JCLI2619.

Meehl, G. A., J. M. Arblaster, K. Matthes, F. Sassi, and H. van Loon (2009), Amplifying the pacific climate system response to a small 11-year solar cycle forcing, *Science*, *325*(5944), 1114–1118, doi:10.1126/science.1172872.

Miyazaki, K., S. Watanabe, Y. Kawatani, Y. Tomikawa, M. Takahashi, and K. Sato (2010a), Transport and mixing in the extratropical tropopause region in a high-vertical-resolution gcm. part i: Potential vorticity and heat budget analysis, *J. Atmos. Sci.*, *67*(5), 1293–1314, doi:10.1175/2009JAS3221.1.

Miyazaki, K., S. Watanabe, Y. Kawatani, K. Sato, Y. Tomikawa, and M. Takahashi (2010b), Transport and mixing in the extratropical tropopause region in a high-vertical-resolution gcm. part ii: Relative importance of large-scale and small-scale dynamics, *J. Atmos. Sci.*, *67*(5), 1315–1336, doi:10.1175/2009JAS3334.1.

Morgenstern, O., et al. (2010), Review of the formulation of present-generation stratospheric chemistry-climate models and associated external forcings, *J. Geophys. Res.*, *115*, D00M02, doi:10.1029/2009JD013728.

Newman, M., G. P. Compo, and M. A. Alexander (2003), Enso-forced variability of the pacific decadal oscillation, *16*(23), 3853–3857, doi:http://dx.doi.org/10.1175/1520-0442(2003)016<3853:EVOTPD>2.0.CO;2.

Oberländer, S., U. Langematz, and S. Meul (2013), Unraveling impact factors for future changes in the Brewer-Dobson circulation, *J. Geophys. Res.*, *118*(18), 10296–10312, doi:10.1002/jgrd.50775.

Omrani, N.-E., N. S. Keenlyside, J. Bader, and E. Manzini (2014), Stratosphere key for wintertime atmospheric response to warm atlantic decadal conditions, *Climate Dyn.*, *42*(3-4), 649–663, doi:10.1007/s00382-013-1860-3.

Otsuka, S., M. Takeshita, and S. Yoden (2014), A numerical experiment on the formation of the tropopause inversion layer associated with an explosive cyclogenesis: possible role of gravity waves, *Progress in Earth and Planetary Science*, *1*(1), 1–14, doi:10.1186/s40645-014-0019-0.

Pan, L. L., L. C. Paulik, S. B. Honomichl, L. A. Munchak, J. Bian, H. B. Selkirk, and H. Vömel (2014), Identification of the tropical tropopause transition layer using the ozone-water vapor relationship, *J. Geophys. Res.*, *119*(6), 3586–3599, doi:10.1002/2013JD020558.

Park, W., and M. Latif (2012), Atlantic meridional overturning circulation response to idealized external forcing, *39*(7-8), 1709–1726, doi:10.1007/s00382-011-1212-0.

Plumb, R. A. (2007), Tracer interrelationships in the stratosphere, *Rev. Geophys.*, *45*(4), doi:10.1029/2005RG000179.

Randel, W. J., and E. J. Jensen (2013), Physical processes in the tropical tropopause layer and their roles in a changing climate, *Nature Geoscience*, *6*(3), 169–176, doi:10.1038/ngeo1733.

Randel, W. J., and F. Wu (2010), The polar summer tropopause inversion layer, *J. Atmos. Sci.*, *67*(8), 2572–2581, doi:http://dx.doi.org/10.1175/2010JAS3430.1.

Randel, W. J., and F. Wu (2015), Variability of zonal mean tropical temperatures derived from a decade of gps radio occultation data, *J. Atmos. Sci.*, *72*, 1261–1275, doi:10.1175/JAS-D-14-0216.1.

Randel, W. J., F. Wu, and P. Forster (2007), The extratropical tropopause inversion layer: Global observations with GPS data, and a radiative forcing mechanism, *J. Atmos. Sci.*, *64*(12), 4489–4496, doi:http://dx.doi.org/10.1175/2007JAS2412.1.

Randel, W. J., et al. (2009), An update of observed stratospheric temperature trends, *J. Geophys. Res.*, *114*(D2), doi:10.1029/2008JD010421.

Rayner, N., D. Parker, E. Horton, C. Folland, L. Alexander, D. Rowell, E. Kent, and A. Kaplan (2003), Global analyses of sea surface temperature, sea ice, and night marine air temperature since the late nineteenth century, *J. Geophys. Res.*, *108*(D14), 4407–4453, doi:10.1029/2002JD002670.

Richter, J. H., A. Solomon, and J. T. Bacmeister (2014a), Effects of vertical resolution and nonorographic gravity wave drag on the simulated climate in the community atmosphere model, version 5, *Journal of Advances in Modeling Earth Systems*, *6*(2), 357–383, doi:10.1002/2013MS000303.

Richter, J. H., A. Solomon, and J. T. Bacmeister (2014b), On the simulation of the quasi-biennial oscillation in the community atmosphere model, version 5, *Journal of Geophysical Research: Atmospheres*, *119*, doi:10.1002/2013JD021122.

Rienecker, M. M., et al. (2011), Merra: Nasa's modern-era retrospective analysis for research and applications, *24*(14), 3624–3648, doi:http://dx.doi.org/10.1175/JCLI-D-11-00015.1.

Rind, D., J. Lerner, J. Jonas, and C. McLinden (2007), Composition and chemistry-d09315-effects of resolution and model physics on tracer transports in the nasa goddard institute for space studies general circulation models (doi 10.1029/2006jd007476), *J. Geophys. Res.*, *112*(9), doi:10.1029/2006JD007476.

Roeckner, E., R. Brokopf, M. Esch, M. Giorgetta, S. Hagemann, L. Kornblueh, E. Manzini, U. Schlese, and U. Schulzweida (2006), Sensitivity of simulated climate to horizontal and vertical resolution in the echam5 atmosphere model, *J. Climate*, *19*(16), 3771–3791, doi:http://dx.doi.org/10.1175/JCLI3824.1.

Roy, I., and J. D. Haigh (2012), Solar cycle signals in the pacific and the issue of timings, *J. Atmos. Sci.*, *69*(4), 1446–1451, doi:http://dx.doi.org/10.1175/JAS-D-11-0277.1.

Santer, B. D., et al. (2003), Behavior of tropopause height and atmospheric temperature in models, reanalyses, and observations: Decadal changes, *J. Geophys. Res.*, *108*(D1), ACL–1, doi:10.1029/2002JD002258.

Scaife, A. A., S. Ineson, J. R. Knight, L. Gray, K. Kodera, and D. M. Smith (2013), A mechanism for lagged north atlantic climate response to solar variability, *Geophys. Res. Lett.*, *40*(2), 434–439, doi:10.1002/grl.50099.

Scherllin-Pirscher, B., C. Deser, S.-P. Ho, C. Chou, W. Randel, and Y.-H. Kuo (2012), The vertical and spatial structure of enso in the upper troposphere and lower stratosphere from gps radio occultation measurements, *Geophys. Res. Lett.*, *39*(20), 20,801, doi:10.1029/2012GL053071.

Schieferdecker, T., S. Lossow, G. Stiller, and T. von Clarmann (2015), A solar signal in lower stratospheric water vapour?, *Atmos. Chem. Phys. Discuss.*, *15*(8), 12,353–12,387, doi:10.5194/acpd-15-12353-2015.

Schmidt, T., J.-P. Cammas, H. Smit, S. Heise, J. Wickert, and A. Haser (2010), Observational characteristics of the tropopause inversion layer derived from CHAMP/GRACE radio occultations and MOZAIC aircraft data, *J. Geophys. Res.*, *115*(D24), D24,304, doi:10.1029/2010JD014284.

Schoeberl, M., and A. Dessler (2011), Dehydration of the stratosphere, *Atmos. Chem. Phys.*, *11*(16), 8433–8446, doi:10.5194/acp-11-8433-2011.

Schoeberl, M., A. Dessler, and T. Wang (2012), Simulation of stratospheric water vapor and trends using three reanalyses, *Atmos. Chem. Phys.*, *12*(14), 6475–6487, doi:10.5194/acp-12-6475-2012.

Shepherd, T. G. (2002), Issues in stratosphere-troposphere coupling., *J. Meteor. Soc. Japan.*, *80*(4B), 769–792, doi:http://dx.doi.org/10.2151/jmsj.80.769.

Sherwood, S. C., and A. E. Dessler (2001), A model for transport across the tropical tropopause, *J. Atmos. Sci.*, *58*(7), 765–779, doi:http://dx.doi.org/10.1175/1520-0469(2001)058<0765:AMFTAT>2.0.CO;2.

Simpson, I. R., M. Blackburn, and J. D. Haigh (2009), The role of eddies in driving the tropospheric response to stratospheric heating perturbations, *J. Atmos. Sci.*, *66*(5), 1347–1365, doi:http://dx.doi.org/10.1175/2008JAS2758.1.

Simpson, I. R., T. G. Shepherd, and M. Sigmond (2011), Dynamics of the lower stratospheric circulation response to enso, *Journal of the Atmospheric Sciences*, *68*(11), 2537–2556, doi:10.1175/JAS-D-11-05.1.

Solomon, S., K. H. Rosenlof, R. W. Portmann, J. S. Daniel, S. M. Davis, T. J. Sanford, and G.-K. Plattner (2010), Contributions of stratospheric water vapor to decadal changes in the rate of global warming, *Science*, *327*(5970), 1219–1223, doi:10.1126/science.1182488.

Solomon, S., J. Daniel, R. Neely, J.-P. Vernier, E. Dutton, and L. Thomason (2011), The persistently variable "background" stratospheric aerosol layer and global climate change, *Science*, *333*(6044), 866–870, doi:10.1126/science.1206027.

SPARC-CCMVal (2010), Sparc report on the evaluation of chemistry-climate models, *SPARC Report 5*, *WCRP-132*, WMO/TD–1526.

Staniforth, A., and J. Thuburn (2012), Horizontal grids for global weather and climate prediction models: a review, *Quart. J. Roy. Meteor. Soc.*, *138*(662), 1–26, doi:10.1002/qj.958.

Taguchi, M. (2009), Wave driving in the tropical lower stratosphere as simulated by waccm. part i: Annual cycle, *J. Atmos. Sci.*, *66*(7), 2029–2043, doi:10.5194/acp-11-3701-2011.

Thieblemont, R., K. M. Matthes, N.-O. Omrani, K. Kodera, and F. Hansen (2015), Solar forcing synchronizes decadal north atlantic climate variability, *Under Review*.

Tian, W., M. P. Chipperfield, L. J. Gray, and J. M. Zawodny (2006), Quasi-biennial oscillation and tracer distributions in a coupled chemistry-climate model, *J. Geophys. Res.*, *111*(D20), doi:10.1029/2005JD006871.

Tian, W., M. P. Chipperfield, and D. Lü (2009), Impact of increasing stratospheric water vapor on ozone depletion and temperature change, *Advances in Atmospheric Sciences*, *26*, 423–437, doi:10.1007/s00376-009-0423-3.

Torrence, C., and G. P. Compo (1998), A practical guide to wavelet analysis, *Bulletin of the American Meteorological society*, *79*(1), 61–78, doi:http://dx.doi.org/10.1175/1520-0477(1998)079<0061:APGTWA>2.0.CO;2.

Trenberth, K. E., J. T. Fasullo, G. Branstator, and A. S. Phillips (2014), Seasonal aspects of the recent pause in surface warming, *Nature Clim. Change*, *4*(10), 911–916, doi:10.1038/NCLIMATE2341.

van Loon, H., and G. A. Meehl (2014), Interactions between externally forced climate signals from sunspot peaks and the internally generated pacific decadal and north atlantic oscillations, *Geophysical Research Letters*, *41*(1), 161–166, doi:10.1002/2013GL058670.

Wang, J. S., D. J. Seidel, and M. Free (2012), How well do we know recent climate trends at the tropical tropopause?, *J. Geophys. Res.*, *117*(D16), 09,118, doi:10.1029/2012JD017444.

Wang, W., K. Matthes, T. Schmidt, and L. Neef (2013), Recent variability of the tropical tropopause inversion layer, *Geophys. Res. Lett.*, *40*(23), 6308–6313, doi:10.1002/2013GL058350.

Wang, W., K. Matthes, and T. Schmidt (2015a), Quantifying contributions to the recent temperature variability in the tropical tropopause layer, *Atmos. Chem. Phys.*, *15*(10), 5815–5826, doi:10.5194/acp-15-5815-2015.

Wang, W., M. Matthes, N.-E. Omrani, and M. Latif (2015b), Multidecadal variability of tropical tropopause temperature and its relation to the pacific decadal oscillation, *Under Review*.

White, W. B., and Z. Liu (2008), Non-linear alignment of el nino to the 11-yr solar cycle, *Geophys. Res. Lett.*, *35*(19), 19,607, doi:10.1029/2008GL034831.

Wickert, J., et al. (2001), Atmosphere sounding by GPS radio occultation: First results from CHAMP, *Geophys. Res. Lett.*, *28*(17), 3263–3266, doi:10.1029/2001GL013117.

Wickert, J., et al. (2009), GPS radio occultation: Results from CHAMP, GRACE and FORMOSAT-3/COSMIC, *Terr. Atmos. Oceanic Sci.*, *20*(1), 35–50, doi:10.3319/TAO.2007.12.26.01(F3C).

Wilks, D. S. (2011), *Statistical methods in the atmospheric sciences*, vol. 100, Academic press.

Wirth, V. (2004), A dynamical mechanism for tropopause sharpening, *Meteor. Z.*, *13*(6), 477–484, doi:10.1127/0941-2948/2004/0013-0477.

Wirth, V., and T. Szabo (2007), Sharpness of the extratropical tropopause in baroclinic life cycle experiments, *Geophys. Res. Lett.*, *34*(2), L02,809, doi:10.1029/2006GL028369.

WMO, M. (1957), A three-dimensional science, *WMO Bull*, *6*, 134–138.

Xie, F., J. Li, W. Tian, J. Feng, and Y. Huo (2012), Signals of el niño modoki in the tropical tropopause layer and stratosphere, *Atmos. Chem. Phys.*, *12*(11), 5259–5273, doi:10.5194/acp-12-5259-2012.

Xie, F., J. Li, W. Tian, Y. Li, and J. Feng (2014), Indo-pacific warm pool area expansion, modoki activity, and tropical cold-point tropopause temperature variations, *Scientific reports*, *4*, 4552, doi:10.1038/srep04552.

Xue, X.-H., H.-L. Liu, and X.-K. Dou (2012), Parameterization of the inertial gravity waves and generation of the quasi-biennial oscillation, *J. Geophys. Res.*, *117*(D6), 6103, doi:10.1029/2011JD016778.

Yulaeva, E., and J. M. Wallace (1994), The signature of enso in global temperature and precipitation fields derived from the microwave sounding unit, *J. Climate*, *7*(11), 1719–1736, doi:http://dx.doi.org/10.1175/1520-0442(1994)007<1719:TSOEIG>2.0.CO;2.

Yulaeva, E., J. R. Holton, and J. M. Wallace (1994), On the cause of the annual cycle in tropical lower-stratospheric temperatures, *J. Atmos. Sci.*, *51*(2), 169–174, doi:http://dx.doi.org/10.1175/1520-0469(1994)051<0169:OTCOTA>2.0.CO;2.

Zhou, X.-L., M. A. Geller, and M. Zhang (2001), Cooling trend of the tropical cold point tropopause temperatures and its implications, *J. Geophys. Res.*, *106*(D2), 1511–1522, doi:10.1029/2000JD900472.

Own Publications

Part of this thesis:

- **Wang, W.**, Matthes, K., Schmidt, T., and Neef, L.: Recent variability of the tropical tropopause inversion layer, Geophys. Res. Lett., 40, 6308–6313, doi:10.1002/2013GL058350, 2013.
- **Wang, W.**, Matthes, K., and Schmidt, T.: Quantifying contributions to the recent temperature variability in the tropical tropopause layer, Atmos. Chem. Phys., 15, 5815-5826, doi:10.5194/acp-15-5815-2015, 2015.
- **Wang, W.**, Matthes, M., Omrani, N.-E., and Latif, M.: Multidecadal variability of tropical tropopause temperature and its relation to the Pacific Decadal Oscillation, 2015. (to be submitted)
- **Wang, W.**, Matthes, K. and Xie, F. Decadal variability of lower stratospheric water vapour: links to the solar cycle and sea surface temperatures, 2015. (to be submitted)

Others:

- **Wang, W.**, Tian, W., Dhomse, S., Xie, F., Shu, J., and Austin, J.: Stratospheric ozone depletion from future nitrous oxide increases, Atmos. Chem. Phys., 14, 12967-12982, doi:10.5194/acp-14-12967-2014, 2014.
- Hansen, F., K. Matthes, C. Petrick, and **W. Wang** (2014), The influence of natural and anthropogenic factors on major stratospheric sudden warmings, J. Geophys. Res. Atmos., 119, 8117–8136, doi:10.1002/2013JD021397.

Abbreviations

BDC	Brewer–Dobson circulation
CCA	Canonical Correlation Analysis
CCM	Chemistry Climate Model
CCMVal	Chemistry-Climate Model Validation Activity
CESM	Community Earth System Model
CPT	Cold Point Tropopause
E-P flux	Eliassen-Palm flux
ECMWF	European Center for Medium rage Weather Forecasting
ENSO	El-Niño Southern Oscillation
EOF	Empirical Orthogonal Function
FFT	Fast Fourier Transform
GHG	GreenHouse Gas
GPS-RO	Global Positioning System Radio Occultation
HadISST	Hadley Centre SST
IPWP	Indo-Pacific Warm Pool
ITCZ	Intertropical Convergence Zone
LS	Lower Stratospheric
MCA	Maximum Covariance Analysis
MERRA	Modern Era Retrospective-Analysis for Research and Applications
MLR	Multiple linear regression
NCAR	National Center for Atmospheric Research
NCEP	National Centers for Environmental Prediction
NOAA	National Oceanic and Atmospheric Administration
PC	Principal Component
PDO	Pacific Decadal Oscillation
QBO	Quasi-Biennial Oscillation
SPARC	Stratospheric Processes and their Role in Climate
SST	Sea Surface Temperature

SSW	Sudden Stratospheric Warming
STIL	Strength of the Tropopause Inversion Layer
SWOOSH	Stratospheric Water and OzOne Satellite Homogenized
TEM	Transformed Eulerian Mean
TIL	Tropopause Inversion Layer
TPT	Tropopause Temperature
TTL	Tropical Tropopause Layer
USSA	U.S. standard atmosphere
UTLS	Upper Troposphere and Lower Stratosphere
WACCM	Whole Atmosphere Community Climate Model
WMO	World Meteorological Organization

Acknowledgements

I would like to first thank my family. Without them this work would have not been possible and I am forever grateful to them for their support. In particular, my loving wife Ming has helped me through difficult times and was always there when I needed her.

Warm acknowledgments to my supervisor Prof. Dr. Katja Matthes, who guides and supports all the work in this thesis. In particular, her encouragements help me to overcome all difficulties in work. I would also like to thank Dr. Torsten Schmidt for providing the GPS-RO data and also many of valuable discussions. Sincere thanks to the current and former members of the NATHAN research group, in particular Lisa Neef for checking the English and grammar in most of my written work, and Felicitas Hansen, Robin Pilch Kedzierski, Sandro Lubis and Nour-Eddine Omrani for enlightening discussions and advice. I appreciate the great support from all my former colleagues at GEOMAR - Helmholtz Centre for Ocean Research Kiel and GFZ - the German Research Centre of Geosciences in Potsdam.

I am grateful to Prof. Dr. Ulrike Langematz for preparing a review of this thesis. Many thanks to Prof. Dr. Mojib Latif, Prof. Dr. Wenshou Tian, Hui Ding, Kuni Kodera, Wonsun Park, Jianchuan Shu, Fei Xie and Jiankai Zhang for their scientific advice and valuable suggestions. I thank Prof. Dr. Douglas Maraun, Markus Kunze, Sandro Lubis and Thomas Martin for helping with statistic analysis methods.

I would also like to thank Felicitas Hansen, Christof Petrick, Rémi Thiéblemont and Sebastian Wahl for carrying out some of the simulations in this thesis. I thank Andrew Gettelman and Dan Marsh from NCAR for their help in setting up the WACCM high vertical resolution model runs. Thanks the Deutsche Klimarechen-zentrum (DKRZ) in Hamburg, Germany, at where model calculations have been performed. I thank Gabriele Stiller and the MIPAS-Envisat team at the Karlsruhe Institute of Technology for the provision of and insights into the MIPAS data.

My final acknowledgments shall go to the Chinese Scholarship Council (CSC) and Free University of Berlin for the financial support. This work was also performed within the Helmholtz-University Young Investigators Group NATHAN, funded by the Helmholtz Association, GFZ and GEOMAR.

Declaration

I hereby declare that except where specific reference is made to the work of others, the contents of this dissertation are original and have not been submitted in whole or in part for consideration for any other degree or qualification in this, or any other university. This dissertation is my own work and contains nothing which is the outcome of work done in collaboration with others, except as specified in the text and acknowledgements.

Wuke Wang
Berlin, 2015